Review

Recent Progress of Two-Dimensional Materials for Ultrafast Photonics

Aojie Zhang [1,2,†], **Zihao Wang** [1,2,†], **Hao Ouyang** [1,2,†], **Wenhao Lyu** [1,2], **Jingxuan Sun** [1,2], **Yuan Cheng** [1,2] **and Bo Fu** [1,2,3,*]

1 BUAA-CCMU Advanced Innovation Center for Big Data-Based Precision Medicine, School of Engineering Medicine, Beihang University, Beijing 100191, China; 18375484@buaa.edu.cn (A.Z.); 18374419@buaa.edu.cn (Z.W.); haooy@buaa.edu.cn (H.O.); 18375219@buaa.edu.cn (W.L.); sjxxjs@buaa.edu.cn (J.S.); zy2017317@buaa.edu.cn (Y.C.)
2 School of Instrumentation and Optoelectronic Engineering, Beihang University, Beijing 100191, China
3 Key Laboratory of Big Data-Based Precision Medicine Ministry of Industry and Information Technology, Interdisciplinary Innovation Institute of Medicine and Engineering, Beihang University, Beijing 100191, China
* Correspondence: fubo10@buaa.edu.cn
† These authors contributed equally to this work.

Abstract: Owing to their extraordinary physical and chemical properties, two-dimensional (2D) materials have aroused extensive attention and have been widely used in photonic and optoelectronic devices, catalytic reactions, and biomedicine. In particular, 2D materials possess a unique bandgap structure and nonlinear optical properties, which can be used as saturable absorbers in ultrafast lasers. Here, we mainly review the top-down and bottom-up methods for preparing 2D materials, such as graphene, topological insulators, transition metal dichalcogenides, black phosphorus, and MXenes. Then, we focus on the ultrafast applications of 2D materials at the typical operating wavelengths of 1, 1.5, 2, and 3 μm. The key parameters and output performance of ultrafast pulsed lasers based on 2D materials are discussed. Furthermore, an outlook regarding the fabrication methods and the development of 2D materials in ultrafast photonics is also presented.

Keywords: two-dimensional materials; fabrications; saturable absorbers; ultrafast lasers

1. Introduction

Nanomaterials are ultrathin materials with at least one-dimensional size in nanometers in three-dimensional space [1,2]. Nanomaterials have unique quantum natures, which make their properties different from general materials in the fields of force, heat, light, electricity, and magnetism [3–9]. In accordance with the structure morphology, nanomaterials can be divided into zero, one, two, and three dimensions. As a kind of nanomaterial, two-dimensional (2D) materials are composed of single or several atomic layers. Strong covalent or ionic bond forces in layers and weak van der Waals forces between layers endow 2D materials with fascinating electrical and optical properties, including the quantum Hall effect, high carrier mobility, and nonlinear optical properties [10,11].

In particular, 2D materials have attracted much attention in the field of ultrafast photonics due to their excellent saturable absorption properties [12]. Ultrafast lasers are the key development direction of ultrafast photonics, which have been widely used in various fields owing to their outstanding advantages, such as short pulse duration, high peak power, high repetition frequency, and wide spectral range [13–15]. The origin of ultrafast lasers can be traced back to 1966. At that time, DeMaria et al. obtained the first picosecond laser pulse output based on a neodymium glass laser by using passive mode-locking technology, opening up a new world for the research of ultrafast pulsed lasers [16].

Q-switching and mode-locking are two typical methods to achieve ultrafast pulsed lasers, both of which can be achieved by active and passive modulation [17,18]. Saturable absorber (SA) is an important medium for passive operation and can be divided into

artificial and real ones. Artificial SA refers to forming a similar SA through nonlinear optical effects, such as nonlinear polarization rotator (NPR) and nonlinear optic loop mirror (NOLM) [19–21].

The first real SA is a semiconductor saturable absorber mirror (SESAM), which can realize mode-locking in different bands through parameter design with stable operation and low loss [22,23]. However, SESAM has a narrow working band, low damage threshold, complex preparation process, and high cost [24]. In the past few decades, nanomaterials have shown potential to be excellent SAs. Carbon nanotubes (CNTs) are a kind of one-dimensional materials with simple preparation and high cost-effectiveness that also have the key advantage of a high damage threshold [25–27]. However, the development of CNTs is restricted by non-saturable loss [28].

Three-dimensional (3D) materials, such as Dirac semimetal cadmium arsenide (Cd_3As_2), metal nanospheres, and nanoscale charcoal powder, can also be used as SAs. However, most 3D materials do not possess the saturable absorption property, and the large insertion loss limits further applications in ultrafast pulsed lasers [29–37]. Compared with artificial SAs, CNTs, and 3D materials, 2D materials are extensively used in ultrafast pulsed lasers as superior SAs owing to the excellent saturable absorption properties, tunable modulation depths, and broadband responses. Moreover, 2D materials possess various preparation methods and easy integration with laser cavities, as well as simplifying the light path of laser systems, which make them promising candidates for further applications in ultrafast lasers.

In 2004, Novoselov et al. used tape to repeatedly peel the bulk graphite according to the mechanical exfoliation (ME) method and acquired the stable single-layer graphene, which opened the door to the world of 2D materials [38]. Graphene, with its unique zero-band gap structure and excellent photoelectric properties [39–41], has rapidly become a research hotspot in the fields of optics, electricity, and biology. In 2009, Bao et al. embedded graphene as a SA in a fiber laser resonator for the first time, and then obtained a picosecond mode-locked pulse output [41]. Since then, 2D materials have gradually become a reliable choice of SAs for ultrafast pulse lasers due to their unique low dimensional physical characteristics, as well as the advantages of a wide working band, controllable modulation depth, and ultrafast relaxation time [42,43].

Thus far, the most widely studied 2D materials in the field of pulsed laser applications are graphene [40,41,44], topological insulators (TIs) [45,46], transition metal disulfides (TMDs) [47,48], and black phosphorus (BP) [49,50]. In addition, a growing number of novel 2D materials have been added to the 2D family, such as MXenes [51], bismuthine [52], and antimonene [53]. The above 2D materials have been widely explored for ultrafast laser applications from the visible to mid-infrared (mid-IR) wavelengths [54–56]. Various gain media have been combined with 2D SAs to achieve 1, 1.5, 2, and 3 μm, as well as other output wavelength pulsed lasers [57–60]. Methods for preparing 2D crystals have also been expanded, such as chemical vapor deposition (CVD), liquid phase exfoliation (LPE), and pulsed laser deposition (PLD) [61,62].

Here, we introduce a variety of methods for preparing 2D materials, and then the applications of typical 2D materials as SAs in ultrafast pulsed lasers are also summarized. Finally, we discuss the state of the art and challenges, as well as the future development of 2D materials in the Perspectives section.

2. Synthesis

In the past decade, 2D materials have attracted wide attention in applications of ultrafast lasers due to their excellent optical and electrical properties [43,63]. In this paper, we focus on the synthesis methods and the applications of widely studied 2D materials in common wavelength of ultrafast lasers (Figure 1). The synthesis of 2D materials is generally divided into top-down and bottom-up methods. In top-down methods, bulk materials are usually exfoliated to obtain 2D materials by physical or chemical methods to overcome the van der Waals force between layers.
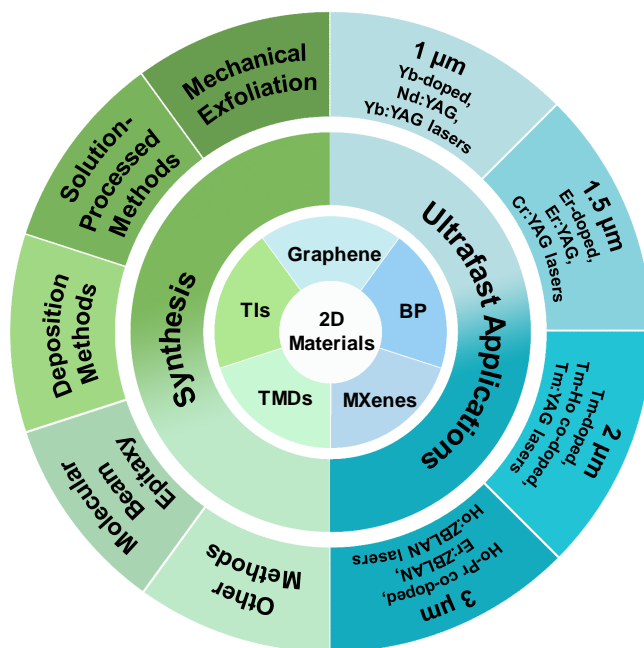
Figure 1. Synthesis and ultrafast applications of 2D materials.

As for bottom-up methods, 2D materials are usually obtained on the substrate by deposition or growth. As shown in Figure 2, we selected the widely used methods, including ME, solution-progressing methods, deposition methods, molecular beam epitaxy (MBE), and other methods. The principles, preparation processes, characteristics, and applications of these methods are also discussed.

Figure 2. The synthesis of 2D materials.

2.1. Top-Down Methods

2.1.1. Mechanical Exfoliation

The ME can separate single- and few-layer materials from bulk materials by overcoming the van der Waals force. Layered materials prepared by ME can be deposited on quartz substrates, such as silicon/silica (Si/SiO_2), and cleaned by acetone, methanol, or isopropyl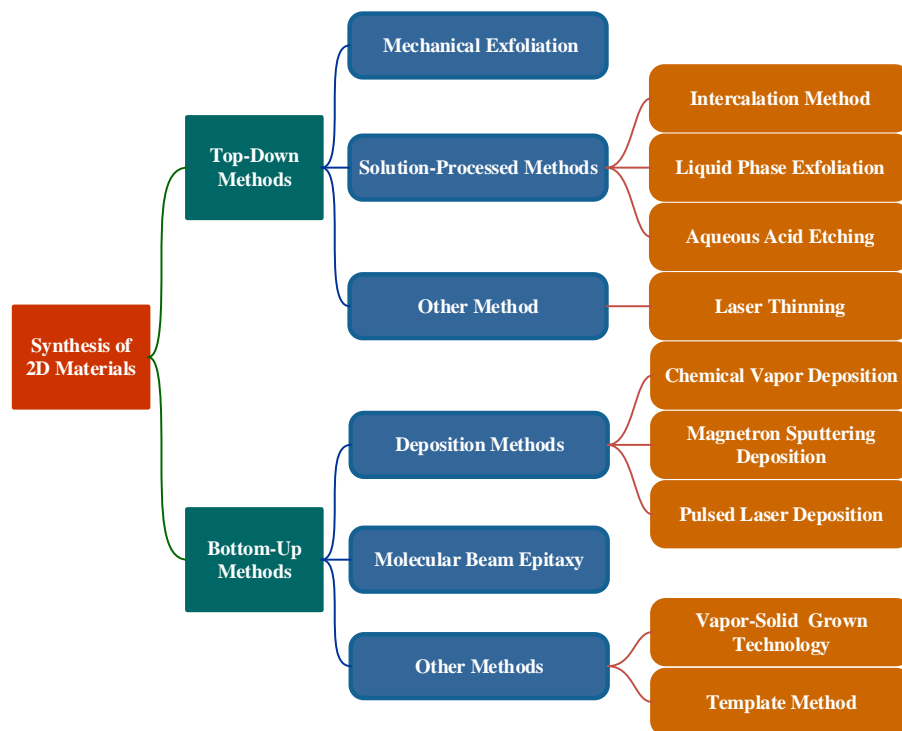 alcohol (IPA) to remove the scotch tape residue [64]. This method has the advantages of being simple, fast, and low cost, and the prepared layered materials have fewer defects and high integrity; therefore, ME is suitable for basic scientific research in laboratory. The ME method based on tape is the most widely used method.

In 2004, Novoselov et al. used scotch tape to repeatedly peel the graphite sheet on mesas attached to the photoresist layer and first obtained single- and few-layer graphene (Figure 3) [38]. Yin et al. peeled a single-layer molybdenum dioxide (MoS_2) sheet from a bulk sample and captured it onto on a Si/SiO_2 substrate by using cellophane tape-based exfoliation. The height of the single-layer MoS_2 obtained was ∼0.8 nm and the phototransistor made of it had good photo-responsivity [65]. ME is also widely used in the preparation of many other 2D materials. In 2010, Desalegne et al. described a method for "graphene-inspired" exfoliation of crystalline bismuth telluride (Bi_2Te_3) films with a thickness of a few atoms [66].
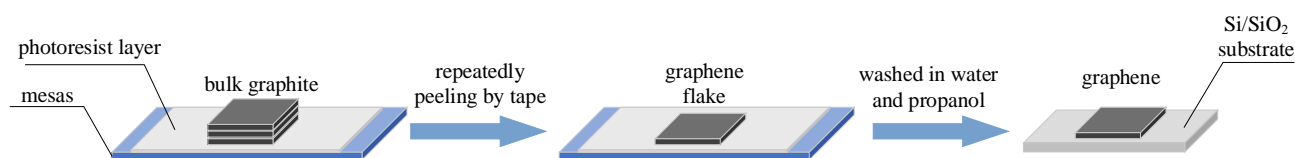

Figure 3. The preparation of a 2D material based on the ME method.

In 2013, Li et al. prepared single-layer TMDs sheets, such as tungsten diselenide (WSe_2), tantalum disulfide (TaS_2), and $TaSe_2$, by using tape-based ME and then using Raman microscopy to characterize them [67]. Then, in 2014, Liu et al. made single-layer BP of ∼0.85-nm step height by tape-based exfoliation [64]. Other topological materials, including Bi_2Se_3 and tellurium antimonide (Sb_2Te_3), can also be obtained by the "graphene-like" ME from the bulk crystals [68].

In 2020, Gkountaras et al. obtained MXenes by the ME method with adhesive tape, in which the prepared MXenes had fewer defects than when using the etching method. This result indicated that ME can peel off some materials with a strong interlayer force, which could broaden the applications of the ME method [69]. However, the efficiency of ME is very low because it requires repeated peeling to obtain a certain number of monolayer materials. Therefore, this method is suitable for scientific research in laboratory; however, it is difficult to realize for mass production.

2.1.2. Solution-Processed Methods

The solution-processed method is one of the most common methods to prepare 2D materials. This method is low cost, and the produced materials are easy to integrate [70]. Different from ME, this is a reliable method for the mass production of layered 2D materials. There are two main methods to prepare 2D materials in solution, including intercalation and LPE methods.

In the intercalation method, an ion or a molecule is usually inserted into the material to destroy the interlayer force [71]. Lithium (Li)-ion intercalation is the most commonly used method, which uses the reaction of water and Li atoms to generate a suspension in deionized water. After filtration or centrifugation, single-layer materials can be obtained. In 1986, Joensen et al. first prepared single-layer MoS_2 by Li-ion intercalation, in which MoS_2 was immersed in a solution of n-butyl Li in hexane for 48 h to achieve intercalation. The intercalated materials were placed into water, and then the monolayer MoS_2 was obtained by ultrasonic treatment and centrifugation after the gas was released [71].

In 1996, Yang et al. also prepared monolayer WS_2 by the intercalation method. They soaked the WS_2 powder in the solution of butyl Li in hexane to obtain Li_xWS_2 and controlled the temperature to ensure x > 1. Then, in order to obtain a WS_2 suspension, Li_xWS_2 was placed into distilled water. After washing and centrifugation repeatedly, single-layer WS_2 was obtained [72]. However, the ion intercalation method is time-consuming and sensitive to the environment, and the prepared material tends to aggregate during deposition [73]. On the basis of the ion intercalation method, some improved methods have been proposed.

In 2012, Ren et al. proposed the hydrothermal intercalation/exfoliation method, which can synthesize Bi_2Te_3 nanosheets on a large scale conveniently. They placed Bi_2Te_3 bulk crystals into a teflon-lined autoclave (30 mL) filled with an ethylene glycol solution of Li hydroxide at 200 °C heated for 24 h to finish Li-ion intercalation. Then, a Bi_2Te_3 colloidal suspension was prepared in deionized water, and the nanosheets were obtained after filtration and drying [74].

In 2014, Zhang et al. completed the intercalation of Li ion by the hydrothermal method and obtained a MoS_2 nanoparticle membrane. As shown in Figure 4a, they placed bulk MoS_2 in an autoclave filled with Li ions and heated it at 200 °C for 72 h to achieve Li-ion intercalation. Then, as with other Li-ion intercalation methods, after placing the intercalated materials into water, a MoS_2 nanoparticle membrane was obtained by filtration [47]. The hydrothermal intercalation/exfoliation method was also used to prepare Bi_2Se_3 [75,76]. Apart from Li-ion intercalation and hydrothermal intercalation/exfoliation, electrochemical intercalation that is slow but can precisely control the number of layers is also a commonly used method [77,78].
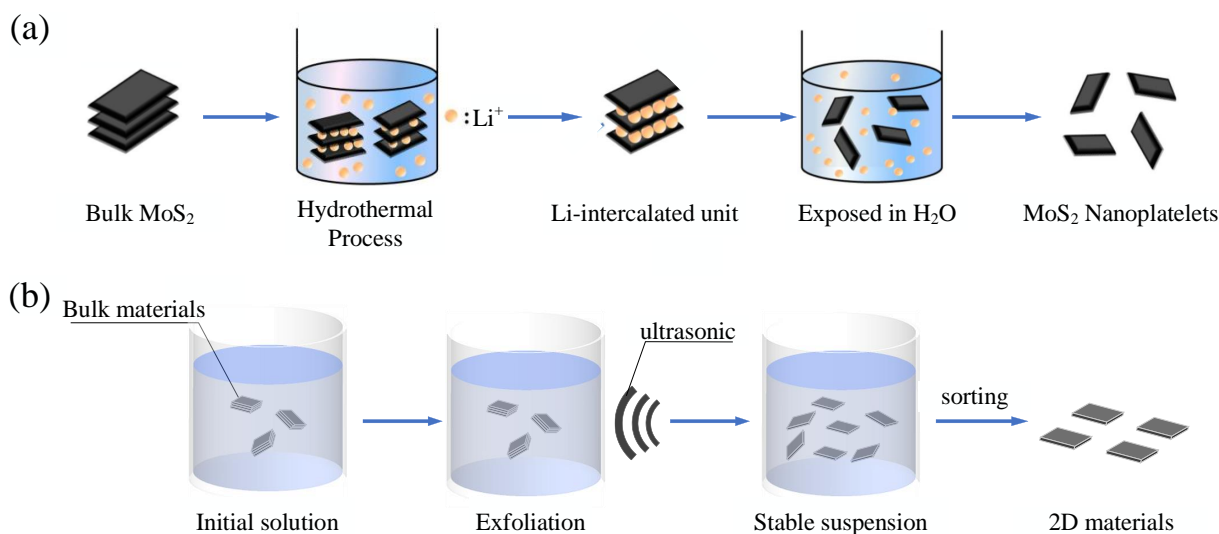
(a)

Bulk MoS_2 — Hydrothermal Process — :Li^+ — Li-intercalated unit — Exposed in H_2O — MoS_2 Nanoplatelets

(b)

Bulk materials — Initial solution — Exfoliation — ultrasonic — Stable suspension — sorting — 2D materials

Figure 4. The preparation of 2D materials based on solution-processed methods. (**a**) Schematic of MoS_2 fabricated by hydrothermal intercalation/exfoliation. Adapted from [47]. (**b**) Schematic of 2D materials fabricated by liquid phase exfoliation (LPE) .

Different from the ion intercalation that often occurs in chemical reactions, LPE is a kind of physical method with a simple process and easy realization. In general, the van der Waals force between the layers of materials is destroyed by using high-intensity ultrasound, and then 2D materials are selected by centrifugation to prepare layered 2D nanomaterials. In 2008, Hernandez et al. demonstrated, for the first time, that LPE can be used to prepare a large number of graphene nanosheets [61]. Subsequently, other 2D materials, such as BP [79–82], boron nitride (BN) [83,84], TMDs [83,84], and TIs [85–89], were also fabricated successfully by LPE.

LPE is generally divided into three main steps, including exfoliation, stabilization, and sorting (Figure 4b). Exfoliation is the process of breaking the force between layers of materials and generating a single or multi-layer structure. The most commonly used

method of exfoliation in liquid is ultrasonication, which has the advantages of being simple, low cost, and of immediate use [90,91]. High-power sonic probes [92,93], sonic baths [61,94–96], and tip ultrasonicators [92,93] are usually used to produce ultrasonication.

There are also other methods for exfoliation, such as ball milling [97–99] and shear exfoliation [100]. After exfoliation, the 2D material needs to be stabilized in the liquid phase. In order to avoid material reaggregation and to reduce the net energy cost of exfoliation, suitable stabilizers are needed, of which the solvent, surfactant, and polymer are the three main ones. N-methyl-2-pyrrolidone and dimethylformamide are two common organic solvents used in the LPE method. However, due to their high boiling point and toxicity, people have also attempted to use IPA with a low boiling point [80,81,101], co-solvent, such as water/ethanol [102,103], or water/isopropanol [103] as a substitute.

Sodium dodecylbenzene sulfonate and sodium cholate can be used as surfactants to prevent reaggregation of materials in the liquid by electrostatic or spatial repulsion [84,96,104,105]. Moreover, simple kitchen soap [106] and aromatic molecules [107] have also been shown to be used as surfactants in the preparation of 2D materials. Sometimes polymers, such as proteins and copolymers with hydrophobic centers and hydrophilic chains, can be used as substitutes for surfactants, which are adsorbed on the surface of nanosheets, increasing the repulsive force between the nanosheets, thus, maintaining the stability of 2D materials [108–110]. Reserach proved that these polymers can be used in graphene [108] and some TMDs [109,111].

After stabilization, 2D materials with the appropriate transverse size and thickness need to be sorted from the stripped dispersions. The commonly used method is ultracentrifugation, which can be realized by sedimentation based-separation (SBS) and density gradient ultracentrifugation (DGU) [112]. SBS separates different dispersions by their different sedimentation rates and the larger dispersions generally settle faster than the smaller ones [112]. At present, using SBS can sort many 2D materials [83,84,113]; however, it can only separate dispersions with a small transverse size. For a dispersion with a large settlement coefficient, it is not effective.

Compared with SBS, DGU can achieve more accurate control of layer number, in which the dispersed nanomaterials are ultracentrifuged in the preformed density gradient medium (DGM) [114]. In this process, dispersions move along the tube under the action of centrifugal force until they reach the point where their buoyancy density equals the buoyancy density of the surrounding DGM, and therefore materials with different layers are in different gradient positions [115]. However, DGU is time-consuming and low yield; thus, researchers can choose the appropriate method according to the actual situation between SBS and DGU.

In general, LPE has the advantages of scalability, room temperature treatment, and high yield; however, the problems of difficulty to accurately control the size and thickness of the exfoliated layer materials also limit its applications.

Aqueous acid etching (AAE) is the most commonly used and efficient method to prepare MXenes, which are exfoliated from MAX phases. The molecular formula of the MAX phase is $M_{n+1}AX_n$, where M is early transition metal elements, A represents group IIIA or IVA elements, and X represents C and/or N. In AAE, M-A bonds are destroyed in the MAX phase by chemical etching the atomic layer. Hydrogen fluoride (HF) is the main etchant to prepare MXenes with low cost and mature technology. In 2011, Naguib et al. used HF to etch titanium aluminum carbide (Ti_3AlC_2) and obtained the first MXene ($Ti_3C_2T_x$) [116].

Later, HF was gradually used in more MAX phases to prepare MXenes [117–121]. However, when manufacturing MXenes with HF, the parameters, such as the HF concentration and etching time, need to be strictly controlled, and HF is highly corrosive and harmful to human body. As a result, other etching solutions for the acid etching of MXenes have been explored. For example, Halim et al. prepared Ti_3C_2 by selectively etching Al in Ti_3AlC_2 thin films with ammonium hydrogen fluoride (NH_4HF_2) aqueous solution [122].

Moreover, lithium fluoride (LiF) and hydrogen chloride (HCl) mixed solution has also been proven to be able to prepare MXenes, such as Ti_3C_2 [123], Ti_2C [124,125], and Ti_3CN [126].

2.1.3. Other Methods

Laser thinning is a top-down method to obtain 2D materials by laser thinning multi-layer materials on the substrate. It can realize the precise control of the number of layers and patterns and has high repeatability, indicating the potential for preparing 2D materials [127–129]. In the laser thinning method, multi-layer thin films are deposited on the substrate by ME [127–130] or chemical deposition [131–133], then laser scanning is used to refine the multi-layer into a single layer.

The process of laser thinning is shown in Figure 5. In 2011, Han et al. thinned the CVD-grown graphene film by laser irradiation, realized the preparation of single-layer graphene, and investigated the key parameters of the thinning effect [131]. In 2012, Castellanos-Gomez et al. deposited multi-layer MoS_2 films on a Si/SiO_2 substrate by ME, which was thinned by a high-power scanning laser. Finally, they reduced the multi-layer MoS_2 into a single-layer 2D crystal at a rate of 8 μm^2/min by laser thinning [127]. Later, in order to make the 2D materials prepared by laser thinning better used in electronic devices, precise controls of layer number and pattern have been widely studied. In 2015, Lin et al. thinned multi-layer graphene by using a picosecond laser, which obtained the required number of layers [133].
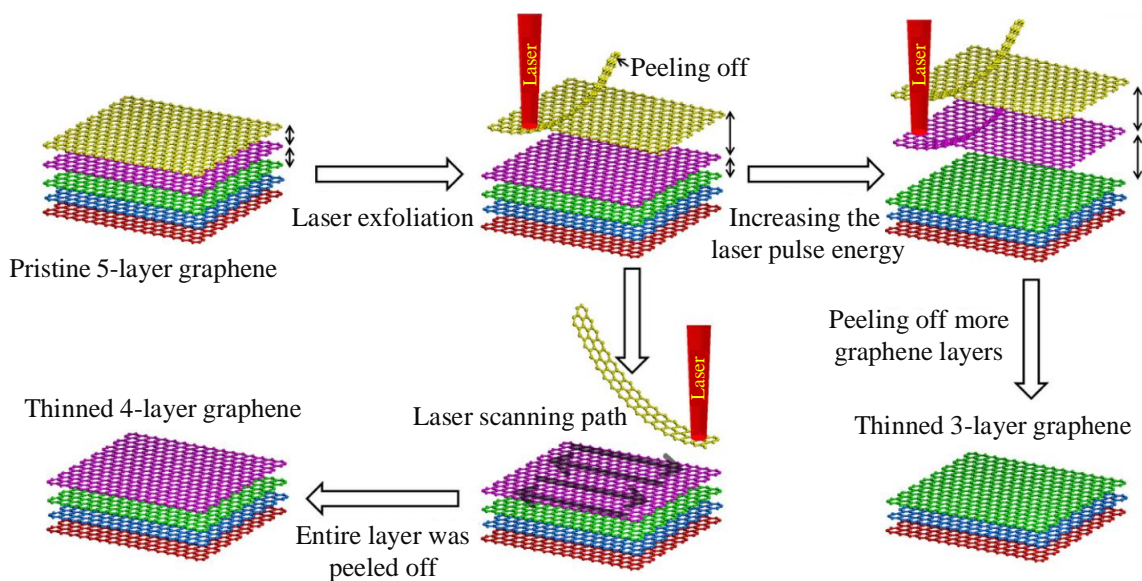

Figure 5. The preparation of 2D material based on the laser thinning method. Adapted from [133].

In the same year, Li et al. realized the thinning of graphene to a specific thickness by using femtosecond laser grating scanning [132]. In 2017, Hu et al. also achieved layer-by-layer precision patterning in the preparation of MoS_2 films by vertical and lateral control, where they also quantitatively designed the laser power and exposure time for accurate thinning and patterning [129]. Up to now, laser thinning has been mainly used in the preparation of graphene and MoS_2; however, as a method of high precision and repeatability, laser thinning also has potential in the preparation of other 2D materials.

2.2. Bottom-Up Methods

2.2.1. Deposition Methods

CVD is a process where a gaseous substance reacts in the gas phase or on the substrate surface to produce 2D material films. LPE and ME can only produce 2D materials with a small size, while CVD can produce large-area and uniform materials [134,135]. In 2008, Yu et al. used CVD to synthesize graphene for the first time, as well as investigating the

effects of cooling rate and other growth conditions on the thickness and defect number of graphene [136]. A year later, Li et al. grew uniform graphene on a metal surface by CVD, in which they used a mixture of methane and hydrogen to grow graphene on 25-mm copper foil [134]. In 2014, Chang et al. prepared crystalline monolayer $MoSe_2$ by CVD with MoO_3 and Se powder. As shown in Figure 6a, argon and hydrogen bring MoO_3 and Se vapor onto sapphire substrate, then the two react to grow $MoSe_2$ on the substrate [137]. In 2015, Xu et al. first prepared large-area and high-quality 2D ultrathin Mo_2C crystals on copper foil using the CVD method, and it was easy for them to adjust the size and thickness of 2D α-Mo_2C crystal by changing the experimental regulation [138]. One advantage of CVD is that, for SA, the modulation depth can be increased by controlling the number of layers. In 2018, Liu et al. prepared WSe_2 thin films by CVD and successfully obtained different modulation depths by controlling the thickness of WSe_2 thin films [139].
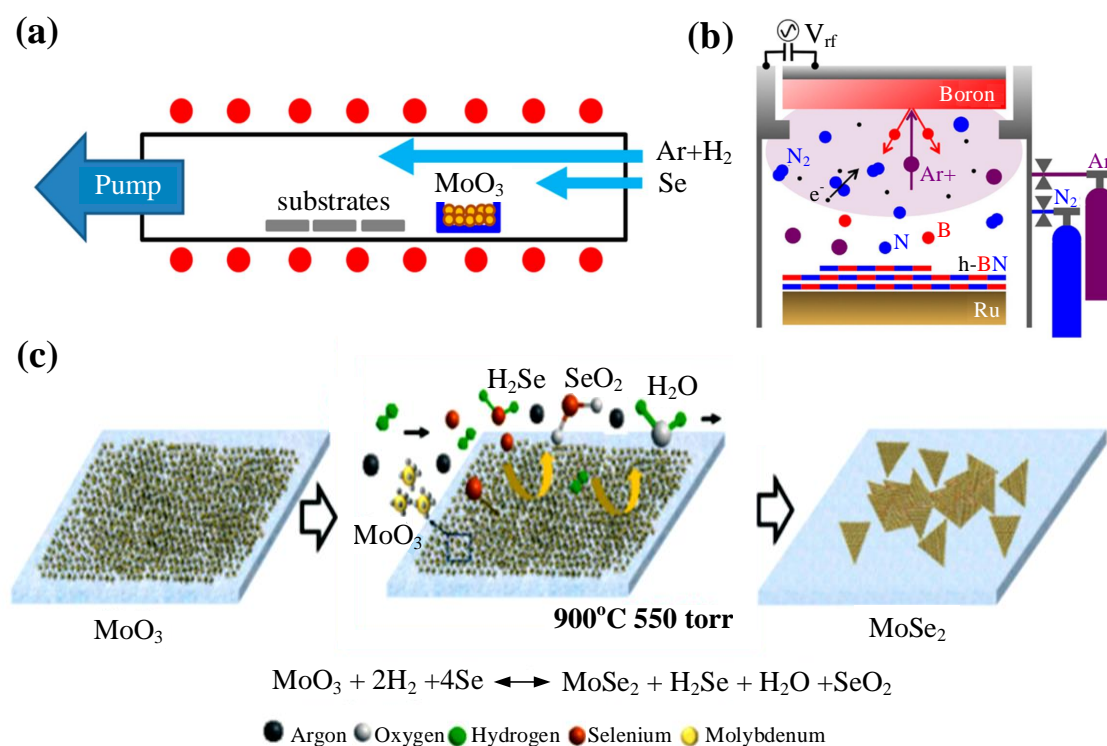

$$MoO_3 + 2H_2 + 4Se \longleftrightarrow MoSe_2 + H_2Se + H_2O + SeO_2$$

● Argon ○ Oxygen ● Hydrogen ● Selenium ○ Molybdenum

Figure 6. The preparation of 2D materials based on deposition methods. (**a**) Schematic of layered $MoSe_2$ grown by CVD. Adapted with permission from reference [137]. Copyright 2010 American Chemical Society. (**b**) Schematic of BN films grown by MSD. Adapted with permission from [140]. Copyright 2012 American Chemical Society. (**c**) Schematic of $MoSe_2$ monolayer grown by PLD and selenidation techniques. Adapted with permission from [141]. Copyright 2016 The Royal Society of Chemistry.

Another advantage of CVD is the good versatility can be used to prepare a variety of 2D materials. In 2010, Shi et al. obtained hexagonal boron nitride (h-BN) films with a thickness between 5 and 50 μm and transverse size up to 20 μm on nickel (Ni) films by CVD under atmospheric pressure [142]. In 2014, Zhang et al. obtained uniform and high-quality Bi_2Se_3 thin films in a selenium-enriched environment by CVD without a catalyst, which reduced the preparation cost, and the effects of certain parameters on the growth process were discussed in detail [143]. In 2020, Gu et al. prepared high-quality 2D palladium selenide ($PdSe_2$) crystals based on atmospheric pressure CVD method and studied the growth process and morphology of $PdSe_2$ crystals by experimentation and theoretical calculations [144].

In order to prepare high-quality 2D materials by CVD, it is also necessary to control the parameters that have great influence on the size and number of layers of the final 2D materials [145]. For example, in 2020, Tang et al. proposed a vertical CVD method to

achieve uniform, high-quality, and reproducible growth of single-layer TMDs by controlling the precursor concentration, gas flow, and temperature [146]. In general, the superiorities of CVD are that it can prepare large-area and uniform 2D materials, the yield is high, and the number of layers is easy to control. However, there are certain drawbacks, such as the complex preparation process [147], high cost [148], and certain risk [149], which need to be considered in the actual situation.

During the preparation process of magnetron sputtering deposition (MSD), the target material is bombarded by the ions, which are accelerated in a strong magnetic and electric field. Then, the splashed material reacts with the material in the gas to obtain 2D materials on the substrate. MSD has a high deposition rate and low growth temperature, in which the deposition rate can be controlled by adjusting the effect of the radio-frequency (RF) power [150]. Li et al. prepared polycrystalline indium selenide (In_2Se_3) thin films by MSD at 270 and 380 °C, as well as found a linear relationship between the deposition rate and effect of RF power where the fastest speed could reach 121.7 nm/min.

In 2013, Sutter et al. obtained high-quality and controllable thickness BN films by designing different schemes MSD of B in N_2/argon (Ar). As shown in Figure 6b, the collision of high-energy Ar ions with a solid B target resultd in the evaporation of B. Then, h-BN was obtained by the combination of evaporated B and dissociated N_2 on the substrate [140]. In 2015, Ling et al. prepared MoS_2 by MSD, and the film thickness could be controlled to 0.75 nm [151]. In the same year Tao et al. demonstrated a MSD method for synthesizing uniform MoS_2 with controllable number of layers in a large area [152].

In 2016, Zhang et al. deposited Bi_2Se_3 thin films with good crystalline quality on Si within 10 min by using Bi_2Se_3 alloy with purity of 99.999% as target in MSD and discussed the resistivity characteristics of the films [153]. MSD has the advantages of simple and easy control, as well as low cost and high speed; however, it also has the problems of high energy consumption and poor material quality [28,152].

In 1987, Dijkkamp et al. successfully prepared yttrium–barium–copper–oxygen superconductor thin films by pulsed excimer laser evaporation of single bulk target in a vacuum for the first time [154]. Since then, PLD technology has gradually emerged. PLD is a bottom-up physical vapor deposition technology, which uses high-energy pulsed laser to impact the target in a high vacuum and then produce a plasma plume. The plume reaches the substrate and crystallizes into the target material [155]. A PLD system generally consists of an excimer laser, optical system, and growth chamber equipped with a vacuum pump and gas path [155].

Thus far, PLD has been widely used in the synthesis of 2D materials. In 2011, Wang et al. achieved the synthesis of large-area graphene (1×1 cm^2) on Ni thin films by PLD [156]. Subsequently, Onsoe et al. synthesized high-quality Bi_2Se_3 atom planar topological insulator epitaxial films with controllable thickness in the range of 6–120 nm using the same method [157]. In 2014, Lee et al. also obtained high-quality Bi_2Se_3 thin films on a Al_2O_3 substrate with low repetition rate and deposition temperature in a multi-target PLD cavity [158]. In 2015, Yang et al. grew ultrathin BP films on graphene/copper or SiO_2/Si substrates with bulk BP crystal as target, in which uniform film growth was achieved by rotating the substrate and target [159].

In 2016, Farman et al. first deposited MoO_3 thin films by PLD, and then obtained $MoSe_2$ thin films by selenization in a two zone hot-wall furnace, as shown in Figure 6c [141]. Moreover, PLD is also a high degree of freedom technology, and thus many requirements can be achieved by adjusting the parameters, such as the substrate cooling rate, gas atmosphere, gas pressure, laser frequency, and laser energy. PLD has the advantages of simple operation, high efficiency, low pollution, good versatility, and substrate compatibility [28]. However, the research of PLD has just begun. PLD is expected to produce a variety of 2D materials in a large area and realize industrialization in the future.

2.2.2. Molecular Beam Epitaxy

MBE is a layer by layer deposition technique, which can epitaxially grow 2D thin films on substrates. It is noted that MBE is a clean, safe, expandable, and highly controllable method and has the advantages of low growth temperature and low impurity caused by a high vacuum [160,161]. In 2014, Zhang et al. grew Sb_2Te_3 thin films with a thickness of 28–121 nm on Si substrates at 280 °C by MBE [162]. Zhu et al. successfully prepared 2D stanine based on Bi_2Te_3 substrates, in which 40-nm Bi_2Te_3 thin films were first grown on Si wafers by MBE [163].

In later research, plasma was proven to play an auxiliary role in MBE. Therefore, Mishra et al. grew Gallium nitride (GaN) on a monolayer-MoS_2/c-sapphire substrate by plasma-assisted MBE [161]. Yang et al. also successfully obtained large-area graphene single crystals on h-BN with fixed stacking orientation by plasma assisted deposition for the first time. As shown in Figure 7a, on the h-BN crystal obtained by ME, various free radicals decomposed from methane epitaxially grew graphene along the edge, thus, expanding the area of graphene [164].
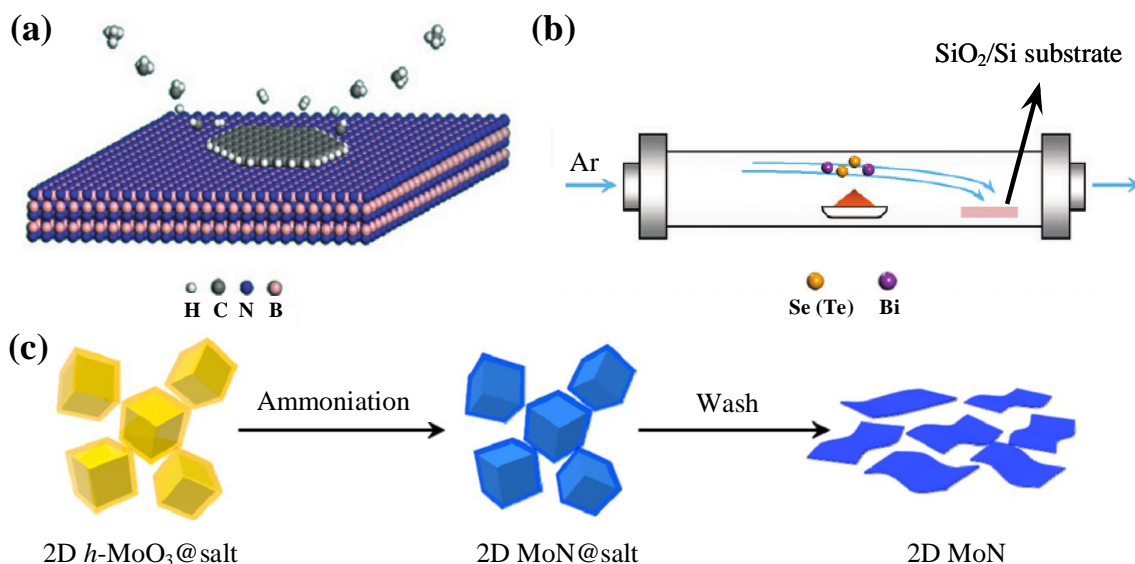

Figure 7. The preparation of 2D materials based on MBE, VS, and template methods. (**a**) Schematic of graphene fabricated by epitaxial growth. Adapted with permission from [164]. Copyright 2013 Macmillan Publishers Limited. (**b**) Schematic of Bi_2Se_3 and Bi_2Te_3 fabricated by VS growth. Adapted with permission from [165]. Copyright 2010 American Chemical Society. (**c**) Schematic of 2D MoN fabricated by template method. Adapted with permission from [166]. Copyright 2017 American Chemical Society.

Currently, many 2D materials can be prepared by MBE, such as $MoTe_2$ [167], WTe_2 [168], Bi_2Te_3 [169], Bi_2Se_3 [170], MoS_2 [161], $MoSe_2$ [171], and WSe_2 [172]. However, MBE also faces some challenges, such as high cost caused by the complex ultra-high vacuum system, slow speed caused by precise control, as well as limitations on the available materials and substrates caused by strict lattice matching constraints [28].

2.2.3. Other Methods

In addition to the general methods described above, there are also some specific methods to prepare a certain kind of 2D materials. In 2010, Kong et al. developed a catalyst free vapor-solid (VS) growth technology. They placed Bi_2Se_3 or Bi_2Te_3 powder of 99.999% purity as raw materials in a horizontal tube furnace, then heated and deposited them on SiO_2/Si substrate by Ar gas transport (Figure 7b). Using this method, they obtained Bi_2Se_3 and Bi_2Te_3 ultrathin nanoplates with a thickness of 3 nm [165].

In 2019, Khan et al. obtained 2D Bi_2O_2Se single crystals at the millimeter scale by VS growth technology in atmospheric pressure and proved that this material had good

crystalline quality, chemical uniformity, and stoichiometry [173]. The template method has also received wide attention in recent years. In 2016, Xiao et al. used salt microcrystals as substrates/templates to guide the growth of oxides at elevated temperature, which can synthesize transition metal oxides, such as hexagonal-MoO_3, MoO_2, MnO, and WO_3 [174].

In 2017, Xiao et al. also obtained 2D nitrides, such as MoN, W_2N, and V_2N, by ammoniating the oxide, as well as confirming the metal properties of 2D MoN and its excellent rate performance in sulfuric acid electrolytes. As shown in Figure 7c, they first obtained 2D hexagonal MoO_3-coated NaCl (2D h-MoO_3@NaCl) through the salt template method, and then the powder was annealed at 650 °C for 5 h in a mixture of NH_3 (5%) and Ar to obtain 2D MoN@NaCl. Finally, 2D MoN was obtained after deionized water cleaning. By changing the parameters and precursors, other 2D metal nitrides or carbides can also be synthesized by the template method [166].

To sum up, there are a variety of methods to prepare 2D materials, each of which has its own characteristic and application scenarios. In top-down methods, ME is often used in the scientific research of laboratories due to its high integrity of materials. However, there is a problem meaning that it cannot be used in mass production. Solution-processed methods, especially LPE, provide the method for large-scale preparation of 2D materials owing to the low cost and simple operation. As for the accurate and reproducible preparation of 2D materials, we introduce the laser thinning method. Although this method is mainly used to prepare graphene and MoS_2, its potential and possibility are also worth exploring.

In terms of bottom-up methods, CVD is a common preparation method, which can produce uniform and large-area materials with high yield, as well as control the number of layers and size by adjusting the parameters. In view of the high cost and complex operation of CVD, MSD with low cost and simple operation can be used to replace CVD in some application scenarios, where the quality requirements of materials are not particularly high. If the requirements for thickness and shape are high, PLD with a high degree of freedom is a better choice. MBE as a mature method, and its vacuum and pure characteristics make it suitable for the preparation of high-purity 2D materials in the laboratory for research. In addition to general top-down and bottom-up methods, AAE, VS growth technology, and the template method, which are used for the synthesis of specific categories of 2D materials are also being explored.

3. Applications of 2D Materials in Ultrafast Lasers

Ultrafast lasers are the key component of ultrafast photonics, which have come into practice in various fields, such as micromachining [175], communication [176], medical procedures [177,178], gas detection [179], and remote sensing [180]. With the advantages of stability, compactness, and easy implementation, mode-locking and Q-switching are two notable techniques to achieve ultrafast pulsed lasers, where SAs perform crucial roles in many types of ultrafast lasers, such as fiber, solid-state, and waveguide lasers [17,18,49,181–183].

Over the last decade, 2D materials have been extensively investigated and applied as reliable SAs in ultrafast lasers at series of wavelengths due to their innate nonlinear saturable absorption properties, broadband operation, and ultrafast relaxation time [43,184,185]. Here, we summarize and discuss diverse types of ultrafast lasers operated at the commonly used wavelengths (1, 1.5, 2, and 3 μm), which are enabled by the most widely studied 2D materials, including graphene, TIs, TMDs, BP, MXenes, and their heterostructures.

3.1. Graphene

As the pioneer of 2D materials, graphene came to the first use as SA in 1.5-μm region due to the telecommunication boom. In 2009, Hasan et al. first reported on an ultrafast laser mode-locked by a solution-processed graphene-polymer at 1557 nm with a pulse duration of ∼800 fs [40]. Almost at the same time, Bao et al. demonstrated the use of graphene SA as mode-locker in an erbium-doped fiber laser (EDFL) at 1565 nm, in which a graphene film was synthesized by CVD and coated on the core of a fiber [41]. Subsequently, Zhang et al. employed a graphene-polymer and atomic layer graphene as SAs in an EDFL

to achieve large-energy mode-locked pulses with single pulse energies of 3 and 7.3 nJ, respectively [186].

Since this pioneering work, the applications of 2D materials including graphene in ultrafast lasers started flourishing [187]. In 2010, Sun et al. proposed a broadband tunable ultrafast laser mode-locked by graphene at the central wavelengths ranging from 1525 to 1559 nm with a pulse width about 1 ps near transform limitation [188]. Such wavelength-tunable pulsed lasers enjoy great potential in various applications, such as spectroscopy and sensing [189]. Figure 8a shows the transmission electron microscope (TEM) image of the folded graphene flake. The output spectra, corresponding autocorrelation traces, and output pulse train are shown in Figure 8b–d, respectively.
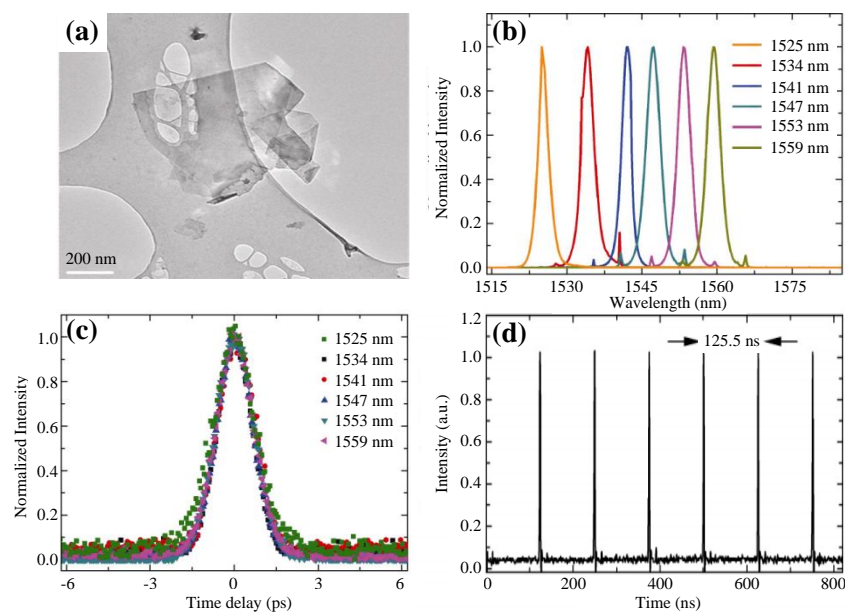

Figure 8. The experimental results of mode-locked EDFL enabled by graphene SA. (**a**) TEM image of a folded graphene flake. (**b**) Output spectra. (**c**) Autocorrelation traces. (**d**) Output pulse train. (**a**–**d**) adaped from [188].

After abundant work on mode-locked lasers, graphene started to be applied in Q-switched lasers to gain pulses with high pulse energy [190]. Luo et al. first exploited graphene as SA to obtain Q-switched pulses in EDFL, which achieved dual-wavelength pulses at 1566.17 and 1566.35 nm with a pulse width of 3.7 µs and pulse energy up to 16.7 nJ [39]. In the next year, a graphene-based Q-switched fiber laser with a tunable broadband between 1522 and 1555 nm was demonstrated by Popa et al., in which a pulse width of 2 µm and pulse energy of 40 nJ were obtained [191]. Such a broadband laser could be applied as the light source for metrology [192], biomedical diagnostics [193], and environmental sensing [194].

In 2012, Gao et al. reported on the first use of graphene SA in a Q-switched Er-doped yttrium aluminum garnet (Er:YAG) laser at 1645 nm with a repetition rate of 35.6 kHz and maximum output power of 251 mW [195]. Soon after that, Sobon et al. realized a passive harmonic mode-locked EDFL with atomic multilayer graphene SA, where a high repetition rate of 2.22 GHz was achieved at the 21st harmonic [196]. In 2013, Fu et al. also reported on a 32nd harmonic mode-locked laser with excellent stability, in which the supermode suppression was up to 50 dB and the signal-to-noise ratio (SNR) was better than 67 dB [44]. Cafiso et al. deployed monolayer graphene in a Chromium-doped YAG (Cr:YAG) laser, obtaining stable mode-locked pulses with a short pulse duration of 91 fs [197].

In 2015, Sotor et al. integrated a CVD-grown graphene-polymer composite (60-layer) into a dispersion-managed fiber laser and obtained a stretched mode-locked pulse of 88 fs in 1.5 µm [198]. The study also validated that the modulation depth of multilayer graphene was proportional to the number of its layers, which can reach up to the 10% level. In 2019,

Fu et al. demonstrated the bound states of solitons and harmonic mode-locking from a fiber laser based on graphene [199]. The laser could produce 26th harmonic stable pulses with a pulse duration of 720 fs and an SNR of 65 dB at the repetition rate of 409.6 MHz, which promoted the applications of graphene-based lasers, including spectroscopy and nonlinear imaging.

The research of graphene-based ultrafast laser in 1 μm was carried out simultaneously along with that in 1.5 μm. In 2010, Yu et al. reported on the first Q-switched ultrafast laser by employing graphene epitaxially grown on silicon carbide (SiC) in a neodymium-doped YAG (Nd:YAG) crystal laser centered at 1064 nm, obtaining a maximum pulse energy of 159.2 nJ [200]. Subsequently, Zhao et al. proposed the first mode-locked ytterbium-doped fiber laser (YDFL) based on CVD-grown graphene film with a dissipative soliton pulse of 580 ps [201]. In 2011, a graphene-based Q-switched YDFL was demonstrated by Liu et al. [202]. In the experiment, the graphene polyvinyl-alcohol (PVA) composite was deposited on a broadband reflective mirror, and the laser generated stable pulses with a pulse width of 70 ns at maximum output power of 12 mW.

In 2011, Cho et al. proposed the first graphene-based solid-state laser with a tunable wavelength from 1.22 to 1.25 μm, where stable 94-fs pulses with an SNR of 62.2 dB were achieved at a repetition rate of 75 MHz [203]. In 2014, Zhao et al. realized a rectangular pulsed fiber laser mode-locked by microfiber-based graphene, the operating wavelength of which could be set to 1061.8 and 1068.8 nm by tuning the bandpass filter or rotating the polarization controllers [204].

In 2011, Wang et al. first used graphene as SA in a Q-switched thulium-doped YAG (Tm:YAG) laser at the wavelength of 2-μm, achieving a pulse energy up to 1.74 μJ and a maximum average output power of 38 mW [205]. In 2012, Ma et al. reported on the first mode-locked laser enabled by graphene-polymer composite at 2018 nm with a pulse width of 729 fs, where Tm-doped calcium lithium niobium gallium garnet (Tm:CLNGG) crystal was used as gain media [206]. Later, Zhang et al. reported on a Tm-doped fiber laser (TDFL) mode-locked by graphene-polymer, achieving low-noise pulses with a pulse width of 3.6 ps and an SNR of ∼70 dB [207].

Liu et al. achieved the first Q-switched operation based on graphene SA in 2 μm, which possessed a pulse duration of 1.4 μs and a single pulse energy of 85 nJ [208]. These works laid the foundation for the applications of graphene SA in 2-μm region. In 2013, Fu et al. achieved a pulse energy up to 35 nJ in a graphene-based mode-locked Tm-Ho co-doped fiber laser (THDFL), which possessed a tunable waveband from 1897.69 to 1930.27 nm [209]. Jiang et al. proposed an ultrafast TDFL Q-switched by CVD-grown graphene SA with a maximum output power of 96 mW at the repetition rate of 202 kHz [210].

In 2014, Zhao et al. achieved Q-switched pulses in a graphene-based holmium-doped YAG (Ho:YAG) ceramic laser, obtaining a pulse energy up to 9.3 μJ [211]. Furthermore, Fu et al. employed graphene as SA in ytterbium (Yb)-, Er-, and Tm-Ho co-doped fiber lasers successively and all achieved passively mode-locking, which demonstrated the broadband operation property of graphene in wide operating wavelengths from 1 to 2 μm [55].

As for the mid-IR region, the first graphene mode-locked Cr:Zinc Selenide (Cr:ZnSe) laser centered around 2.5 μm was proposed by Cizmeciyan et al. in 2013 [212]. Soon after that, Tokita et al. reported on the first graphene Q-switched laser in 3 μm by incorporating a graphene SA mirror in an Er-doped ZBLAN fiber laser, obtaining a repetition rate of 59 kHz, a pulse width of 400 ns, and an average output power of 380 mW, respectively [213].

In 2015, Zhu et al. demonstrated a mode-locked fiber laser in 3-μm region for the first time based on graphene SA mirror [214]. According to the results, mode-locked pulses had a pulse width of 42 ps at a repetition rate of 25.4 MHz. Without stopping, the working wavelength of ultrafast mode-locked laser based on graphene kept extending, which reached up to 4.4 μm under Pushkin et al.'s work in 2020 [215].

Unfortunately, the application of graphene SA is limited due to its low absorption co-efficiency (2.3% per layer) and absence of bandgap [41,82]. However, the modulation depth of graphene increases with number of its layers, which enables the remarkable

performance of graphene in broadband operations [41,70]. Additionally, other merits compared with traditional SA, such as the ultrafast recovery time, lower saturation intensity, and wavelength-independent saturable absorption, make graphene an outstanding SA that is widely used in mode-locked and Q-switched lasers [201,216]. It is the applications of graphene in ultrafast lasers that opened the curtain on the research of 2D materials in ultrafast photonics with excellent performance.

3.2. Topological Insulators

Due to the similarity to graphene in band structure [87,217,218], TIs, such as Bi_2Te_3, Bi_2Se_3, and Sb_2Te_3, have also been widely studied and applied in ultrafast photonics. In 2012, Bernard et al. made a preliminary exploration of the optical properties about Bi_2Te_3 and used it as SA to realize a mode-locked fiber laser in the 1.5-μm region [45]. Triggered by this work, Zhao et al. also demonstrated a mode-locked laser based on Bi_2Te_3 that was fabricated by the hydrothermal intercalation/exfoliation method [217].

Figure 9c,d shows the spectrum centered at 1558.4 nm and the pulse width of 1.86 ps. Scanning electron microscopy (SEM) and TEM images of the as-prepared Bi_2Te_3 are shown in Figure 9a,b. Later, the saturable absorption property of Bi_2Se_3 was experimentally investigated by Zhao et al. from a mode-locked fiber laser with a tunable waveband ranging from 1557 to 1565 nm [87]. This pioneering work paved the path for applications of TIs in ultrafast photonics.
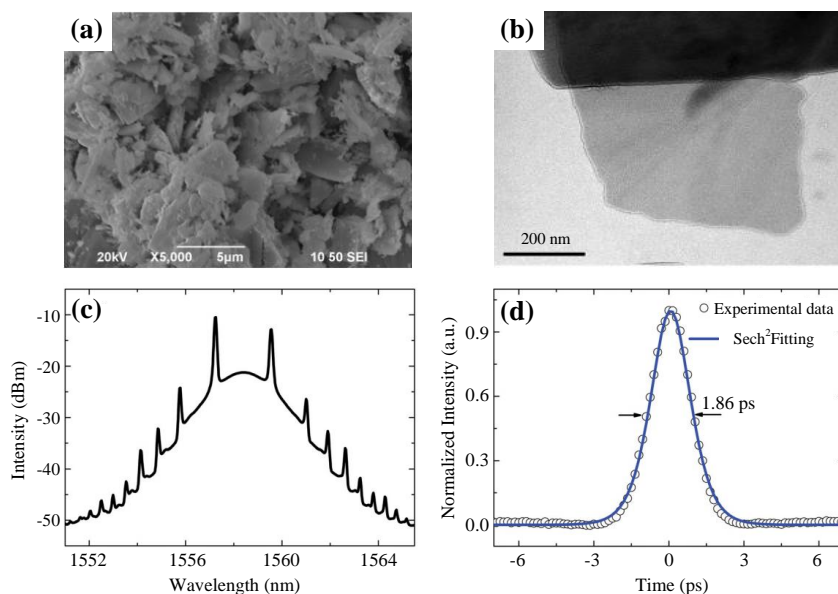

Figure 9. The experimental results of mode-locked EDFL enabled by Bi_2Te_3 SA. (**a**) SEM and (**b**) TEM images of Bi_2Te_3 nanosheets prepared by the hydrothermal intercalation/exfoliation method. (**c**) Soliton spectrum. (**d**) Autocorrelation trace. (**a**–**d**) adapted with permission from [217]. Copyright 2012 American Institute of Physics.

In 2013, Tang et al. obtained Q-switched operation from a Bi_2Te_3-induced Er:YAG ceramic laser at 1.645 μm with a maximum output power of 210 mW, which indicated that TIs SAs could be suitable candidates for high-power applications [46]. In the same year, Chen et al. achieved a dual-wavelength fiber laser at 1545.85 and 1565.84 nm, and a wavelength-tunable fiber laser ranging from 1510.9 to 1589.1 nm both Q-switched by Bi_2Se_3 successively, which confirmed the potential of TIs in broadband optical operation [86].

In 2014, Lee et al. demonstrated a femtosecond mode-locked fiber laser at the central wavelength of 1547 nm [219]. Different from previous work that used high-quality nanosheet-based TIs as mode-lockers, they used bulk-structured Bi_2Te_3 fabricated by ME and finally obtained 600-fs pulses with an average output power of 0.8 mW. The results illustrated that the bulk-structured TI could also be an efficient mode-locker with the advan-

tages of low cost and easy fabrication. After that, Liu et al. used a Bi_2Se_3-PVA composite as SA in an anomalous dispersion fiber ring laser and achieved femtosecond mode-locked pulses of ∼660 fs with an SNR more than 55 dB, indicating its high stability [85].

Sotor et al. reported on the first stretched-pulse mode-locked laser based on TIs. In this work, they deposited bulk Sb_2Te_3 on the side-polished fiber and spliced it to a dispersion-managed laser resonator, which generated 128-fs pulses with an average output power of 1 mW [220]. In 2015, Yan et al. proposed a passive harmonic mode-locked fiber laser operating at 1562.4 nm enabled by a Bi_2Te_3 film SA, where the microfiber-based TI SA was fabricated by the PLD method for the first time [221]. As a result, stable fundamental mode-locking was demonstrated with a pulse width of 320 fs and an output power of 45.3 mW at the repetition rate of 2.95 GHz.

In 2015, the dissipative solitons operation of a fiber laser based on Sb_2Te_3 was proposed by Boguslawski et al. for the first time, which possessed a central wavelength of 1558 nm with a pulse duration of 167 fs and pulse energy of 0.21 nJ [222]. In 2019, Wei et al. reported a passively mode-locked all-fiber EDFL based on CVD-grown Bi_2Te_3 film with the maximum output power, as well as pulse energy of 40.37 mW and 23.9 nJ [223]. Later, Guo et al. employed CVD-grown Bi_2Se_3 as SA in a bidirectional pumped laser cavity, raising the parameters to 82.6 mW and 48.3 nJ [224] and 185.3 mW and 171.3 nJ [225], successively. The improvement of the parameters validated that CVD-grown Bi_2Se_3 exhibits a remarkable capability in high power mode-locked lasers.

In 2013, Luo et al. proposed the first passively Q-switched YDFL based on Bi_2Se_3 at 1067 nm, indicating that TIs SAs had come on the stage in ultrafast lasers at 1 μm [226]. In 2014, Li et al. achieved both Q-switched and Q-switched mode-locked operation in a solid-state laser in 1-μm band by using a Bi_2Te_3 SA mirror, obtaining the maximum output power of 183 and 247 mW, respectively [183]. Shortly afterward, Chi et al. reported on the generation of all-normal-dispersion dissipative-soliton pulses with a bulk Bi_2Te_3 at 1.06 μm [227]. At a repetition rate of 1.44 MHz, stable mode-locked pulses had a pulse duration of 230 ps. Equally important is that Dou et al. also exploited Bi_2Se_3 as SA in an all-normal-dispersion YDFL, which possessed a pulse width of 46 ps and maximum average output power of 33.7 mW at 44.6 MHz [88].

In 2015, Xu et al. achieved Q-switched operation at 1313 nm by using LPE-prepared Bi_2Se_3 nanosheets as SA and $Nd:LiYF_4$ (YLF) crystals as the gain medium, obtaining pulse energy up to 1.23 μJ at a repetition rate of 161.3 kHz [228]. Later, Xu et al. proposed passively Q-switched mode-locked Nd:yttrium vanadate lasers enabled by large-size Bi_2Te_3 sheets at 1064 and 1342 nm separately both with a short pulse duration of a nanosecond, revealing the promising application of large-size Bi_2Te_3 in high-energy short pulse generation [229].

In 2018, Wang et al. demonstrated an all-solid-state mode-locked laser based on a large-area Bi_2Te_3 SA mirror prepared by the spinning coating-co-reduction approach (SCCA), which had a repetition rate up to 1 GHz, output power up to 180 mW, and SNR of 61 dB [230]. These results indicates that TIs could be potential SAs in solid-state lasers for the generation of highly stable ultrafast pulses.

In 2014, Luo et al. employed TIs as SA in a Q-switched TDFL at 1.98 μm for the first time, where TI-Bi_2Se_3 nanosheets were prepared by the LPE method [231]. Later, the first mode-locked fiber laser based on Bi_2Te_3 in the 2-μm region was obtained by Jung et al. [232]. They utilized the bulk-structured Bi_2Te_3 prepared by ME and achieved 795-fs pulses at a repetition rate of 27.9 MHz. In 2015, Yin et al. demonstrated the generation of stable bunched solitons and harmonically mode-locked solitons in a Bi_2Te_3-based mode-locked THDFL, obtaining a pulse duration of 1.26 ps at a repetition rate of 21.5 MHz [233].

Compared with Bi_2Te_3, the other commonly used TI (Bi_2Se_3) was applied to mode-locked fiber lasers in 2 μm very late until 2018, when Lee et al. proposed a mode-locked THDFL enabled by a bulk-structured Bi_2Se_3 with a pulse duration of ∼853 fs [234]. In the same year, Loiko et al. demonstrated a Q-switched thulium-doped gadolinium vanadate

laser based on a Sb_2Te_3 film that was fabricated by the MSD method, obtaining a maximum average output power of 0.70 W at the repetition rate of ∼200 kHz [235].

In 2015, Yin et al. reported on the first mid-IR fiber laser mode-locked by Bi_2Te_3 SA mirror at 2830 nm with a pulse duration of ∼6 ps and maximum pulse energy up to 8.6 nJ [236]. Li et al. achieved passively Q-switched operation in a Ho-doped ZrF_4-BaF_2-LaF_3-AlF_3-NaF (ZBLAN) fiber laser induced by Bi_2Te_3 SA, which produced high-energy pulses with a maximum output power of 327.4 mW and pulse energy of 3.99 μJ [237]. This work indicated that TIs could be reliable SAs for mid-IR pulse generation.

In 2016, Tang et al. demonstrated a Q-switched Er-doped ZBLAN fiber laser by utilizing Bi_2Te_3 as SA, which possessed an average power up to 856 mW at the repetition rate of 92 kHz [238]. In 2018, Li et al. reported on a miniaturized all-fiber Ho-doped fiber laser (HDFL) Q-switched by Bi_2Se_3 nanosheets, in which the shortest pulse duration was 1.54 μs at the maximum output power of 315 μW [239].

As another 2D material widely applied in ultrafast photonics right after graphene, TIs enjoy various merits , including broadband saturable absorption properties, a large nonlinear refractive index, and an innate giant modulation depth (up to 95%) [217,240,241]. Therefore, TIs have been considered as remarkable SAs for the generation of ultrashort, high energy, and high repetition rate pulses within a wide wavelength ranging from visible to mid-IR regions [223,242–244]. However, the relatively slow relaxation time, complicated fabrication process, and relatively low mode-locking stability limit the applications of TIs in ultrafast photonics [49,70,245].

In addition, although Sb_2Te_3 SA demonstrated reliable performance in ultrashort and high power pulses generation [246,247], the majority of applications focus on the telecommunication band. Hence, it is worthwhile to explore more operating wavelengths of Sb_2Te_3 SA. Apart from that, more fabrication methods for TIs with lower cost and easier manipulation, as well as applications in a higher wavelength band of mid-IR region also need to be further studied.

3.3. Transition Metal Dichalcogenides

Since Wang et al. investigated the excellent saturable absorption properties of MoS_2 at 800 nm [248], TMDs, such as MoS_2, $MoSe_2$, WS_2, and WSe_2, have come to the stage of ultrafast photonics applications. In 2014, Zhang et al. first reported on a mode-locked fiber laser at 1054.3 nm with a pulse width of 800 ps, in which a few-layer MoS_2 film was fabricated through the hydrothermal exfoliation method [47]. Later, the first Q-switched fiber laser based on a MoS_2-polymer composite SA was demonstrated by Woodward et al. obtaining a typical Q-switched pulse operated at 1068.2 nm with a pulse width of 2.7 μs [48]. Xu et al. realized a Q-switched solid-state laser by employing LPE-prepared MoS_2 nanosheets in an Nd:yttrium aluminum perovskite (Nd:YAP) laser cavity, where high energy pulses with a peak power of 4.92 W were generated, revealing the promising potential of MoS_2 SA for ultrafast solid-state lasers [249].

In 2015, Zhao et al. proposed a simple chemical weathering-assisted exfoliation method to fabricate MoS_2 and WS_2 monolayers, which exhibited extraordinary performance in Q-switched and mode-locked all-solid-state lasers [250]. Based on this fabrication method, Hou et al. further disposed WS_2 through ultrasonic treatment and used it as SA to obtain a mode-locked Yb:YAG laser with a pulse duration of 736 fs at a repetition rate of 86.7 MHz, further proving that WS_2 could be an excellent SA for ultrafast solid-state lasers [251]. In the same year, Lin et al. demonstrated the first tunable Q-switched YDFL based on WS_2 that prepared by the intercalation method, and the SEM image is shown in Figure 10a [252]. As shown in Figure 10b–d, the typical Q-switched pulses operated at 1048.1 nm with a pulse duration of 1.65 μs and an SNR of ∼50 dB at the repetition rate of 81.5 kHz.
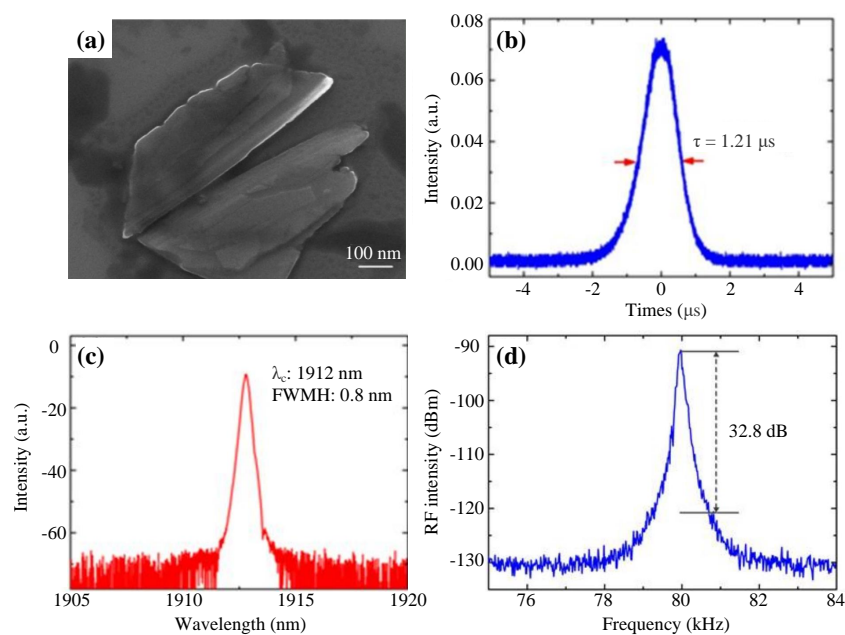
Figure 10. The experimental results of Q-switched YDFL enabled by WS$_2$ SA. (**a**) SEM image of WS$_2$ nanoplates. (**b**) Output spectrum, (**c**) single pulse profile, and (**d**) radio frequency (RF) spectrum at the repetition rate of 81.5 kHz. (**a–d**) adapted from [252].

In 2016, Cheng et al. reported on waveguide Nd:YAG lasers passively Q-switched by CVD-grown MoSe$_2$ and WSe$_2$ respectively, both achieving nanosecond pulse durations [253]. Adopting almost the same scheme, Wang et al. realized Q-switched Nd:YAG lasers based on WS$_2$ solution of different concentrations [254]. By changing the concentrations of the WS$_2$ solutions, they uncovered that the pulse width decreased and the repetition rate rose along with the increase of concentration.

In 2014, Liu et al. demonstrated a femtosecond mode-locked fiber laser at 1569.5 nm with a pulse duration of 710 fs, and a repetition rate of 12.09 MHz by exploiting a firmly MoS$_2$-PVA composite as SA, which was the first application of MoS$_2$ SA in a telecommunication band [255]. Following this work, Liu et al. realized a high-order passively harmonic EDFL mode-locked by microfiber-based MoS$_2$ SA [256]. According to the results, the laser achieved highest harmonic order of 369th at the repetition rate of 2.5 GHz. Soon after that, stable Q-switched operation based on MoS$_2$ with a widely tunable waveband from 1519.6 to 1567.7 nm was achieved by Huang et al. which possessed a maximum pulse energy of 160 nJ and an SNR of 50 dB [257].

Considering the defect of the polymer binder for decreasing the damage threshold, Khazaeizhad et al. coated the MoS$_2$ film on a side-polished fiber to fabricate a polymer-free MoS$_2$ SA. They used it to obtain not only dissipative soliton pulse trains with a bandwidth of 23.2 nm in the normal dispersion regime but also soliton-like pulses of 637 fs in the anomalous dispersion regime [258]. In addition to MoS$_2$, WS$_2$ is also used as a SA for generating ultrashort pulses. In 2015, Mao et al. uncovered the ultrafast saturable absorption property of WS$_2$ nanosheets with the merit of a high damage threshold and used it as SA to achieve stable soliton mode-locking [259]. In pace with this work, stable Q-switched and femtosecond mode-locked operation in the EDFL based on LPE-grown WS$_2$ were also reported by Kassani et al. and Khazaeinezhad et al. separately [260,261].

Yan et al. realized a harmonic mode-locked EDFL by inserting WS$_2$ film-SA synthesized through the PLD method, where the 53rd harmonic with a pulse width of 452 fs and an SNR of 65 dB was obtained at the repetition rate of 1.04 GHz [262]. This work revealed that WS$_2$ could be an outstanding mode-locker and Q-switcher in ultrafast photonics. In the same year, MoSe$_2$ was first exploited as SA in 1.5 μm by Luo et al. who embedded few-layer MoSe$_2$ in a polymer composite and achieved mode-locked soliton pulses with a pulse duration of 1.45 ps [263]. In 2016, Koo et al. utilized a MoSe$_2$-PVA composite to

demonstrate a femtosecond harmonic mode-locked fiber laser with a maximum harmonic order of 212th at the repetition rate of 3.27 GHz, which is the largest repetition rate achieved by 2D material-based lasers to date [264].

In 2017, Liu et al. transferred PLD-prepared WS_2 on a small waist diameter tapered fiber along with a long fused zone covered by a gold film to obtain a SA that had a large modulation depth [265]. Thus, highly stable pulses with an SNR up to 93 dB and a pulse duration of 67 fs were obtained, which was the shortest pulse duration achieved in mode-locked fiber lasers based on TMDs, confirming the promising future of WS_2 in ultrashort pulse generation. In 2018, a Q-switched EDFL based on CVD-grown $MoSe_2$ was reported by Liu et al. which emitted 207-fs pulses with an SNR of 85 dB, further indicating that the combination of the CVD method and the tapered fiber structure is conducive to fabricate high performance SAs for the generation of stable ultrashort pulses [266].

In 2014, by introducing suitable defects in the process, Wang et al. fabricated a type of few-layered MoS_2 with large broadband saturable absorption extending to 2.4 μm [267]. The MoS_2 was applied to demonstrate Q-switching in solid-state lasers at 1.06, 1.42, and 2.1 μm separately. Later, Luo et al. reported on broadband Q-switched fiber lasers by using a few-layer MoS_2-PVA composite SA at different wavelengths, where the span of the wavelengths covered from 1 to 2 μm [268]. Their work indicated unambiguously that few-layer MoS_2 was a promising broadband SA. In 2015, Kong et al. realized both Q-switching and Q-switched mode-locking in a Tm:CLNGG laser induced by MoS_2 golden mirror SA [269].

Subsequently, the first mode-locked operation based on MoS_2 in 2 μm was achieved by Tian et al., who obtained a pulse energy of 15.5 nJ and a repetition rate of 9.67 MHz [270]. In the same year, Jung et al. proposed the first application of WS_2 in an ultrafast mode-locked fiber laser at 1941 nm with an SNR up to 72 dB [271]. In 2017, Lee et al. achieved a femtosecond mode-locked fiber laser at 1912 nm based on $MoSe_2$-PVA composite SA with a pulse duration of ~920 fs and a repetition rate of 18.21 MHz [272]. Another relatively typical TMD, WSe_2, was not used as a SA in the 2-μm region until 2018 by Wang et al., who demonstrated mode-locked soliton pulses had a pulse duration of 1.16 ps and an average output power of 32.5 mW at a repetition rate of 11.36 MHz [273].

In 2016, TMD SA started to be applied in the 3-μm region. Fan et al. reported on a Q-switched Er:lutetium oxide (Er:Lu_2O_3) laser at the central wavelength of 2.84 μm induced by a few-layer MoS_2-based SA, which possessed a repetition rate of 121 kHz and pulse energy of 8.5 μJ, corresponding to a Watt-level average output power of 1.03 W [274]. Subsequently, Wei et al. achieved Q-switched operation in a fiber laser based on WS_2 at 2865.7 nm [275]. The above are the early demonstrations of TMD SA for Q-switching in 3 μm, which indicated the potential of TMD SA applied in the mid-IR region.

In the next two years, Q-switched solid-state lasers in 3 μm based on MoS_2 and WSe_2 were demonstrated by Zhang and Liu et al. successively [276,277]. In 2020, Guo et al. achieved mode-locked operation based on CVD-grown WSe_2 SA mirror at 2789.6 nm with a maximum average output power of 360 mW and a repetition rate of 42.43 MHz, which is the first time TMD severed as mode-locker in the 3-μm region [278].

Many merits of TMDs, such as layer-dependent bandgap and broadband operation, enable them as outstanding SAs from the visible to mid-IR regions [262,267], especially in the Q-switched operation [70,279]. However, the relatively large direct bandgap and low optical damage threshold limit the applications in long operating wavelength as well as in high power lasers [280]. Additionally, the commonly used methods for integrating TMD SAs thus far are either complex and difficult, or induce additional insertion loss to the cavity, which is worthy of optimization to achieve more fruitful results in the mid-IR region.

For example, Liu et al. prepared a WS_2/SiO_2 SA by the sol-gel method to overcome the shortcomings of scattering loss and a low optical damage threshold, as well as to achieve long-term stable mode-locked pulses under high power operation [281]. Furthermore, although MoS_2, $MoSe_2$, WS_2, and WSe_2 have been widely studied and applied, other

TMDs, such as SnS_2, $SnSe_2$, and platinum diselenide, which show exceptional excellent properties, also deserve more investigation regarding ultrafast photonics [282–286].

3.4. Black Phosphorus

After the broadband nonlinear optical response of BP was reported in 2015 [82], Chen et al. utilized BP as SA to realize not only mode-locking at 1571.45 nm with a pulse duration down to 946 fs but also Q-switching at 1562.87 nm with a maximum pulse energy of 94.3 nJ [49]. Later, Li et al. achieved mode-locked operation based on BP with a pulse duration of 786 fs and Q-switched operation with a maximum pulse energy of 18 nJ in the telecommunication band [50]. They also studied the linear and nonlinear absorption properties of BP and found that it was polarization and thickness dependent.

In 2016, Chen et al. demonstrated the generation of stable mode-locked soliton pulses with a tunable wavelength extending from 1549 to 1575 nm by incorporating LPE-prepared BP into an all anomalous dispersion Er-doped cavity [287]. In the same year, Song et al. achieved a vector soliton fiber laser mode-locked by BP for the first time, where the LPE-prepared BP nanoflakes were transferred onto the end facet of a fiber [288]. According to the results, stable 670-fs soliton pulses centered at ∼1550 nm were obtained with a fundamental repetition rate of 8.77 MHz and an SNR of ∼60 dB.

In 2017, a dual-wavelength mode-locked vector soliton fiber laser based on few-layer BP centered at 1533 and 1558 nm with a pulse duration of ∼700 fs was proposed by Yun et al. which validated the potential of BP SA for ultrafast vector soliton generation [289]. In 2018, Jin et al. obtained stable stretched pulses in a mode-locked EDFL based on inkjet-printed BP with a shorter pulse duration of 102 fs and a wider bandwidth of 40 nm compared with previous reports. According to the results, the SNR was up to 60 dB, and the stable mode-locked operation could be maintained for a long time (>10 days), which indicated that the laser experiences long-term stability [290].

In 2015, Zhang et al. reported on a mode-locked solid-state laser based on BP SA mirror at 1064.1 nm with a pulse width of 6.1 ps and average output power of 460 mW [291]. In the same year, Ma et al. realized the first Q-switched solid-state laser enabled by BP at the central wavelength of 1046 nm where passively Q-switched pulses had an average output power of 37 mW at the maximum repetition rate of 113.6 kHz, corresponding to a pulse energy of ∼325.7 nJ [292]. Their works opened the way for BP SA in applications of ultrafast lasers in 1 µm.

In 2016, Al-Masoodi et al. demonstrated Q-switched operation in a BP-based YDFL, achieving a pulse energy of 328 nJ at the repetition rate of 32.9 kHz [293]. Then, Su et al. obtained femtosecond pulses of 272 fs in a solid-state laser mode-locked by BP for the first time with the maximum average output power as high as 0.82 W [294]. Rashidet et al. proposed a dual-wavelength Q-switched laser with a BP thin film operated at 1038.68 and 1042.05 nm [295]. In addition, Ahmad et al. proposed a wavelength-tunable BP-based Q-switched fiber laser at an operational wavelength ranging from 1056.6 to 1083.3 nm [296].

In 2017, Huang et al. achieved a Q-switched laser at 1064 nm where microfibers were sandwiched by BP flakes to integrate SA, providing an effective way to prolong the life of BP flakes by isolating them from the air [297]. In 2019, Wang et al. demonstrated both Q-switched and mode-locked lasers based on BP by inserting polarization-maintaining fiber Bragg gratings [298]. The operating wavelength could be turned to 1063.8 and 1064.1 nm, respectively, as well as concurrently.

Following the initial applications in 1 µm, BP began to be used in the eye-safe region of 2 µm. In 2015, Sotor et al. first reported on a mode-locked fiber laser enabled by mechanically exfoliated BP films at 1910 nm with a pulse duration of 739 ps and an average output power of 1.5 mW at a repetition rate of 36.8 MHz [181]. In 2016, Yu et al. achieved the first Q-switched operation in 2 µm based on BP with the shortest pulse width of 731 ns. Figure 11a shows the SEM image of the LPE-prepared BP. As shown in Figure 11b–d, the laser produced 1.21-µs pulses with the central wavelength of 1912 nm and an SNR of 32.8 dB at the repetition rate of 79.8 kHz [299].
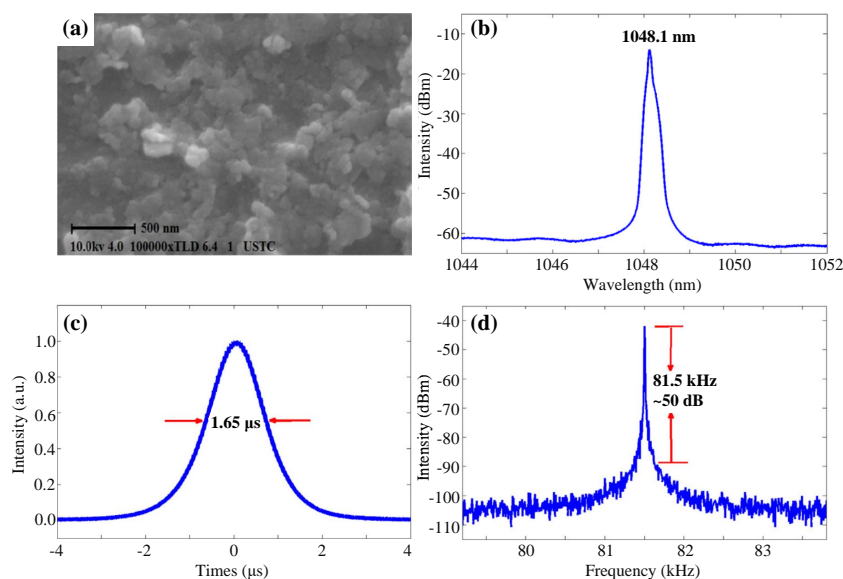
Figure 11. The experimental results of Q-switched THDFL enabled by BP SA. (**a**) SEM image of LPE-grown BP nanoplatelets. (**b**) Single pulse profile, (**c**) output spectrum, and (**d**) RF spectrum at a repetition rate of 113.3 kHz. (**a–d**) adapted from [299].

Later, the earliest solid-state laser Q-switched by BP in 2 μm was demonstrated by Chu et al., who achieved the shortest pulse duration of 1.78 μs at the repetition rate of 19.25 kHz, corresponding to a pulse energy of 7.84 μJ [300]. Then, Zhang et al. reported on a dual-wavelength Q-switched Tm:YAP bulk laser operating at 1969 and 1979 nm, which further proved the capability of BP for Q-switched operation in 2 μm [301]. When it came to 2017, Pawliszewska et al. proposed the first use of BP SA as a mode-locker in HDFL, where harmonic operation up to 10th order was demonstrated with a pulse duration of 1.3 ps at the repetition rate of 290 MHz [302].

In 2015, Qin et al. demonstrated Q-switched operation at 2.8 μm based on a BP SA mirror for the first time obtaining a maximum average output power of 485 mW and pulse energy of 7.7 μJ [81]. Without stopping, in the next year, they adopted the same method to fabricate BP SA and obtained a mode-locked Er-doped ZBLAN fiber laser with a pulse duration of 42 ps and a repetition rate of 24 MHz, which promoted the applications of BP as SA for ultrafast lasers in the mid-IR region [303]. In 2016, Kong et al. reported on a BP-based Q-switched Er:Y_2O_3 ceramic laser at 2.72 μm with a pulse energy of 0.48 μJ at 12.6 kHz [304].

Soon after that, Li et al. inserted LPE-prepared BP into rare earth ion doped fluoride fiber lasers to realize mode-locked and Q-switched operation, respectively, thus, further enhancing the working wavelength of BP-based fiber lasers [80]. In the same year, a dual-wavelength Q-switched solid-state laser at 2.79 μm was demonstrated by Liu et al. [305]. They adopted BP nanoflakes as SA in an Er:strontium fluoride (Er:SrF_2) bulk laser that generated 702-ns pulses at a repetition rate of 77.03 kHz.

In 2018, Qin et al. demonstrated both mode-locked and Q-switched lasers in 3.5 μm enabled by BP SA, which was the first time mode-locking and Q-switching are operated in such a high spectral region, validating the superb potential of BP as SA in the mid-IR region. In 2019, Woodward et al. reported on a dysprosium-doped fiber laser Q-switched by BP SA with a tunable wavelength from 2.97 to 3.32 μm by using an acousto-optic tunable filter [306].

Benefiting from the layer-dependent direct bandgap that can be broadly turned from ∼0.3 (bulk) to ∼2 eV (monolayer), BP stands out as an excellent filler between zero-bandgap graphene and wide-bandgap TMDs [307–309]. Although BP can be fabricated conveniently with low cost [81], its instability in air and water molecules requires relatively strict conditions for its preparation and operation, which restricts the application especially

in high power regimes [310–312]. For now, there is a need for more research on not only economic fabrication methods for stable BP SA but also its application in certain types of ultrafast lasers; for example, harmonic mode-locked lasers with high repetition rate pulses, which possess critical applications in optical communication [313], spectroscopy [43], and frequency bombing [314].

3.5. MXenes

Since Naguib et al. first exfoliated Ti_3C_2 nanosheets from Ti_3AlC_2, MXenes joined the 2D materials family [51,116]. In 2017, Jhon et al. utilized Ti_3CNT_x monolayers to obtain both stable Q-switched and mode-locked pulses at 1558 and 1557 nm [315]. According to the experimental results, a EDFL generated a pulse width of 660 fs, and the main properties were well retained from the Ti_3CNT_x monolayers to stacked ones, which indicated that femtosecond pulses can be demonstrated conveniently by using MXenes as SA without the troublesome process of monolayer dispersion.

In the same year, Jiang et al. discovered the broadband light signal manipulating capabilities of $Ti_3C_2T_x$ films and deposited them onto a side-polished fiber to obtain a mode-locked EDFL with a pulse duration of 159 fs [316]. In 2018, Kim et al. realized a passively mode-locked laser at 1556 nm based on $Ti_3C_2T_x$ fabricated by the AAE method, where a soliton pulse with a pulse width of 800 fs was generated at a repetition rate of 6.22 MHz [317]. In 2019, Li et al. reported on a mode-locked EDFL based on $Ti_3C_2T_x$, which was also synthesized by the AAE method [318].

Figure 12a shows the SEM image of the $Ti_3C_2T_x$ flakes. As shown in Figure 12b–d, the laser yielded 946-fs pulses at 1567.3 nm with a bandwidth of 3.1 nm and an SNR up to 70.7 dB, which meant the pulse generation was highly stable. In the same year, Feng et al. demonstrated a 39th order harmonic mode-locked EDFL enabled by $Ti_3C_2T_x$ SA for the first time [319]. The pulse width was 850 fs, and the repetition rate was up to 218.4 MHz with high commercial value in certain fields, such as electronic communication. Later, Yi et al. investigated the broadband SA properties of Ti_2CT_x and incorporated the solution-processed Ti_2CT_x onto a D-shape fiber to obtain a mode-locked pulse at 1565 nm with a pulse duration of 5.3 ps [56].
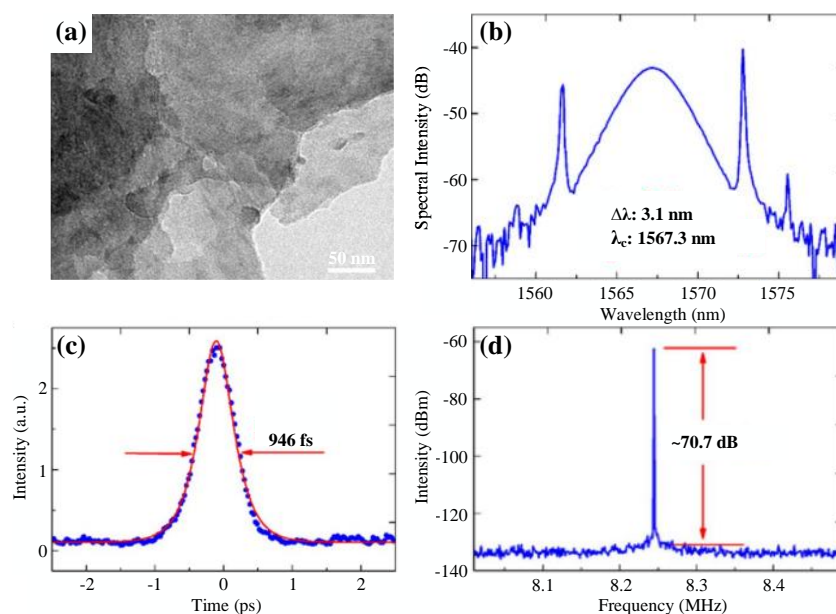

Figure 12. The experimental results of mode-locked EDFL enabled by MXene SA. (**a**) TEM image of the $Ti_3C_2T_x$ flakes. (**b**) Output spectrum. (**c**) Autocorrelation trace. (**d**) RF spectrum. (**a**–**d**) adapted from [318].

Wu et al. proposed a dispersion-managed fiber laser mode-locked by microfiber-based $Ti_3C_2T_x$ SA with a stretched pulse of 104 fs [320]. In 2020, Huang et al. realized the highest harmonic MXene-based mode-locked fiber laser so far, where 206th harmonic order pulses at 1559.1 nm were generated with a pulse width of 940 fs and a high repetition rate of 1.01 GHz [321]. Li et al. first achieved a square-shaped mode-locked fiber laser based on Nb_2C, which was fabricated through the MSD technique [322]. In 2021, Jafry et al. demonstrated mode-locked EDFLs with thin films of $Ti_3C_2T_x$ and $Ti_3C_2T_x$, separately, achieving the highest pulse energies (6.03 and 7.69 nJ) generated by MXene-based SA up to now [323].

In 2018, Jiang et al. obtained an ultrafast fiber laser mode-locked by few-layer $Ti_3C_2T_x$ deposited onto a side-polished fiber at 1065.89 nm, which possessed a pulse duration of 480 ps, repetition rate of 18.96 MHz, and pulse energy of 0.47 nJ [316]. In the same year, Feng et al. reported on a Q-switched Nd:YAG ceramic laser enabled by $Ti_3C_2T_x$ at 1064 nm, which was the first time a Q-switched solid-state laser in the 1-μm region with MXene SA had been achieved [324]. At a repetition rate of 186 kHz, the shortest pulse width was 359 ns and the maximum pulse energy was 0.66 μJ. Soon after that, the first mode-locked solid-state laser with MXene was realized by Sun et al. where LPE-prepared $Ti_3C_2T_x$ was implemented into a Yb:potassium yttrium tungstate (Yb:KYW) laser, and 316-fs pulses at a repetition rate of 64.06 MHz were produced [325].

In 2020, Shi et al. obtained a stable mode-locked fiber laser based on Ti_2CT_x nanosheets with an SNR up to 75 dB [326]. Subsequently, Ma et al. demonstrated a hybrid mode-locked fiber laser by employing nonlinear polarization evolution to YDFL together with vanadium carbide MXene (V_2CT_x) nanosheets, enhancing the output performance regarding the pulse stability and cavity efficiency [327]. Self-starting stable 72-fs pulses with a high pulse energy of 1 nJ were produced in the laser cavity, which is the shortest pulse duration from MXene-based lasers. The experimental results confirmed that V_2CT_x SA is promising in ultrashort pulse generation with high energy.

In 2017, Jhon et al. reported on a passively Q-switched THDFL by using Ti_3CNT_x as SA at the central wavelength of 1875 nm, indicating that the operating range of MXenes could be further extended [315]. In 2019, Zu et al. demonstrated a solid-state laser Q-switched by MXene SA in 2 μm, where the AAE-processed $Ti_3C_2T_x$ was integrated with Tm, Gadolinium doped Calcium fluoride crystal and a pulse width of 2.39 μs at the repetition rate of 19.61 kHz was obtained [328]. In this year, the first self-starting mode-locked TDFL with $Ti_3C_2T_x$ SA was reported by Jiang et al. at 1862 nm with a pulse duration of 2.11 ps and a repetition rate of 13.45 MHz, which further showed the applicability of MXene SA in broadband operation [329].

In 2020, Wang et al. demonstrated a mode-locked fiber laser based on Ti_3C_2, where the vector solitons were generated at the central wavelength of 1965 nm with a 19th harmonic pulse train [330]. They also obtained noise-like pulses evolving from vector solitons with a bandwidth of 3.3 nm by changing the polarization in the cavity, and made the first contribution to explorations of the polarization-independent property of Ti_3C_2. Later, Ahmad et al. realized a $Ti_3C_2T_x$-based passively Q-switched fiber laser with a widely tunable wavelength ranging from 1895 to 2050 nm [331].

In 2021, Gao et al. proposed a passively mode-locked fiber laser by depositing Nb_2C on the tapered fiber, achieving a maximum harmonic order of 69th at the repetition rate of 411 MHz [332]. The results suggested the potential of Nb_2C SA in the mode-locked device. Soon after that, Niu et al. demonstrated a doubly Q-switched Tm:lutetium aluminum garnet (Tm:LuAG) laser by using $Ti_3C_2T_x$ SA and an acousto-optic modulator, which possessed a shorter pulse width of 178 ns and higher pulse peak power of 1062 W compared with the singly Q-switched laser [333].

In 2019, Zhou et al. obtained passively Q-switched pulses in 3 μm based on $Ti_3C_2T_x$ with a maximum output power of 517 mW at the repetition rate of 78.12 kHz, which carved the way for the MXene used in mid-IR pulse generation [334]. Later, Yi et al. realized a Q-switched Er-doped ZBLAN fiber laser based on Ti_2CT_x, obtaining a pulse duration of 730 ns and repetition rate of 99.5 kHz [56]. Subsequently, Bharathan et al. reported on a

mid-IR fiber laser mode-locked by MXene SA operated near 2.8 µm, which had a pulse width of 223.7-ns and an average power of 223 mW [335].

In 2020, the first Watt-level 2D material-based Q-switched fiber laser in the mid-IR region was reported by Wei et al., who achieved a maximum average output power of 1.09 W by using $Ti_3C_2T_x$ as the SA [336]. The study demonstrated that $Ti_3C_2T_x$ is an outstanding SA for mid-IR pulse generation with high power. In 2021, Feng et al. proposed an Er:Lu_2O_3 laser Q-switched by LPE-prepared Nb_2CT_x nanosheets [337]. According to the experimental results, the Q-switched laser could generate a laser pulse of 223.7 ns, which is the shortest pulse duration of MXene-based Q-switched lasers in 3-µm region to date.

As a kind of novel 2D material, MXenes have become a hotspot as prominent SAs in recent years accounting for the excellent damage threshold, ultrafast recovery time, and broadband operation [56,318,338]. Currently, MXene-SAs have achieved mode-locking and Q-switching in a broad waveband from the visible to mid-IR regions, excelling at the generation of ultrashort pulses with good stability and high energy. However, the operating wavelength is still limited to under 3 µm, and the applications of various MXene-SAs in each waveband are uneven, which mainly focus on $Ti_3C_2T_x$ and Ti_3C_2. Therefore, more efforts should be taken to expand the operating wavelength of MXene-based lasers. Meanwhile, more exciting properties and applications in ultrafast lasers of other MXenes, such as Nb_2CT_x and V_2CT_x, are worth exploring further.

3.6. Heterostructures

In order to improve the performance of SAs based on 2D materials, researchers combined the advantages of different 2D materials by forming van der Waals heterostructures, which exhibits superior potential in applications of ultrafast photonics [339]. In 2015, Mu et al. first demonstrated Q-switched and mode-locked fiber lasers based on graphene/Bi_2Te_3 heterostructure SA [340]. The SEM image of the heterostructure is shown in Figure 13a. Mode-locked pulses centered at 1568.07 nm with a pulse duration of 837 fs, repetition rate of 17.3 MHz, and an SNR of 60.7 dB are shown in Figure 13b–d. According to the results, they found that the heterostructure combined the advantages of high modulation depth of Bi_2Te_3 and fast carrier dynamics of graphene, which can be tunable by controlling the coverage of Bi_2Te_3 on graphene.

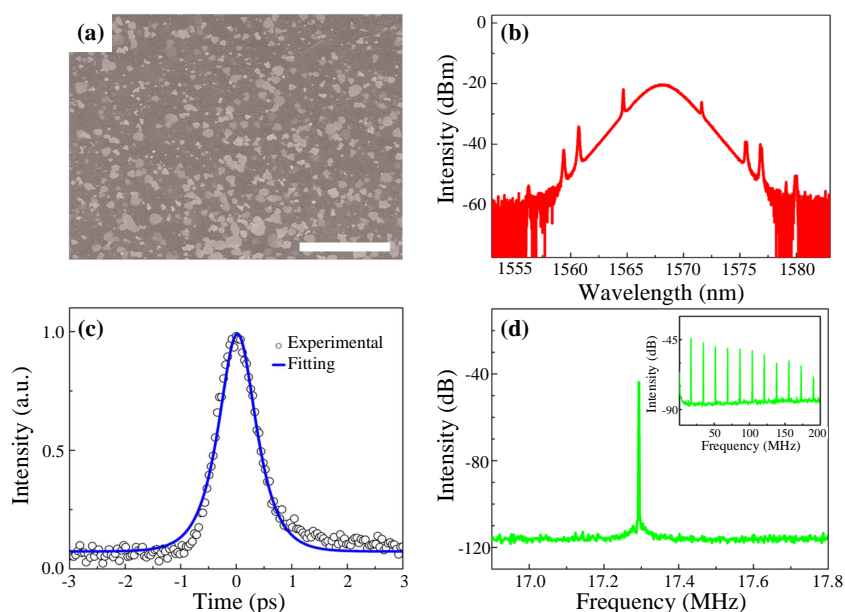**Figure 13.** The experimental results of mode-locked fiber laser enabled by graphene/Bi_2Te_3 heterostructure SA. (**a**) SEM image of graphene/Bi_2Te_3 heterostructure with 15% coverage of Bi_2Te_3. (**b**) Output spectrum. (**c**) Autocorrelation trace. (**d**) RF spectrum (insert: RF spectrum with a wideband up to 200 MHz). (**a**–**d**) adapted from [340].

Later, Jiang et al. used MoS_2/graphene nanocomposites as SA in EDFLs, where both mode-locked and Q-switched operations were achieved [341]. From then on, various heterostructure SAs based on different 2D materials started sparking in ultrafast photonics. In 2017, Liu et al. fabricated a graphene/BP heterostructure to overcome the instability of BP in the air [342]. Furthermore, they used it as a SA to realize not only high energy Q-switching of 267.5 nJ but also mode-locking with a 148-fs pulse width, which exhibited better performance than the laser based on single graphene or BP. Li et al. reported a Q-switched waveguide laser with a maximum output power of 275 mW in 1-μm band, in which the graphene/WS_2 heterostructure was used to enhance the output pulse energy [343]. Tan et al. proposed an Nd:YAG ceramic waveguide laser based on a graphene/WSe_2 heterostructure that was modified by ion beam technology [344].

You et al. proposed passively Q-switched solid-state lasers in 2- and 3-μm bands based on a Bi_2Te_3/graphene heterostructure [345]. The presence of graphene made up for the defect of easy oxidation and the low thermal conductivity of Bi_2Te_3, revealing the feasibility of Bi_2Te_3/graphene SA to generate high energy pulses at a long wavelength. Zhao et al. demonstrated Q-switched operation at the wavelength of 2.8 μm based on MoS_2/graphene heterostructure that was prepared through the hydrothermal method, thus, further promoting the applications of heterostructure SA in the mid-IR region [346]. Chen et al. applied WS_2-MoS_2-WS_2 heterostructure into mode-locked EDFLs and obtained 296-fs pulses with an SNR up to 90.3 dB, which revealed the capability of TMD-based heterostructure SA in ultrafast applications [147].

In 2018, Liu et al. achieved both mode-locking and Q-switching based on a MoS_2-Sb_2Te_3-MoS_2 heterostructure SA with a large modulation depth and high damage threshold [347]. Xue et al. fabricated a MoS_2/BP heterostructure SA through LPE and the spin-coating method [348]. They adopted it in a Tm:YAP laser and realized Q-switched operation with an average output power of 3.6 W and pulse energy of 41.8 nJ, validating its excellent saturable absorption properties. In 2019, MoS_2/WS_2 heterostructure SA was asserted in an EDFL by Liu et al. where 154-fs pulses with a maximum output power of 19.8 mW and an SNR of 91.2 dB were generated at a repetition rate of 74.6 MHz [349].

In 2021, Xia et al. combined the advantages of BP and MXene to fabricate the BP/Ti_3C_2 heterojunction, which possessed a large modulation depth of 58.2% and a small saturation intensity of 1.13 GW/cm^2 in the communication band [350]. They further proved the applicability of BP/Ti_3C_2 heterojunction in ultrafast photonics by inducing it as a SA in a mode-locked EDFL. As a result, a 753-fs pulse width was achieved at 11.7 MHz with a high SNR of 75 dB, and a harmonic mode-locked operation up to the 51st order was also realized at 588 MHz.

In general, 2D material-based heterostructure SAs have attracted wide attention in ultrafast photonics due to excellent merits of modifying the nonlinear optical properties and broadening the response wavelength range [190,340,347,350–352]. Moreover, heterostructures offer a prominent alternative for optoelectronic devices to achieve desirable performance, such as photodetectors, lithium-ion batteries, and field-effect transistors [352–359].

Currently, the operated wavelengths of lasers enabled by heterostructure SAs mainly focus on the 1- and 1.5-μm bands. Graphene and TMD are the most commonly used 2D materials to form heterostructure SAs in ultrafast lasers, while the novel MXenes are relatively rarely used. Therefore, in order to achieve higher performance ultrafast lasers, it is necessary to explore the heterostructure SAs based on MXenes and other 2D materials.

Ultrafast lasers have attracted wide attention owing to the generation of ultrashort pulses with high peak power and pulse energy. The emergency of 2D material SAs has brought bright prospects for ultrafast lasers, which are key components to realize high-performance mode-locked and Q-switched operation [43]. Table 1 summarizes the recent developments of ultrafast lasers based on typical 2D material SAs. Ultrafast pulsed lasers have been mostly investigated in the 1-, 1.5- and 2-μm regions, even up to the mid-IR region of 3 μm. Different gain media are selected in these lasers to obtain pulses centered at diverse wavelengths. Yb-doped fiber, Nd:YAG, and Yb:YAF crystals are commonly used as

gain media in 1 μm, while Er-doped fiber, Er:YAG, and Cr:YAG crystals are widely utilized to achieve ultrafast pulses at the wavelength of 1.5 μm.

In the case of the 2-μm region, researchers tend to employ Tm-doped, Tm-Ho co-doped fibers, and Tm:YAG crystals to obtain ultrafast pulses. In order to realize ultrafast pulsed lasers in the mid-IR region, the ZBLAN fiber is the general gain medium in laser cavities. Ultrafast pulsed lasers based on 2D materials, such as graphene, TIs, TMDs, BP, MXenes, and their heterostructures, can be achieved in 1, 1.5, 2, and 3 μm with corresponding gain media. Moreover, the performances of ultrafast pulsed lasers using 2D materials as SAs are generally outstanding, including a short pulse width, high repetition rate, large pulse energy, and high stability. Each 2D material possesses unique properties, which results in superior output performances of ultrafast pulses at different wavelengths.

Short pulse width is one of the most remarkable merits of ultrafast lasers with 2D materials. In the telecommunication band, the pulse width could achieve the order of femtosecond in mode-locking. For instance, mode-locked pulses with the pulse widths of 870, 128, 163.5, 102, and 159 fs could be generated from EDFLs without amplification or compression based on graphene, TIs, TMDs, BP, and MXenes, respectively. A high repetition rate is another superior output performance, which can be realized by harmonic mode-locked operation. Sobon et al. used graphene to achieve harmonic mode-locked EDFL with the repetition rate of 2.22 GHz [196]. A 2.95-GHz repetition rate was obtained in a harmonic mode-locked fiber laser with TI-Bi_2Te_3 centered at 1.5 μm [221]. With a TMD-WS_2 film SA in a fiber laser, Yan et al. obtained a repetition rate up to 1 GHz at the wavelength of 1559.7 nm [360].

In the next year, Koo et al. raised the repetition rate up to 3.27 GHz by integrating $MoSe_2$-PVA SA into EDFL [264]. In 2020, Huang et al. realized a harmonic mode-locked fiber laser with $Ti_3C_2T_x$ up to 1.01 GHz, which is the highest repetition rate of MXene-based lasers to date [321]. The above experimental results indicated that graphene and TIs are promising candidates for generating harmonic mode-locked pulses with a high repetition rate. In addition, ultrafast lasers based on BP have not achieved a repetition rate up to the order of GHz, which are worthy of further investigations. Compared with mode-locking, Q-switching more is easier to realize ultrafast pulsed lasers with high pulse energy and output power. Li et al. utilized Bi_2Te_3 to obtain a Q-switched fiber laser in the 3-μm region, generating 3.99 μJ-pulses with the output power of 327.4 mW [237]. Wei et al. reported on a MXene-based Er-doped ZBLAN fiber laser with the maximum pulse energy of 28 μJ and the output power of 1.9 W [336]. However, the output power and pulse energy of graphene and TMDs in Q-switched fiber lasers are commonly below 150 mW and 2 μJ [361,362]. Moreover, a BP-based Q-switched laser at 3 μm was achieved with a pulse energy of 7.7 μJ and output power of 485 mW, whereas its easy oxidation under high laser excitation limits the applications [81,288,363]. Hence, TIs and MXenes are expected to achieve pulses with high pulse energy and output power in mid-IR region.

2D materials possess various characteristics and diverse preparation methods, which have an impact on the output performance of ultrafast pulsed lasers. Lasers enabled by graphene cover a wide waveband from the visible to mid-IR regions, which is fabricated mostly by ME and CVD methods [196,201,208,214,364]. Although TIs can be applied for broadband operation, the operating wavelengths of mode-locked lasers based on TIs focus on the telecommunication band, indicating that more applications in other wavebands need to be studied [88,220,221,234]. CVD and LPE are typical methods to fabricate TMDs that always serve as Q-switchers in near-infrared lasers.

However, the investigations of mode-locked lasers based on TMDs in the mid-IR region are restricted by the large direct bandgap in the monolayer state and low damage threshold [280,365,366]. BP not only enjoys broadband operation up to 3.5 μm but is capable of achieving femtosecond mode-locked pulses from the 1- to 2-μm regions as well [181,191,294,367]. Although BP can be easily prepared by ME or LPE methods, the easy oxidation in the air requires strict conditions for its preparation and operation [310–312].

Table 1. Summary of ultrafast lasers based on 2D material SAs. Note that the results obtained from different conditions including various 2D materials, gain media, and experimental purposes.

2D Materials		Fabrication Methods	Gain Media	λ (nm)	τ (s)	f_{rep} (Hz)	Energy (nJ)	Power (mW)	SNR (dB)	Ref.
Graphene	Graphene	CVD	Alexandrite	750	65 f	5.56 M	1.4	8	75	[364]
	Graphene	CVD	Yb	1069.8	580 p	0.9 M	0.41	0.37	70	[201]
	Graphene	MBE	Nd:YAG	1064	161 n	660 k	159.2	105	–	[200]
	Graphene	LPE	Er	1525	~1.15 p	~8 M	~125 p	~1	~80	[188]
	Graphene	Modified Hummers	Er	1566.2, 1566.4	3.7 µ	3.3–65.9 k	16.7	1.1	–	[39]
	Graphene	ME	Er	1560.5	900 f	2.22 G	4.3 p	9.6	50	[196]
	Graphene	LPE	Er	1550	~29 f	18.67 M	2.8	52	62	[368]
	Graphene	CVD	Tm:CLNGG	2018	729 f	98.7 M	0.6	60.2	–	[206]
	Graphene	CVD	Tm	2007.1, 2010.4	1.4 µ	44–53 k	85	4.5	40	[208]
	Graphene	LPE	Tm	1940	3.6 p	6.46 M	~0.4	~2	~70	[207]
	Graphene	CVD	Tm	1897.7	122 n	0.964 M	35.2	34	67	[209]
			Yb	1035	6.5 n	16.29 M	0.81	13	55	
	Graphene	CVD	Er	1564	870 f	19.30 M	10.4 p	0.2	64	[55]
			Tm-Ho	1908	65 n	1.82 M	16.2	29	60	
	Graphene	–	Er-doped ZBLAN	2783	2.9 µ	18.9–37.2 k	0.74–1.67 µ	15–62	30	[361]
	Graphene	CVD	Er-doped ZBLAN	2784.5	42 p	25.4 M	0.7	18	43.5	[214]
TIs	Bi_2Se_3	LPE	Pr-doped ZBLAN	635.5, 635.7	244–761 n	191.6–454.5 k	22.3	7.6	~43	[243]
	Bi_2Se_3	LPE	Yb	1067.66	1.95 µ	8.3-29.1 k	17.9	0.46	48	[226]
	Bi_2Se_3	PM	Yb	1031.7	46 p	44.6 M	0.756	33.7	58	[88]
	Bi_2Se_3	PM	Er	1565.1	14 µ	8.865 k	12.6	112 µ	–	[86]
	Bi_2Se_3	ME	Tm-Ho	1912.12	853 f	~18.37 M	–	–	65	[234]
	Bi_2Se_3	LPE	Tm	1980	4.18 µ	8.4–26.8 k	313	8.4	43	[231]
	Bi_2Se_3	LPE	Ho-doped ZBLAN	2920.6	1.54–3.47 µ	24.97–56.13 k	6	315 µ	~43	[239]
	Bi_2Te_3	ME	Yb	1057.82	230 p	1.44 M	0.599	0.86	~77	[227]
	Bi_2Te_3	Spin coating- co-reduction	$Nd:YVO_2$	1064	7.9 p	949 M	0.1 n	181	61	[230]
	Bi_2Te_3	ME	$Nd:YVO_3$	1064	97 n	47 k	0.6 µ	26.1	–	[229]
			$Nd:YVO_4$	1342	93 n	75 k	0.4 µ	33.2		
	Bi_2Te_3	HI/E	Er:YAG	1645	6.3 µ	40.7 k	5.3 µ	210	–	[46]
	Bi_2Te_3	LPE	Er	1566.9	14 µ	6.97 k	–	–	36.4	[369]
	Bi_2Te_3	PLD	Er	1562.4	920 f	2.95 G	15.4 p	45.3	60	[221]
	Bi_2Te_3	HI/E	Ho-doped ZBLAN	2979.9	1.37–4.83 µ	46.20–81.96 k	3.99 µ	327.38	37.4	[237]
	Sb_2Te_3	ME	Er	1565	128 f	22.32 M	44.8 p	1	65	[220]
	Sb_2Te_3	MSD	Er	1558	167 f	25.38 M	0.21	5.34	68	[222]
	$CoSb_3$	–	Er	1557.9	~833 f	14.48 M	6.9 p	0.1	57	[370]

Table 1. *Cont.*

2D Materials		Fabrication Methods	Gain Media	λ (nm)	τ (s)	f_{rep} (Hz)	Energy (nJ)	Power (mW)	SNR (dB)	Ref.
TMDs	MoS$_2$	HI/E	Yb	1054.3	800 p	6.58 M	1.41	9.3	50	[47]
	MoS$_2$	LPE	Nd:YAP	1079.5	227–580 n	32–232.5 k	1.11 μ	0.26	–	[254]
	MoS$_2$	CVD	Er	1568	4.98 p	26.02 M	–	–	63	[258]
			Er	1568	637 f	33.48 M			61	
	MoS$_2$	LPE	Er	1551.2	5.7 μ	16.78 k	–	–	~50	[257]
			Yb	1066.5	5.8 μ	6.4–28.9 k	32.6	0.9	44.6	
	MoS$_2$	LPE	Er	1565	5.4–23.2 μ	6.5–27.0 k	63.2	1.7	54.5	[268]
			Tm	2032	1.76 μ	33.6–48.1 k	~1 μ	47.3	54.6	
	MoS$_2$	LPE	Er-doped ZBLAN	2754	1.84 μ–806 n	36–70 k	1–2 μ	37–140	40	[362]
	WS$_2$	Chemical weathering exfoliation	Yb:YAG	1057.5	736 f	86.7 M	3.11	27	~51	[251]
	WS$_2$	LPE	Nd:YAG	1064.5	1.28–2.36 μ	28.59–45.25 k	1.2 μ	54	–	[254]
	WS$_2$	CVD	Er	1557.4	163.5 f	63.133 M	0.45	28.5	96	[371]
	WS$_2$	PLD	Er	1559.7	452 f	1.04 G	10.87 p	11.3	48	[360]
	WS$_2$	LPE	Tm-Ho	1941	1.3 p	34.8 M	~17.2 p	~0.6	72	[271]
	WS$_2$	Sulfidation grown	Ho/Pr co-doped ZBLAN	2865.7	1.73–3.8 μ	25.6–131.6 k	0.17–0.42 μ	4–48.4	40.5	[275]
BP	BP	LPE	Yb:CYA	1064	620 n–1.2 μ	~87.7–113.6 k	182.4–325.7	16-37	–	[292]
	MoSe$_2$	CVD	Nd:YAG	1064	80–290 n	0.995-3.334 M	35.9	115.1	–	[253]
	WSe$_2$	CVD	Nd:YAG	1064	52–400 n	0.781–2.938 M	19	45.7	–	
	WSe$_2$	CVD	Tm	1863.96	1.16 p	11.36 M	2.89	32.5	53	[273]
	PtSe$_2$	CVD	Ho/Pr co-doped ZBLAN	2865	620 n–1.72 μ	104.2–238.1 k	0.14–0.39 μ	15-93	30	[372]
	BP	LPE	Yb, Lu:CALGO	1053.4	272 f	63.3 M	6.48	0.82	~62	[294]
	BP	ME	Yb	1038.7, 1042.1	1.16–2.05 μ	52.52-58.73 k	2.09	0.12	50	[295]
	BP	ME	Er	1532.5	9.5–3.1 μ	26–40 k	~18.6	728 μ	–	[50]
	BP	ME	Er	1558.7	~786 f	14.7 M	~0.1	1.6	~56	
	BP	LPE	Er	1555	102 f	23.9 M	71 p	1.7	60	[290]
	BP	ME	Tm	1910	739 f	36.8 M	40.7 p	1.5	70	[181]
	BP	LPE	Tm-Ho	1912	731 n–1.42 μ	69.4-113.3 k	632.4	71.7	32.8	[299]
	BP	LPE	Tm:YAP	1969, 1979	181–720 n	~41–81 k	39.5 μ	3100	–	[301]
			Tm:CYA	1029	1.73 μ	63.9 k	0.09 μ	6		
	BP	LPE	Tm:CYA	1930	3.7 μ	17.7 k	0.68 μ	12	–	[304]
			Er:Y$_2$O$_3$	2720	4.47 μ	12.6 k	0.48 μ	6		
	BP	ME	Er-doped ZBLAN	2783	42 p	24 M	25.5	613	60	[303]
	BP	LPE	Er-doped ZBLAN	3462	2.05 μ	66.3 k	1.8 μ	120	–	[367]
			Er-doped ZBLAN	3489	–	28.91 M	1.38	40	54	
	BP	LPE	Dy-doped ZBLAN	3040	740 n–1.8 μ	47–86 k	0.5–1.0 μ	24–87	–	[306]

Table 1. *Cont.*

2D Materials	Fabrication Methods	Gain Media	λ (nm)	τ (s)	f_{rep} (Hz)	Energy (nJ)	Power (mW)	SNR (dB)	Ref.
$Ti_3C_2T_x$	AAE	Nd:YAG	1064	359–688 n	109–186 k	0.66 μ	94.8	–	[324]
$Ti_3C_2T_x$	AAE	Yb	1065.89	480 p	18.96 M	0.47	9	56	[316]
$Ti_3C_2T_x$	AAE	Er	1555.01	159 f	7.28 M	410 p	3	~62	
$Ti_3C_2T_x$	LPE	Er	1573.2	1.73 p	11.1 M	–	–	62.2	[373]
$Ti_3C_2T_x$	AAE	Tm	1976	2.4 μ	59 k	–	–	52	[331]
$Ti_3C_2T_x$	AAE	Er-doped ZBLAN	2786.2	1.04–28 μ	32.47–78.12 k	6.52–13.93 μ	210–1090	42.1	[336]
Ti_2CT_x	AAE	Yb	1037.8	792 p	16.5 M	0.72	6.57	75	[326]
Ti_2CT_x	AAE	Yb	1565.4	164 p	8.25 M	–	–	62	[56]
Ti_2CT_x	AAE, LPE	Tm:LuAG	2027	178 n	1 k	189 μ	189	–	[333]
Ti_2CT_x	AAE	Ho:YLF	2062.2	837 n	35.5 k	20.8 μ	341	–	[374]
Ti_2CT_x	AAE	Er-doped ZBLAN	2798	1.83 μ–730 n	44.1–99.5 k	0.35–0.81 μ	16–80	33.1	[56]
V_2CT_x	AAE	Yb	1064	72 f	38.5 M	1	38.5	71	[327]
Ti_3C_2	AAE	Tm-Ho	1964	–	–	–	–	56	[330]
Ti_3CNT_x	AAE	Er	1557	660 f	15.4 M	3.2 p	0.05	60	[315]
Nb_2C	MSD	Yb	1031.5	271 p	14.8 M	0.89	13.2	62	[375]
$α$-Mo_2C	CVD	Yb	1061.8	418 p	3.22 M	–	–	64	[376]
		Er	1602.6	1.81 p	1.88 M			45	
Graphene/WS_2	CVD	Nd:YVO$_4$	1064	66–149 n	3.528–7.777 M	33.1	275	–	[343]
Graphene/Bi_2Te_3	CVD	Yb:KYW	1037.2	236 f	41.84 M	19	550	65	[377]
BP/Ti_3C_2	–	Er	1559.8	735 f	11.7 M	–	–	75	[350]
Graphene/Bi_2Te_3	CVD	Er	1568.07	837 f	17.3 M	0.178	3.07	60.7	[340]
MoS_2/Graphene	Modified Hummers	Er	1567.2	9.31–19.12 μ	6.312–21.9 k	73.5–98.6	0.464–2.16	–	[341]
Graphene/BP	LPE	Er	1529	865 f	295.6 M	–	–	48	[342]
WS_2/MoS_2/WS_2	MSD	Er	1562.66	296 f	36.46 M	0.686	25	90.3	[147]
Bi_2Te_3/Graphene	Solvothermal synthesis	Nd:YAG	1980	238 n–1.22 μ	46–108 k	21.7 μ	2340	–	[344]
MoS_2/ Graphene	HI/E	Er:YSGG	2797	355 n	126 k	0.889 μ	112	–	–	[346]

λ, central wavelength; τ, pulse width; f_{rep}, repetition rate; Power, average output power; Energy, single pulse energy; SNR, signal to noise ratio; CVD, chemical vapor deposition; MBE, molecular beam epitaxy; LPE, liquid phase exfoliation; ME, mechanical exfoliation; PM, polyol method; MSD, magnetron sputtering deposition; PLD, pulsed laser deposition; HI/E, hydrothermal intercalation/exfoliation method; Yb, ytterbium; Nd, neodymium-doped; Er, erbium; Tm, thulium; Ho, holmium; ZBLAN, ZrF_4-BaF_2-LaF_3-AlF_3-NaF; Pr, praseodymium; Lu, lutetium; and Dy, dysprosium.

Note: The leftmost column groups rows as MXenes (first block), Hetero structures (second block), and MoS_2/ Graphene (last row).

MXenes, mostly fabricated by AAE method, have been widely used as SAs within a waveband from 1 to 3 μm due to the broadband saturable absorption property [316,324,331,336]. However, more research in the farther mid-infrared region deserve to be explored [318]. As for lasers enabled by 2D material-based heterostructures, the majority of them work in telecommunication bands, as well as using graphene and TMDs as SAs. Heterostructures based on other 2D materials, such as MXenes, are also worth investigating at higher operating wavelengths in lasers.

4. Perspectives

The unique optical properties of the newly developed 2D materials overcome the performance defects of traditional SAs and have been widely applied in various ultrafast lasers. The performance of SAs, such as the modulation depth and response time, has a crucial impact on the generation of ultrashort and high-energy pulses. Therefore, it is worth exploring SAs used in ultrafast lasers with excellent properties. In the early stage, NPR and NOLM were commonly used as artificial SAs. However, the instability of NPR makes it easy to be affected by the environment and hard to realize self-starting operations. NOLM possesses a low damage threshold that hinders the applications in ultrafast lasers with high power and a narrow wavelength range [43].

The emergence of low dimensional nanomaterials, including 2D and 3D materials, offers reliable options for SAs. 3D materials, such as Dirac semimetal Cd_3As_2, metal nanosphere, and nanoscale charcoal powder, have been investigated in the past few years [29–36]. Cd_3As_2 showed significant saturable absorption properties in the near- and mid-infrared regions [31]. Metal nanospheres have the advantages of wideband adjustability and an ultrafast response time [29]. In addition, nanoscale charcoal powder has a higher modulation depth of 26% and transmittance of 0.91 that benefits from the decrease of size [36].

2D and 3D materials both entail superiorities as SAs, such as excellent saturable absorption characteristics, ultrafast response times, and rich preparation methods. Compared with 3D SAs, 2D materials are worth investigating owing to their unique advantages. First, the controllability of the atomic layer thickness and bandgap structure of 2D materials provide a favorable condition for the adjustment of the physical and chemical properties [15]. Then, the insertion loss caused by the thin thickness of 2D materials is also lower than that of 3D materials in a laser cavity [37]. Moreover, a larger family of 2D materials can serve as SAs in the field of ultrafast photonics, which provide complementary properties among each other.

The performance of SAs can be enhanced by stacking van der Waals heterostructures made of different 2D materials [13,339]. Furthermore, the carrier migration and heat diffusion of 2D materials are confined in plane, making them possess specific optical and electrical properties, such as quantum Hall effect and ultrahigh carrier mobility [378–380]. However, the study of 2D materials started relatively late, and there are still many potential areas to be further explored. Here, the future developments of 2D materials in the field of ultrafast photonics are presented.

Exploiting high-performance SA materials: On the one hand, it is necessary to further discover new 2D materials with high performance, such as a wide operating band, high damage threshold, and fast relaxation time. On the other hand, we can adjust the structural parameters of existing 2D materials by means of surface modification, doping, and intercalation, so as to improve the properties of 2D materials and make them desirable SAs [63]. Taking graphene as an example, we can use polyethyleneimine for surface treatment to improve its wettability and optical properties, and the bandgap of graphene can be controlled by doping oxygen atoms. Furthermore, intercalating with bromine can maintain the high light transmittance and electrical conductivity of graphene [381–383].

Extending the broadband response range: Owing to the broadband absorption properties of 2D materials, they have an optical response from the visible to infrared bands. Therefore, the ultrafast laser can further extend the operating wavelength range. At

present, ultrafast fiber lasers based on 2D materials have been widely used from the 1- to 3-μm bands, while the research on the mid-IR band beyond 3.5 μm is still in the early stages [63,190]. By further optimizing the laser design and selecting the ideal gain medium and SA, a wider range of ultrafast laser pulses can be obtained.

Improving the preparation methods: Bottom-up growth and top-down exfoliation methods can be used to prepare 2D materials; however, they both have disadvantages. Cost-effective microwave and LPE technologies are difficult to ensure high crystallinity and the quality of materials, and ME—which can produce high quality products—is complex and difficult to operate. Moreover, the consistency and reproducibility of 2D material samples still struggle to meet the requirements. In order to transform laboratory-scale production into industrial large-scale production, it is necessary to strengthen preparation theory research and explore the growth mechanism.

At present, CVD is a promising method due to its large size, good uniformity, and controllable number of layers [25]. However, due to the use of a variety of precursors and the complex growth process, there are still many problems in maintaining the controllability of 2D film preparations. Thus, it makes sense to further study the key parameters affecting the growth process of CVD, which can realize the quantity production of 2D materials with high quality and productivity.

Combining advantages through heterostructure: Although the current 2D materials used for SA have unique advantages, the limitations of a single material impede their potential as excellent SAs. The low saturation intensity of graphene has a positive effect on the SA, yet the 2.3% single-layer modulation depth places restrictions on its applications [384]. TIs have an ultrafast recovery time; however, the mode-locking stability and continuity are lower than that of graphene [70]. TMDs possess a large modulation depth and high damage threshold; however, the bandgap is too wide for pulse operation in the mid-IR band [385]. The BP-based ultrafast laser can be extended to the 3.5-μm band; nevertheless, BP is very unstable and easily oxidized in the air [49].

Despite the broadband optical response and strong absorption coefficient of MX-enes, the limited preparation methods hinder their development and applications [316]. Therefore, combining the optical advantages of two or more 2D materials has become a new development direction of SA, which can effectively avoid the limitations of single material applications. At present, the commonly used method is stacking 2D materials by heterostructure, which can improve the performance of the materials based on theoptical complementary effect. In this way, one can obtain SAs with a larger modulation depth, wider absorption bandwidth, higher peak power, and better stability [345,386,387].

Exploring other ultrafast laser applications: In addition to saturable absorption, 2D materials have distinct optical and electrical anisotropy, which indicates their potential in light modulation and polarization detection. For example, in 2020, Sakakura et al. found that laser writing in quartz glass can produce geometric phase shifts [388], and thus the study of new characteristics, such as the polarization properties of 2D materials, could broaden their applications in ultrafast lasers.

5. Conclusions

In this review, we introduced the principles, preparation processes, characteristics, and applications of ME, solution-processed methods, deposition methods, MBE, and other widely used methods. Then, we made conclusions regarding the applications of commonly used 2D materials as SAs from the 1- to 3-μm wavelengths and further discussed the state of the art and challenges. Furthermore, an outlook for optimizing preparation methods and broadening the applications of 2D materials was also presented in the section on perspectives. Graphene can be prepared by multiple methods, including ME, CVD, and LPE. ME is often used in laboratory research due to its simple operation and high material integrity, while industrial large-area graphene can be prepared by LPE and CVD.

However, the ultrasonic process of LPE may lead to structural defects [389]. Thus, it is necessary to optimize the conditions of the ultrasonic process, such as the time, temperature,

and reaction space [390]. CVD can achieve high quality and fast growth of graphene under a suitable pressure, temperature, and substrate, which is one of the main research directions. For example, graphene can be rapidly prepared by a static atmospheric pressure CVD system based on molecular thermal motion and a Cu substrate [391]. High-quality TIs can be obtained by ME with low cost; however, this has the drawbacks of low yield and difficulty in controlling the thickness [66,392].

In order to obtain high-purity TIs with uniform thickness, MBE can be used despite the need for vacuum environment and long preparation time [162,393,394]. LPE and the hydrothermal method can obtain high-quality TIs with simple processes, in which the suitable doping of impurities has important impacts on the characteristics of the TIs [88,89,395,396]. Linear, banded, and flake TIs can be prepared by the CVD method, whereas the growth rate is still a problem to be solved [143,396,397]. MBE is the earliest developed method to synthesize TMDs, and is mainly used in scientific experiments due to the high cost and low speed [28,398].

Later, the exfoliation of high-purity natural or synthetic bulk crystals by ME accelerated the research of TMDs [65,67,398,399]. However, ME lacks repeatability, and the products are not homogeneous. Therefore, CVD methods for large-scale preparation of TMDs were explored [146]. Recently, LPE and ME have been the two main methods for preparing BP. LPE is simple and effective but the layers of prepared BP are uncontrollable, which hinders the subsequent research on the optical properties of BP [82]. The ME method can obtain few or even single layer BP, while the yield and quality of BP remain to be improved. As an option, viscoelastic poly-dimethylsiloxane (PDMS) can be used for exfoliation rather than utilizing tapes [312].

Furthermore, BP is unstable, and the optical properties can be affected when exposed to air; thus, exploring proper methods for better storage is worthy of study. For example, we can use polymethyl methacrylate (PMMA) for surface encapsulation to inhibit the oxidation of BP material [400]. As a kind of novel 2D material, MXenes can be prepared by the AAE method [116,122,123], in which HF was used at first. Later, in view of safety and efficiency, HCl-LiF and fluorides, such as NH_4HF, gradually became substitutes [123–126].

In addition, CVD can be used to prepare large-area MXenes without external functional groups, which are mostly used in the research of electronics and optics [138,401]. However, considering that CVD requires an ultrahigh reaction temperature, plasma-enhanced pulsed-laser deposition (PEPLD) is another adoptable method to decrease the preparation temperature and synthesize high-quality MXenes [402].

Regarding the performance of ultrafast pulses, the pulse energy and output power can reach up to the order of μJ and Watts, respectively [231,336,344]. In 2D material-based lasers, ultrashort pulses with a femtosecond width are preferred to be obtained by mode-locked operation in 1.5 μm. Most of Q-switched lasers using 2D materials as SAs generate pulses with pulse width from nanosecond to picosecond. Concretely, graphene and BP are mostly used in solid-state lasers that are commonly applied in the 1-μm region. TMDs and TIs both tend to generate Q-switched pulses with high pulse energy and output power, which are beneficial to the applications in high power lasers.

MXenes and heterostructures are desirable alternatives to generate pulses with high SNR, indicating high stability. In terms of broadband operations, graphene, BP, and MXenes have priorities due to broadband saturable absorption properties; however, the easy oxidation of BP limits its practical applications. In addition, graphene, TIs, and MXenes show innate talent for high pulse energy while there is still room for TIs to enhance the mode-locked stability. As for BP and TMDs, SAs with better properties and stability as well as convenient and low-cost fabrication methods are worth exploring in order to take advantages of their full potential in ultrafast lasers.

2D materials are popular in applications of ultrafast photonics, such as detection, luminescence, and modulation, due to the outstanding photoelectric properties. Ultrafast photonics based on 2D materials have become a highly active field of research. Since graphene was applied in ultrafast lasers, people have concentrated an enormous amount of

effort on the characteristics of 2D materials, in order to develop the excellent performance of ultrafast photonic devices. Although some difficulties and challenges inhibit the large-scale and high-quality preparation of 2D materials, the broad development prospect serves as an irresistible trend of the times. We believe that, with the in-depth study of the properties and preparation processes, ultrafast photonics based on 2D materials will gradually develop from scientific research to industrial technology applications and, thus, bring innovation to fields such as optics, electronics, and biology.

Author Contributions: B.F. conceived the project and supervised the whole work; A.Z., Z.W., H.O., and W.L. wrote the original draft; A.Z. and Z.W. drew figures; J.S. and Y.C. reviewed and edited the manuscript. All authors have read and agreed to the published version of the manuscript.

Institutional Review Board Statement: Not applicable.

Informed Consent Statement: Not applicable.

Data Availability Statement: Not applicable.

Conflicts of Interest: The authors declare no conflict of interest.

References

1. Martin, C.R. Nanomaterials: A membrane-based synthetic approach. *Science* **1994**, *266*, 1961–1966. [CrossRef]
2. Gleiter, H. Nanostructured materials: Basic concepts and microstructure. *Acta Mater.* **2000**, *48*, 1–29. [CrossRef]
3. Gajewicz, A.; Cronin, M.T.D.; Rasulev, B.; Leszczynski, J.; Puzyn, T. Novel approach for efficient predictions properties of large pool of nanomaterials based on limited set of species: Nano-read-across. *Nanotechnology* **2015**, *26*, 015701. [CrossRef]
4. Salata, O. Applications of nanoparticles in biology and medicine. *J. Nanobiotechnol.* **2004**, *2*, 3. [CrossRef] [PubMed]
5. Kumar, C.S.S.R.; Mohammad, F. Magnetic nanomaterials for hyperthermia-based therapy and controlled drug delivery. *Adv. Drug Deliv. Rev.* **2011**, *63*, 789–808. [CrossRef]
6. Langhammer, C.; Larsson, E.M.; Kasemo, B.; Zoric, I. Indirect nanoplasmonic sensing: Ultrasensitive experimental platform for nanomaterials science and optical nanocalorimetry. *Nano Lett.* **2010**, *10*, 3529–3538. [CrossRef] [PubMed]
7. Leonard, F.; Talin, A.A. Electrical contacts to one- and two-dimensional nanomaterials. *Nat. Nanotechnol.* **2011**, *6*, 773–783. [CrossRef] [PubMed]
8. Goldstein, R.V.; Morozov, N.F. Mechanics of deformation and fracture of nanomaterials and nanotechnology. *Phys. Mesomech.* **2007**, *10*, 235–246. [CrossRef]
9. Chen, W.Y.; Wang, Y.Z.; Kuo, S.W.; Huang, C.F.; Tung, P.H.; Chang, F.C. Thermal and dielectric properties and curing kinetics of nanomaterials formed from poss-epoxy and meta-phenylenediamine. *Polymer* **2004**, *45*, 6897–6908. [CrossRef]
10. Huang, X.; Tan, C.L.; Yin, Z.Y.; Zhang, H. 25th anniversary article: Hybrid nanostructures based on two-dimensional nanomaterials. *Adv. Mater.* **2014**, *26*, 2185–2204. [CrossRef]
11. You, J.; Bongu, S.; Bao, Q.; Panoiu, N. Nonlinear optical properties and applications of 2D materials: Theoretical and experimental aspects. *Nanophotonics* **2019**, *8*, 63–97. [CrossRef]
12. Yu, S.L.; Wu, X.Q.; Wang, Y.P.; Guo, X.; Tong, L.M. 2D Materials for Optical Modulation: Challenges and Opportunities. *Adv. Mater.* **2017**, *29*, 1606128. [CrossRef] [PubMed]
13. Woodward, R.I.; Kelleher, E.J.R. 2D saturable absorbers for fibre lasers. *Appl. Sci.* **2015**, *5*, 1440–1456. [CrossRef]
14. Liu, X.; Guo, Q.; Qiu, J. Emerging low-dimensional materials for nonlinear optics and ultrafast photonics. *Adv. Mater.* **2017**, *29*, 1605886. [CrossRef] [PubMed]
15. Wang, J.; Wang, X.; Lei, J.; Ma, M.; Wang, C.; Ge, Y.; Wei, Z. Recent advances in mode-locked fiber lasers based on two-dimensional materials. *Nanophotonics* **2020**, *9*, 2315–2340. [CrossRef]
16. Demaria, A.J.; Glenn, W.H.; Brienza, M.J.; Mack, M.E. Picosecond laser pulses. *Proc. IEEE* **1969**, *57*, 2–25. [CrossRef]
17. Hargrove, L.; Fork, R.L.; Pollack, M. Locking of He–Ne laser modes induced by synchronous intracavity modulation. *Appl. Phys. Lett.* **1964**, *5*, 4–5. [CrossRef]
18. Mocker, H.W.; Collins, R.J. Mode competition and self-locking effects in a Q-switching ruby laser. *Appl. Phys. Lett.* **1965**, *7*, 270–273. [CrossRef]
19. Matsas, V.; Newson, T.; Richardson, D.; Payne, D. Self-starting passively mode-locked fibre ring soliton laser exploiting nonlinear polarisation rotation. *Electron. Lett.* **1992**, *28*, 1391–1393. [CrossRef]
20. Zhang, Z.; Sang, M.; Ye, Z.; Nie, Y. Passively Q-switched erbium-doped fiber laser based on nonlinear polarization rotation. *Microw. Opt. Technol. Lett.* **2008**, *50*, 694–696. [CrossRef]

21. Doran, N.J.; Wood, D. Nonlinear-optical loop mirror. *Opt. Lett.* **1988**, *13*, 56–58. [CrossRef]

22. Barnett, B.C.; Rahman, L.; Islam, M.N.; Chen, Y.C.; Bhattacharya, P.; Riha, W.; Reddy, K.V.; Howe, A.T.; Stair, K.A.; Iwamura, H.; et al. High-power erbium-doped fiber laser mode locked by a semiconductor saturable absorber. *Opt. Lett.* **1995**, *20*, 471–473. [CrossRef] [PubMed]

23. Paschotta, R.; Häring, R.; Gini, E.; Melchior, H.; Keller, U.; Offerhaus, H.L.; Richardson, D.J. Passively Q-switched 0.1-mJ fiber laser system at 1.53 μm. *Opt. Lett.* **1999**, *24*, 388–390. [CrossRef] [PubMed]

24. Okhotnikov, O.; Grudinin, A.; Pessa, M. Ultra-fast fibre laser systems based on SESAM technology: New horizons and applications. *New J. Phys.* **2004**, *6*, 177. [CrossRef]

25. Wang, S.; Wang, W.H.; Lu, J.P.; Ni, Z.H. Chemical vapor deposition growth of large-areas two dimensional materials: Approaches and mechanisms. *Acta Phys. Sin.* **2021**, *70*, 026802. [CrossRef]

26. Fu, B.; Popa, D.; Zhao, Z.; Hussain, S.A.; Flahaut, E.; Hasan, T.; Soavi, G.; Ferrari, A.C. Wavelength tunable soliton rains in a nanotube-mode locked Tm-doped fiber laser. *Appl. Phys. Lett.* **2018**, *113*, 193102. [CrossRef]

27. Set, S.; Yaguchi, H.; Tanaka, Y.; Jablonski, M.; Sakakibara, Y.; Rozhin, A.; Tokumoto, M.; Kataura, H.; Achiba, Y.; Kikuchi, K. Mode-locked fiber lasers based on a saturable absorber incorporating carbon nanotubes. In Proceedings of the Optical Fiber Communication Conference, Optical Society of America, Atlanta, GA, USA, 28 March 2003; p. PD44. [CrossRef]

28. Yao, J.D.; Zheng, Z.Q.; Yang, G.W. Production of large-area 2D materials for high-performance photodetectors by pulsed-laser deposition. *Prog. Mater. Sci.* **2019**, *106*, 100573. [CrossRef]

29. Duan, W.; Nie, H.; Sun, X.; Zhang, B.; He, G.; Yang, Q.; Xia, H.; Wang, R.; Zhan, J.; He, J. Passively Q-switched mid-infrared laser pulse generation with gold nanospheres as a saturable absorber. *Opt. Lett.* **2018**, *43*, 1179–1182. [CrossRef]

30. Yuan, J.; Bai, X.; Fan, D.; Gu, J.; Wang, S.; Zeng, X. Passively mode-locked erbium-doped fiber laser using gold-nanosphere based on double cladding fiber as saturable absorber. In Proceedings of the 2015 11th Conference on Lasers and Electro-Optics Pacific Rim (CLEO-PR), Busan, Korea, 24–28 August 2015; Volume 2, p. 7375961. [CrossRef]

31. Meng, Y.; Zhu, C.; Li, Y.; Yuan, X.; Xiu, F.; Shi, Y.; Xu, Y.; Wang, F. Three-dimensional Dirac semimetal thin-film absorber for broadband pulse generation in the near-infrared. *Opt. Lett.* **2018**, *43*, 1503–1506. [CrossRef]

32. Sun, Y.; Meng, Y.; Jiang, H.; Qin, S.; Yang, Y.; Xiu, F.; Shi, Y.; Zhu, S.; Wang, F. Dirac semimetal saturable absorber with actively tunable modulation depth. *Opt. Lett.* **2019**, *44*, 582–585. [CrossRef]

33. Zhao, Q.Z.; Qiu, J.R.; Jiang, X.W.; Zhao, C.J.; Zhu, C.S. Controllable precipitation and dissolution of silver nanoparticles in ultrafast laser pulses irradiated Ag^+-doped phosphate glass. *Opt. Express* **2004**, *12*, 4035–4040. [CrossRef]

34. Lin, Y.H.; Chi, Y.C.; Lin, G.R. Nanoscale charcoal powder induced saturable absorption and mode-locking of a low-gain erbium-doped fiber-ring laser. *Laser Phys. Lett.* **2013**, *10*, 055105. [CrossRef]

35. Li, W.; Hu, H.; Zhang, X.; Zhao, S.; Fu, K.; Dutta, N.K. High-speed ultrashort pulse fiber ring laser using charcoal nanoparticles. *Appl. Opt.* **2016**, *55*, 2149–2154. [CrossRef]

36. Lin, Y.H.; Lo, J.Y.; Tseng, W.H.; Wu, C.I.; Lin, G.R. Self-amplitude and self-phase modulation of the charcoal mode-locked erbium-doped fiber lasers. *Opt. Express* **2013**, *21*, 25184–25196. [CrossRef]

37. Guinea, F.; Katnelson, M.I.; Wehling, T.O. Two-dimensional materials: Electronic structure and many-body effects. *Ann. Phys.* **2014**, *526*, A81–A82. [CrossRef]

38. Novoselov, K.S.; Geim, A.K.; Morozov, S.V.; Jiang, D.; Zhang, Y.; Dubonos, S.V.; Grigorieva, I.V.; Firsov, A.A. Electric field effect in atomically thin carbon films. *Science* **2004**, *306*, 666–669. [CrossRef] [PubMed]

39. Luo, Z.; Zhou, M.; Weng, J.; Huang, G.; Xu, H.; Ye, C.; Cai, Z. Graphene-based passively Q-switched dual-wavelength erbium-doped fiber laser. *Opt. Lett.* **2010**, *35*, 3709–3711. [CrossRef]

40. Hasan, T.; Sun, Z.; Wang, F.; Bonaccorso, F.; Tan, P.H.; Rozhin, A.G.; Ferrari, A.C. Nanotube polymer composites for ultrafast photonics. *Adv. Mater.* **2009**, *21*, 3874–3899. [CrossRef]

41. Bao, Q.; Zhang, H.; Wang, Y.; Ni, Z.; Yan, Y.; Shen, Z.X.; Loh, K.P.; Tang, D.Y. Atomic-layer graphene as a saturable absorber for ultrafast pulsed lasers. *Adv. Funct. Mater.* **2009**, *19*, 3077–3083. [CrossRef]

42. Wang, G.; Baker-Murray, A.A.; Blau, W.J. Saturable absorption in 2D nanomaterials and related photonic devices. *Laser Photonics Rev.* **2019**, *13*, 1800282. [CrossRef]

43. Ma, C.; Wang, C.; Gao, B.; Adams, J.; Wu, G.; Zhang, H. Recent progress in ultrafast lasers based on 2D materials as a saturable absorber. *Appl. Phys. Rev.* **2019**, *6*, 041304. [CrossRef]

44. Fu, B.; Gui, L.; Zhang, W.; Xiao, X.; Zhu, H.; Yang, C. Passive harmonic mode locking in erbium-doped fiber laser with graphene saturable absorber. *Opt. Commun.* **2013**, *286*, 304–308. [CrossRef]

45. Bernard, F.; Zhang, H.; Gorza, S.P.; Emplit, P. Towards mode-locked fiber laser using topological insulators. In Proceedings of the Advanced Photonics Congress, Optical Society of America, Colorado Springs, CO, USA, 17–21 June 2012; OSA Technical Digest (online), p. NTh1A.5. [CrossRef]

46. Pinghua, T.; Xiaoqi, Z.; Chujun, Z.; Yong, W.; Han, Z.; Deyuan, S.; Shuangchun, W.; Dingyuan, T.; Dianyuan, F. Topological insulator: Bi_2Te_3 saturable absorber for the passive Q-switching operation of an in-band pumped 1645-nm Er:YAG ceramic laser. *IEEE Photonics J.* **2013**, *5*, 1500707. [CrossRef]

47. Zhang, H.; Lu, S.B.; Zheng, J.; Du, J.; Wen, S.C.; Tang, D.Y.; Loh, K.P. Molybdenum disulfide (MoS_2) as a broadband saturable absorber for ultra-fast photonics. *Opt. Express* **2014**, *22*, 7249–7260. [CrossRef] [PubMed]

48. Woodward, R.I.; Kelleher, E.J.R.; Runcorn, T.H.; Popov, S.V.; Torrisi, F.; Howe, R.C.T.; Hasan, T. Q-switched fiber laser with MoS₂ saturable absorber. In Proceedings of the CLEO: Science and Innovations, Optical Society of America, San Jose, CA, USA, 8–13 June 2014; p. SM3H.6. [CrossRef]

49. Chen, Y.; Jiang, G.; Chen, S.; Guo, Z.; Yu, X.; Zhao, C.; Zhang, H.; Bao, Q.; Wen, S.; Tang, D.; et al. Mechanically exfoliated black phosphorus as a new saturable absorber for both Q-switching and Mode-locking laser operation. *Opt. Express* **2015**, *23*, 12823–12833. [CrossRef] [PubMed]

50. Li, D.; Jussila, H.; Karvonen, L.; Ye, G.; Lipsanen, H.; Chen, X.; Sun, Z. Polarization and thickness dependent absorption properties of black phosphorus: New saturable absorber for ultrafast pulse generation. *Sci. Rep.* **2015**, *5*, 15899. [CrossRef] [PubMed]

51. Fu, B.; Sun, J.; Wang, C.; Shang, C.; Xu, L.; Li, J.; Zhang, H. MXenes: Synthesis, optical properties, and applications in ultrafast photonics. *Small* **2021**, *17*, 2006054. [CrossRef] [PubMed]

52. Lu, L.; Liang, Z.M.; Wu, L.M.; Chen, Y.X.; Song, Y.F.; Dhanabalan, S.C.; Ponraj, J.S.; Dong, B.Q.; Xiang, Y.J.; Xing, F.; et al. Few-layer bismuthene: Sonochemical exfoliation, nonlinear optics and applications for ultrafast photonics with enhanced stability. *Laser Photonics Rev.* **2018**, *12*, 1700221. [CrossRef]

53. Pumera, M.; Sofer, Z. 2D monoelemental arsenene, antimonene, and bismuthene: Beyond black phosphorus. *Adv. Mater.* **2017**, *29*, 1605299. [CrossRef]

54. Zhang, Y.; Lu, D.; Yu, H.; Zhang, H. Low-dimensional saturable absorbers in the visible spectral region. *Adv. Opt. Mater.* **2019**, *7*, 1800886. [CrossRef]

55. Fu, B.; Hua, Y.; Xiao, X.; Zhu, H.; Sun, Z.; Yang, C. Broadband graphene saturable absorber for pulsed fiber lasers at 1, 1.5, and 2 μm. *IEEE J. Sel. Top. Quantum Electron.* **2014**, *20*, 411–415. [CrossRef]

56. Yi, J.; Du, L.; Li, J.; Yang, L.; Hu, L.; Huang, S.; Dong, Y.; Miao, L.; Wen, S.; Mochalin, V.N.; et al. Unleashing the potential of Ti₂CTₓ MXene as a pulse modulator for mid-infrared fiber lasers. *2D Mater.* **2019**, *6*, 045038. [CrossRef]

57. Loiko, P.; Bora, T.; Serres, J.M.; Mateos, X.; Yu, H.H.; Baranov, A.; Aguilo, M.; Diaz, F.; Griebner, U.; Petrov, V.; et al. Oriented ZnO nanorods: A novel saturable absorber for lasers at 1–2 μm. In Proceedings of the European Conference on Lasers and Electro-Optics, Optical Society of America, Munich, Germany, 25–29 June 2017; p. CE_7_4. [CrossRef]

58. Baranov, A.I.; Myasnikov, D.V.; Protasenya, D.V.; Demkin, A.S.; Gapontsev, V.P. High power ultrashort fiber laser system at 1.55 um. In Proceedings of the 2016 International Conference Laser Optics, Institute of Electrical and Electronics Engineers Inc., St. Petersburg, Russia, 27 June–1 July 2016; p. 7549939. [CrossRef]

59. Cho, W.B.; Schmidt, A.; Yim, J.H.; Choi, S.Y.; Lee, S.; Rotermund, F.; Griebner, U.; Steinmeyer, G.; Petrov, V.; Mateos, X.; et al. Passive mode-locking of a Tm-doped bulk laser near 2 μm using a carbon nanotube saturable absorber. *Opt. Express* **2009**, *17*, 11007–11012. [CrossRef] [PubMed]

60. Rotermund, F.; Petrov, V.; Noack, F.; Wittmann, M.; Korn, G. Laser-diode-seeded operation of a femtosecond optical parametric amplifier with MgO: LiNbO₃ and generation of 5-cycle pulses near 3 μm. *J. Opt. Soc. Am. B* **1999**, *16*, 1539–1545. [CrossRef]

61. Hernandez, Y.; Nicolosi, V.; Lotya, M.; Blighe, F.M.; Sun, Z.Y.; De, S.; McGovern, I.T.; Holland, B.; Byrne, M.; Gun'ko, Y.K.; et al. High-yield production of graphene by liquid-phase exfoliation of graphite. *Nat. Nanotechnol.* **2008**, *3*, 563–568. [CrossRef] [PubMed]

62. Serna, M.I.; Yoo, S.H.; Moreno, S.; Xi, Y.; Oviedo, J.P.; Choi, H.; Alshareef, H.N.; Kim, M.J.; Minary-Jolandan, M.; Quevedo-Lopez, M.A. Large-area deposition of MoS₂ by pulsed laser deposition with in situ thickness control. *ACS Nano* **2016**, *10*, 6054–6061. [CrossRef] [PubMed]

63. He, J.; Tao, L.; Zhang, H.; Zhou, B.; Li, J. Emerging 2D materials beyond graphene for ultrashort pulse generation in fiber lasers. *Nanoscale* **2019**, *11*, 2577–2593. [CrossRef]

64. Liu, H.; Neal, A.T.; Zhu, Z.; Luo, Z.; Xu, X.F.; Tomanek, D.; Ye, P.D. Phosphorene: An unexplored 2D semiconductor with a high hole mobility. *ACS Nano* **2014**, *8*, 4033–4041. [CrossRef]

65. Yin, Z.Y.; Li, H.; Li, H.; Jiang, L.; Shi, Y.M.; Sun, Y.H.; Lu, G.; Zhang, Q.; Chen, X.D.; Zhang, H. Single-Layer MoS₂ Phototransistors. *ACS Nano* **2012**, *6*, 74–80. [CrossRef]

66. Teweldebrhan, D.; Goyal, V.; Balandin, A.A. Exfoliation and characterization of bismuth telluride atomic quintuples and quasi-two-dimensional crystals. *Nano Lett.* **2010**, *10*, 1209–1218. [CrossRef]

67. Li, H.; Lu, G.; Wang, Y.L.; Yin, Z.Y.; Cong, C.X.; He, Q.Y.; Wang, L.; Ding, F.; Yu, T.; Zhang, H. Mechanical exfoliation and characterization of single- and few-layer nanosheets of WSe₂, TaS₂, and TaSe₂. *Small* **2013**, *9*, 1974–1981. [CrossRef]

68. Shahil, K.M.F.; Hossain, M.Z.; Goyal, V.; Balandin, A.A. Micro-Raman spectroscopy of mechanically exfoliated few-quintuple layers of Bi₂Te₃, Bi₂Se₃, and Sb₂Te₃ materials. *J. Appl. Phys.* **2012**, *111*, 054305. [CrossRef]

69. Gkountaras, A.; Kim, Y.; Coraux, J.; Bouchiat, V.; Lisi, S.; Barsoum, M.W.; Ouisse, T. Mechanical exfoliation of select MAX phases and Mo₄Ce₄Al₇C₃ single crystals to produce MAXenes. *Small* **2020**, *16*, 1905784. [CrossRef] [PubMed]

70. Fu, B.; Sun, J.; Wang, G.; Shang, C.; Ma, Y.; Ma, J.; Xu, L.; Scardaci, V. Solution-processed two-dimensional materials for ultrafast fiber lasers (invited). *Nanophotonics* **2020**, *9*, 2169–2189. [CrossRef]

71. Joensen, P.; Frindt, R.; Morrison, S.R. Single-layer MoS₂. *Mater. Res. Bull.* **1986**, *21*, 457–461. [CrossRef]

72. Yang, D.; Frindt, R.F. Li-intercalation and exfoliation of WS₂. *J. Phys. Chem. Solids* **1996**, *57*, 1113–1116. [CrossRef]

73. Eda, G.; Yamaguchi, H.; Voiry, D.; Fujita, T.; Chen, M.W.; Chhowalla, M. Photoluminescence from Chemically Exfoliated MoS₂. *Nano Lett.* **2011**, *11*, 5111–5116. [CrossRef] [PubMed]

74.   Ren, L.; Qi, X.; Liu, Y.D.; Hao, G.L.; Huang, Z.Y.; Zou, X.H.; Yang, L.W.; Li, J.; Zhong, J.X. Large-scale production of ultrathin topological insulator bismuth telluride nanosheets by a hydrothermal intercalation and exfoliation route. *J. Mater. Chem.* **2012**, *22*, 4921–4926. [CrossRef]

75.   Meng, Y.C.; Semaan, G.; Salhi, M.; Niang, A.; Guesmi, K.; Luo, Z.C.; Sanchez, F. High power L-band mode-locked fiber laser based on topological insulator saturable absorber. *Opt. Express* **2015**, *23*, 23053–23058. [CrossRef]

76.   Gao, L.; Huang, W.; Zhang, J.D.; Zhu, T.; Zhang, H.; Zhao, C.J.; Zhang, W.; Zhang, H. Q-switched mode-locked erbium-doped fiber laser based on topological insulator Bi_2Se_3 deposited fiber taper. *Appl. Opt.* **2014**, *53*, 5117–5122. [CrossRef]

77.   Lin, Y.H.; Yang, C.Y.; Liou, J.H.; Yu, C.P.; Lin, G.R. Using graphene nano-particle embedded in photonic crystal fiber for evanescent wave mode-locking of fiber laser. *Opt. Express* **2013**, *21*, 16763–16776. [CrossRef]

78.   Wang, T.; Zhang, W.C.; Shi, X.Y.; Wang, J.; Ding, X.G.; Zhang, K.; Peng, J.S.; Wu, J.; Zhou, P. Black phosphorus-enabled harmonic mode locking of dark pulses in a Yb-doped fiber laser. *Laser Phys. Lett.* **2019**, *16*, 85102. [CrossRef]

79.   Song, H.Q.; Wang, Q.; Zhang, Y.F.; Li, L. Mode-locked ytterbium-doped all-fiber lasers based on few-layer black phosphorus saturable absorbers. *Opt. Commun.* **2017**, *394*, 157–160. [CrossRef]

80.   Li, J.F.; Luo, H.Y.; Zhai, B.; Lu, R.G.; Guo, Z.N.; Zhang, H.; Liu, Y. Black phosphorus: A two-dimension saturable absorption material for mid-infrared Q-switched and mode-locked fiber lasers. *Sci. Rep.* **2016**, *6*, 30361. [CrossRef]

81.   Qin, Z.; Xie, G.; Zhang, H.; Zhao, C.; Yuan, P.; Wen, S.; Qian, L. Black phosphorus as saturable absorber for the Q-switched Er:ZBLAN fiber laser at 2.8 µm. *Opt. Express* **2015**, *23*, 24713–24718. [CrossRef] [PubMed]

82.   Lu, S.B.; Miao, L.L.; Guo, Z.N.; Qi, X.; Zhao, C.J.; Zhang, H.; Wen, S.C.; Tang, D.Y.; Fan, D.Y. Broadband nonlinear optical response in multi-layer black phosphorus: An emerging infrared and mid-infrared optical material. *Opt. Express* **2015**, *23*, 11183–11194. [CrossRef]

83.   Coleman, J.N.; Lotya, M.; O'Neill, A.; Bergin, S.D.; King, P.J.; Khan, U.; Young, K.; Gaucher, A.; De, S.; Smith, R.J.; et al. Two-dimensional nanosheets produced by liquid exfoliation of layered materials. *Science* **2011**, *331*, 568–571. [CrossRef] [PubMed]

84.   Smith, R.J.; King, P.J.; Lotya, M.; Wirtz, C.; Khan, U.; De, S.; O'Neill, A.; Duesberg, G.S.; Grunlan, J.C.; Moriarty, G.; et al. Large-scale exfoliation of inorganic layered compounds in aqueous surfactant solutions. *Adv. Mater.* **2011**, *23*, 3944–3948. [CrossRef]

85.   Liu, H.; Zheng, X.W.; Liu, M.; Zhao, N.; Luo, A.P.; Luo, Z.C.; Xu, W.C.; Zhang, H.; Zhao, C.J.; Wen, S.C. Femtosecond pulse generation from a topological insulator mode-locked fiber laser. *Opt. Express* **2014**, *22*, 6868–6873. [CrossRef] [PubMed]

86.   Chen, Y.; Zhao, C.; Huang, H.; Chen, S.; Tang, P.; Wang, Z.; Lu, S.; Zhang, H.; Wen, S.; Tang, D. Self-assembled topological insulator: Bi_2Se_3 membrane as a passive Q-switcher in an erbium-doped fiber laser. *J. Light. Technol.* **2013**, *31*, 2857–2863. [CrossRef]

87.   Zhao, C.; Zou, Y.; Chen, Y.; Wang, Z.; Lu, S.; Zhang, H.; Wen, S.; Tang, D. Wavelength-tunable picosecond soliton fiber laser with Topological Insulator: Bi_2Se_3 as a mode locker. *Opt. Express* **2012**, *20*, 27888–27895. [CrossRef] [PubMed]

88.   Dou, Z.Y.; Song, Y.R.; Tian, J.R.; Liu, J.H.; Yu, Z.H.; Fang, X.H. Mode-locked ytterbium-doped fiber laser based on topological insulator: Bi_2Se_3. *Opt. Express* **2014**, *22*, 24055–24061. [CrossRef] [PubMed]

89.   Sun, L.P.; Lin, Z.Q.; Peng, J.; Weng, J.; Huang, Y.Z.; Luo, Z.Q. Preparation of few-layer bismuth selenide by liquid-phase-exfoliation and its optical absorption properties. *Sci. Rep.* **2014**, *4*, 4794. [CrossRef]

90.   Bonaccorso, F.; Bartolotta, A.; Coleman, J.N.; Backes, C. 2D-crystal-based functional inks. *Adv. Mater.* **2016**, *28*, 6136–6166. [CrossRef] [PubMed]

91.   Coleman, J.N. Liquid exfoliation of defect-free graphene. *Acc. Chem. Res.* **2013**, *46*, 14–22. [CrossRef]

92.   Green, A.A.; Hersam, M.C. Solution phase production of graphene with controlled thickness via density differentiation. *Nano Lett.* **2009**, *9*, 4031–4036. [CrossRef]

93.   Kang, J.; Wood, J.D.; Wells, S.A.; Lee, J.H.; Liu, X.L.; Chen, K.S.; Hersam, M.C. Solvent exfoliation of electronic-grade, two-dimensional black phosphorus. *ACS Nano* **2015**, *9*, 3596–3604. [CrossRef] [PubMed]

94.   Nicolosi, V.; Chhowalla, M.; Kanatzidis, M.G.; Strano, M.S.; Coleman, J.N. Liquid exfoliation of layered materials. *Science* **2013**, *340*, 1226419. [CrossRef]

95.   Backes, C.; Smith, R.J.; McEvoy, N.; Berner, N.C.; McCloskey, D.; Nerl, H.C.; O'Neill, A.; King, P.J.; Higgins, T.; Hanlon, D.; et al. Edge and confinement effects allow in situ measurement of size and thickness of liquid-exfoliated nanosheets. *Nat. Commun.* **2014**, *5*, 4576. [CrossRef] [PubMed]

96.   Hassoun, J.; Bonaccorso, F.; Agostini, M.; Angelucci, M.; Betti, M.G.; Cingolani, R.; Gemmi, M.; Mariani, C.; Panero, S.; Pellegrini, V.; et al. An advanced lithium-ion battery based on a graphene anode and a lithium iron phosphate cathode. *Nano Lett.* **2014**, *14*, 4901–4906. [CrossRef] [PubMed]

97.   Knieke, C.; Berger, A.; Voigt, M.; Taylor, R.N.K.; Rohrl, J.; Peukert, W. Scalable production of graphene sheets by mechanical delamination. *Carbon* **2010**, *48*, 3196–3204. [CrossRef]

98.   Yao, Y.G.; Lin, Z.Y.; Li, Z.; Song, X.J.; Moon, K.S.; Wong, C.P. Large-scale production of two-dimensional nanosheets. *J. Mater. Chem.* **2012**, *22*, 13494–13499. [CrossRef]

99.   Ibrahem, M.A.; Lan, T.W.; Huang, J.K.; Chen, Y.Y.; Wei, K.H.; Li, L.J.; Chu, C.W. High quantity and quality few-layers transition metal disulfide nanosheets from wet-milling exfoliation. *RSC Adv.* **2013**, *3*, 13193–13202. [CrossRef]

100. Paton, K.R.; Varrla, E.; Backes, C.; Smith, R.J.; Khan, U.; O'Neill, A.; Boland, C.; Lotya, M.; Istrate, O.M.; King, P.; et al. Scalable production of large quantities of defect-free few-layer graphene by shear exfoliation in liquids. *Nat. Mater.* **2014**, *13*, 624–630. [CrossRef]

101. Cheng, P.W.; Tang, C.Y.; Wang, X.Y.; Ma, S.N.; Long, H.; Tsang, Y.E.H. Passively Q-switched ytterbium-doped fiber laser based on broadband multilayer platinum ditelluride (PtTe$_2$) saturable absorber. *Sci. Rep.* **2019**, *9*, 10106. [CrossRef]

102. Zhou, K.G.; Mao, N.N.; Wang, H.X.; Peng, Y.; Zhang, H.L. A mixed-solvent strategy for efficient exfoliation of inorganic graphene analogues. *Angew. Chem. Int. Ed.* **2011**, *50*, 10839–10842. [CrossRef]

103. Halim, U.; Zheng, C.R.; Chen, Y.; Lin, Z.Y.; Jiang, S.; Cheng, R.; Huang, Y.; Duan, X.F. A rational design of cosolvent exfoliation of layered materials by directly probing liquid-solid interaction. *Nat. Commun.* **2013**, *4*, 2213. [CrossRef] [PubMed]

104. Lotya, M.; Hernandez, Y.; King, P.J.; Smith, R.J.; Nicolosi, V.; Karlsson, L.S.; Blighe, F.M.; De, S.; Wang, Z.M.; McGovern, I.T.; et al. Liquid phase production of graphene by exfoliation of graphite in surfactant/water solutions. *J. Am. Chem. Soc.* **2009**, *131*, 3611–3620. [CrossRef] [PubMed]

105. Niu, L.Y.; Coleman, J.N.; Zhang, H.; Shin, H.; Chhowalla, M.; Zheng, Z.J. Production of two-dimensional nanomaterials via liquid-based direct exfoliation. *Small* **2016**, *12*, 272–293. [CrossRef] [PubMed]

106. Varrla, E.; Paton, K.R.; Backes, C.; Harvey, A.; Smith, R.J.; McCauley, J.; Coleman, J.N. Turbulence-assisted shear exfoliation of graphene using household detergent and a kitchen blender. *Nanoscale* **2014**, *6*, 11810–11819. [CrossRef]

107. Ciesielski, A.; Samori, P. Graphene via sonication assisted liquid-phase exfoliation. *Chem. Soc. Rev.* **2014**, *43*, 381–398. [CrossRef]

108. Zhu, J.; Kang, J.; Kang, J.M.; Jariwala, D.; Wood, J.D.; Seo, J.W.T.; Chen, K.S.; Marks, T.J.; Hersam, M.C. Solution-processed dielectrics based on thickness-sorted two-dimensional hexagonal boron nitride nanosheets. *Nano Lett.* **2015**, *15*, 7029–7036. [CrossRef] [PubMed]

109. Kang, J.; Seo, J.W.T.; Alducin, D.; Ponce, A.; Yacaman, M.J.; Hersam, M.C. Thickness sorting of two-dimensional transition metal dichalcogenides via copolymer-assisted density gradient ultracentrifugation. *Nat. Commun.* **2014**, *5*, 5478. [CrossRef]

110. May, P.; Khan, U.; Hughes, J.M.; Coleman, J.N. Role of solubility parameters in understanding the steric stabilization of exfoliated two-dimensional nanosheets by adsorbed polymers. *J. Phys. Chem. C* **2012**, *116*, 24390–24391. [CrossRef]

111. Vega-Mayoral, V.; Backes, C.; Hanlon, D.; Khan, U.; Gholamvand, Z.; O'Brien, M.; Duesberg, G.S.; Gadermaier, C.; Coleman, J.N. Photoluminescence from Liquid-Exfoliated WS$_2$ Monomers in Poly(Vinyl Alcohol) Polymer Composites. *Adv. Funct. Mater.* **2016**, *26*, 1028–1039. [CrossRef]

112. Svedberg, T.; Pedersen, K.O. *The Ultracentrifuge*; Oxford University Press: Oxford, UK, 1940.

113. O'Neill, A.; Khan, U.; Coleman, J.N. Preparation of high concentration dispersions of exfoliated MoS$_2$ with increased flake size. *Chem. Mater.* **2012**, *24*, 2414–2421. [CrossRef]

114. Williams, J.; Van Holde, K.E.; Baldwin, R.L.; Fujita, H. The theory of sedimentation analysis. *Chem. Rev.* **1958**, *58*, 715–744. [CrossRef]

115. Ifft, J.B.; Vinograd, J. The buoyant behavior of bovine serum mercaptalbumin in salt solutions at equilibrium in the ultracentrifuge. II. net hydration, ion binding, and solvated molecular weight in various salt solutions. *J. Phys. Chem.* **1966**, *70*, 2814–2822. [CrossRef]

116. Naguib, M.; Kurtoglu, M.; Presser, V.; Lu, J.; Niu, J.J.; Heon, M.; Hultman, L.; Gogotsi, Y.; Barsoum, M.W. Two-dimensional nanocrystals produced by exfoliation of Ti$_3$AlC$_2$. *Adv. Mater.* **2011**, *23*, 4248–4253. [CrossRef]

117. Naguib, M.; Mashtalir, O.; Carle, J.; Presser, V.; Lu, J.; Hultman, L.; Gogotsi, Y.; Barsoum, M.W. Two-dimensional transition metal carbides. *ACS Nano* **2012**, *6*, 1322–1331. [CrossRef]

118. Peng, C.; Wei, P.; Chen, X.; Zhang, Y.L.; Zhu, F.; Cao, Y.H.; Wang, H.J.; Yu, H.; Peng, F. A hydrothermal etching route to synthesis of 2D MXene (Ti$_3$C$_2$, Nb$_2$C): Enhanced exfoliation and improved adsorption performance. *Ceram. Int.* **2018**, *44*, 18886–18893. [CrossRef]

119. Naguib, M.; Halim, J.; Lu, J.; Cook, K.M.; Hultman, L.; Gogotsi, Y.; Barsoum, M.W. New two-dimensional niobium and vanadium carbides as promising materials for li-ion batteries. *J. Am. Chem. Soc.* **2013**, *135*, 15966–15969. [CrossRef] [PubMed]

120. Chang, F.Y.; Li, C.S.; Yang, J.; Tang, H.; Xue, M.Q. Synthesis of a new graphene-like transition metal carbide by de-intercalating Ti$_3$AlC$_2$. *Mater. Lett.* **2013**, *109*, 295–298. [CrossRef]

121. Anasori, B.; Shi, C.Y.; Moon, E.J.; Xie, Y.; Voigt, C.A.; Kent, P.R.C.; May, S.J.; Billinge, S.J.L.; Barsoum, M.W.; Gogotsi, Y. Control of electronic properties of 2D carbides (MXenes) by manipulating their transition metal layers. *Nanoscale Horiz.* **2016**, *1*, 227–234. [CrossRef] [PubMed]

122. Halim, J.; Lukatskaya, M.R.; Cook, K.M.; Lu, J.; Smith, C.R.; Naslund, L.A.; May, S.J.; Hultman, L.; Gogotsi, Y.; Eklund, P.; Barsoum, M.W. Transparent conductive two-dimensional titanium carbide epitaxial thin films. *Chem. Mater.* **2014**, *26*, 2374–2381. [CrossRef] [PubMed]

123. Ghidiu, M.; Lukatskaya, M.R.; Zhao, M.Q.; Gogotsi, Y.; Barsoum, M.W. Conductive two-dimensional titanium carbide 'clay' with high volumetric capacitance. *Nature* **2014**, *516*, 78–81. [CrossRef]

124. Ying, G.B.; Dillon, A.D.; Fafarman, A.T.; Barsoum, M.W. Transparent, conductive solution processed spincast 2D Ti$_2$CT$_x$ (MXene) films. *Mater. Res. Lett.* **2017**, *5*, 391–398. [CrossRef]

125. Liu, F.F.; Zhou, A.G.; Chen, J.F.; Jin, J.; Zhou, W.J.; Wang, L.B.; Hu, Q.K. Preparation of Ti$_3$C$_2$ and Ti$_2$C MXenes by fluoride salts etching and methane adsorptive properties. *Appl. Surf. Sci.* **2017**, *416*, 781–789. [CrossRef]

126. Du, F.; Tang, H.; Pan, L.M.; Zhang, T.; Lu, H.M.; Xiong, J.; Yang, J.; Zhang, C. Environmental friendly scalable production of colloidal 2D titanium carbonitride MXene with minimized nanosheets restacking for excellent cycle life lithium-ion batteries. *Electrochim. Acta* **2017**, *235*, 690–699. [CrossRef]

127. Castellanos-Gomez, A.; Barkelid, M.; Goossens, A.M.; Calado, V.E.; van der Zant, H.S.J.; Steele, G.A. Laser-thinning of MoS$_2$: On demand generation of a single-layer semiconductor. *Nano Lett.* **2012**, *12*, 3187–3192. [CrossRef]

128. Gu, E.Y.; Wang, Q.Y.; Zhang, Y.W.; Cong, C.X.; Hu, L.G.; Tian, P.F.; Liu, R.; Zhang, S.L.; Qiu, Z.J. A real-time raman spectroscopy study of the dynamics of laser-thinning of MoS$_2$ flakes to monolayers. *AIP Adv.* **2017**, *7*, 125329. [CrossRef]

129. Hu, L.L.; Shan, X.Y.; Wu, Y.L.; Zhao, J.M.; Lu, X.H. Laser thinning and patterning of MoS$_2$ with layer-by-layer precision. *Sci. Rep.* **2017**, *7*, 15538. [CrossRef] [PubMed]

130. Bala, L.; Lacinska, E.M.; Nogajewski, K.; Molas, M.R.; Wysmolek, A.; Potemski, M. Strong photoluminescence fluctuations in laser-thinned few-layer WS$_2$. *Acta Phys. Pol. A* **2016**, *130*, 1176–1178. [CrossRef]

131. Han, G.H.; Chae, S.J.; Kim, E.S.; Gunes, F.; Lee, I.H.; Lee, S.W.; Lee, S.Y.; Lim, S.C.; Jeong, H.K.; Jeong, M.S.; et al. Laser thinning for monolayer graphene formation: Heat sink and interference effect. *ACS Nano* **2011**, *5*, 263–268. [CrossRef] [PubMed]

132. Li, D.W.; Zhou, Y.S.; Huang, X.; Jiang, L.; Silvain, J.F.; Lu, Y.F. In situ imaging and control of layer-by-layer femtosecond laser thinning of graphene. *Nanoscale* **2015**, *7*, 3651–3659. [CrossRef]

133. Lin, Z.; Ye, X.H.; Han, J.P.; Chen, Q.; Fan, P.X.; Zhang, H.J.; Xie, D.; Zhu, H.W.; Zhong, M.L. Precise control of the number of layers of graphene by picosecond laser thinning. *Sci. Rep.* **2015**, *5*, 11662. [CrossRef] [PubMed]

134. Li, X.S.; Cai, W.W.; An, J.H.; Kim, S.; Nah, J.; Yang, D.X.; Piner, R.; Velamakanni, A.; Jung, I.; Tutuc, E.; Banerjee, S.K.; Colombo, L.; Ruoff, R.S. Large-area synthesis of high-quality and uniform graphene films on copper foils. *Science* **2009**, *324*, 1312–1314. [CrossRef] [PubMed]

135. Khazaeinezhad, R.; Kassani, S.H.; Jeong, H.; Yeom, D.I.; Oh, K. Femtosecond soliton pulse generation using evanescent field interaction through Tungsten disulfide (WS$_2$) film. *J. Light. Technol.* **2015**, *33*, 3550–3557. [CrossRef]

136. Yu, Q.K.; Lian, J.; Siriponglert, S.; Li, H.; Chen, Y.P.; Pei, S.S. Graphene segregated on Ni surfaces and transferred to insulators. *Appl. Phys. Lett.* **2008**, *93*, 113103. [CrossRef]

137. Chang, Y.H.; Zhang, W.; Zhu, Y.; Han, Y.; Pu, J.; Chang, J.K.; Hsu, W.T.; Huang, J.K.; Hsu, C.L.; Chiu, M.H.; et al. Monolayer MoSe$_2$ grown by chemical vapor deposition for fast photodetection. *ACS Nano* **2014**, *8*, 8582–8590. [CrossRef]

138. Xu, C.; Wang, L.B.; Liu, Z.B.; Chen, L.; Guo, J.K.; Kang, N.; Ma, X.L.; Cheng, H.M.; Ren, W.C. Large-area high-quality 2D ultrathin Mo$_2$C superconducting crystals. *Nat. Mater.* **2015**, *14*, 1135–1141. [CrossRef] [PubMed]

139. Liu, W.J.; Liu, M.L.; Yin, J.D.; Chen, H.; Lu, W.; Fang, S.B.; Teng, H.; Lei, M.; Yan, P.G.; Wei, Z.Y. Tungsten diselenide for all-fiber lasers with the chemical vapor deposition method. *Nanoscale* **2018**, *10*, 7971–7977. [CrossRef] [PubMed]

140. Sutter, P.; Lahiri, J.; Zahl, P.; Wang, B.; Sutter, E. Scalable synthesis of uniform few-layer hexagonal boron nitride dielectric films. *Nano Lett.* **2013**, *13*, 276–281. [CrossRef] [PubMed]

141. Ullah, F.; Nguyen, T.K.; Le, C.T.; Kim, Y.S. Pulsed laser deposition assisted grown continuous monolayer MoSe$_2$. *Crystengcomm* **2016**, *18*, 6992–6996. [CrossRef]

142. Shi, Y.M.; Hamsen, C.; Jia, X.T.; Kim, K.K.; Reina, A.; Hofmann, M.; Hsu, A.L.; Zhang, K.; Li, H.N.; Juang, Z.Y.; et al. Synthesis of few-layer hexagonal boron nitride thin film by chemical vapor deposition. *Nano Lett.* **2010**, *10*, 4134–4139. [CrossRef] [PubMed]

143. Zhang, C.; Liu, M.; Man, B.Y.; Jiang, S.Z.; Yang, C.; Chen, C.S.; Feng, D.J.; Bi, D.; Liu, F.Y.; Qiu, H.W.; et al. Facile fabrication of graphene-topological insulator Bi$_2$Se$_3$ hybrid Dirac materials via chemical vapor deposition in Se-rich conditions. *Crystengcomm* **2014**, *16*, 8941–8945. [CrossRef]

144. Gu, Y.; Cai, H.; Dong, J.; Yu, Y.; Hoffman, A.N.; Liu, C.; Oyedele, A.D.; Lin, Y.C.; Ge, Z.; Puretzky, A.A.; et al. Two-dimensional palladium diselenide with strong in-plane optical anisotropy and high mobility grown by chemical vapor deposition. *Adv. Mater.* **2020**, *32*, e1906238. [CrossRef]

145. Cai, Z.Y.; Liu, B.L.; Zou, X.L.; Cheng, H.M. Chemical vapor deposition growth and applications of two-dimensional materials and their heterostructures. *Chem. Rev.* **2018**, *118*, 6091–6133. [CrossRef]

146. Tang, L.; Li, T.; Luo, Y.; Feng, S.; Cai, Z.; Zhang, H.; Liu, B.; Cheng, H.M. Vertical chemical vapor deposition growth of highly uniform 2D transition metal dichalcogenides. *ACS Nano* **2020**, *14*, 4646–4653. [CrossRef]

147. Chen, H.; Yin, J.D.; Yang, J.W.; Zhang, X.J.; Liu, M.L.; Jiang, Z.K.; Wang, J.Z.; Sun, Z.P.; Guo, T.; Liu, W.J.; et al. Transition-metal dichalcogenides heterostructure saturable absorbers for ultrafast photonics. *Opt. Lett.* **2017**, *42*, 4279–4282. [CrossRef]

148. Mao, D.; She, X.Y.; Du, B.B.; Yang, D.X.; Zhang, W.D.; Song, K.; Cui, X.Q.; Jiang, B.Q.; Peng, T.; Zhao, J.L. Erbium-doped fiber laser passively mode locked with few-layer WSe$_2$/MoSe$_2$ nanosheets. *Sci. Rep.* **2016**, *6*, 23583. [CrossRef]

149. Khazaeinezhad, R.; Kassani, S.H.; Jeong, H.; Nazari, T.; Yeom, D.I.; Oh, K. Mode-locked all-fiber lasers at both anomalous and normal dispersion regimes based on spin-coated MoS$_2$ nano-sheets on a side-polished fiber. *IEEE Photonics J.* **2015**, *7*, 1–9. [CrossRef]

150. Li, S.S.; Yan, Y.; Zhang, Y.; Ou, Y.F.; Ji, Y.X.; Liu, L.; Yan, C.P.; Zhao, Y.; Yu, Z. Monophase gamma-In$_2$Se$_3$ thin film deposited by magnetron radio-frequency sputtering. *Vacuum* **2014**, *99*, 228–232. [CrossRef]

151. Ling, Z.P.; Yang, R.; Chai, J.W.; Wang, S.J.; Leong, W.S.; Tong, Y.; Lei, D.; Zhou, Q.; Gong, X.; Chi, D.Z.; et al. Large-scale two-dimensional MoS$_2$ photodetectors by magnetron sputtering. *Opt. Express* **2015**, *23*, 13580–13586. [CrossRef]

152. Tao, J.G.; Chai, J.W.; Lu, X.; Wong, L.M.; Wong, T.I.; Pan, J.S.; Xiong, Q.H.; Chi, D.Z.; Wang, S.J. Growth of wafer-scale MoS$_2$ monolayer by magnetron sputtering. *Nanoscale* **2015**, *7*, 2497–2503. [CrossRef]

153. Zhang, M.; Wei, Z.T.; Jin, R.; Ji, Y.X.; Yan, Y.; Pu, X.Y.; Yang, X.S.; Zhao, Y. Electrical transport properties and morphology of topological insulator Bi$_2$Se$_3$ thin films with different thickness prepared by magnetron sputtering. *Thin Solid Film.* **2016**, *603*, 289–293. [CrossRef]

154. Dijkkamp, D.; Venkatesan, T.; Wu, X.; Shaheen, S.; Jisrawi, N.; Min-Lee, Y.; McLean, W.; Croft, M. Preparation of Y-Ba-Cu oxide superconductor thin films using pulsed laser evaporation from high T c bulk material. *Appl. Phys. Lett.* **1987**, *51*, 619–621. [CrossRef]

155. Lowndes, D.H.; Geohegan, D.; Puretzky, A.; Norton, D.; Rouleau, C. Synthesis of novel thin-film materials by pulsed laser deposition. *Science* **1996**, *273*, 898–903. [CrossRef] [PubMed]

156. Wang, K.; Tai, G.; Wong, K.H.; Lau, S.P.; Guo, W. Ni induced few-layer graphene growth at low temperature by pulsed laser deposition. *AIP Adv.* **2011**, *1*, 183. [CrossRef]

157. Onose, Y.; Yoshimi, R.; Tsukazaki, A.; Yuan, H.T.; Hidaka, T.; Iwasa, Y.; Kawasaki, M.; Tokura, Y. Pulsed laser deposition and ionic liquid gate control of epitaxial Bi$_2$Se$_3$ thin films. *Appl. Phys. Express* **2011**, *4*, 083001. [CrossRef]

158. Lee, Y.F.; Punugupati, S.; Wu, F.; Jin, Z.; Narayan, J.; Schwartz, J. Evidence for topological surface states in epitaxial Bi$_2$Se$_3$ thin film grown by pulsed laser deposition through magneto-transport measurements. *Curr. Opin. Solid State Mater. Sci.* **2014**, *18*, 279–285. [CrossRef]

159. Yang, Z.B.; Hao, J.H.; Yuan, S.G.; Lin, S.H.; Yau, H.M.; Dai, J.Y.; Lau, S.P. Field-effect transistors based on amorphous black phosphorus ultrathin films by pulsed laser deposition. *Adv. Mater.* **2015**, *27*, 3748–3754. [CrossRef]

160. Chen, M.W.; Ovchinnikov, D.; Lazar, S.; Pizzochero, M.; Whitwick, M.B.; Surrente, A.; Baranowski, M.; Sanchez, O.L.; Gillet, P.; Plochocka, P.; et al. Highly oriented atomically thin ambipolar MoSe$_2$ grown by molecular beam epitaxy. *ACS Nano* **2017**, *11*, 6355–6361. [CrossRef]

161. Mishra, P.; Tangi, M.; Ng, T.K.; Hedhili, M.N.; Anjum, D.H.; Alias, M.S.; Tseng, C.C.; Li, L.J.; Ooi, B.S. Impact of N-plasma and Ga-irradiation on MoS$_2$ layer in molecular beam epitaxy. *Appl. Phys. Lett.* **2017**, *110*, 012101. [CrossRef]

162. Zhang, X.P.; Zeng, Z.G.; Shen, C.; Zhang, Z.Q.; Wang, Z.C.; Lin, C.; Hu, Z.Y. Investigation on the electrical transport properties of highly (001)-textured Sb$_2$Te$_3$ films deposited by molecular beam epitaxy. *J. Appl. Phys.* **2014**, *115*, 554. [CrossRef]

163. Zhu, F.F.; Chen, W.J.; Xu, Y.; Gao, C.L.; Guan, D.D.; Liu, C.H.; Qian, D.; Zhang, S.C.; Jia, J.F. Epitaxial growth of two-dimensional stanene. *Nat. Mater.* **2015**, *14*, 1020–1025. [CrossRef]

164. Yang, W.; Chen, G.R.; Shi, Z.W.; Liu, C.C.; Zhang, L.C.; Xie, G.B.; Cheng, M.; Wang, D.M.; Yang, R.; Shi, D.X.; et al. Epitaxial growth of single-domain graphene on hexagonal boron nitride. *Nat. Mater.* **2013**, *12*, 792–797. [CrossRef] [PubMed]

165. Kong, D.S.; Dang, W.H.; Cha, J.J.; Li, H.; Meister, S.; Peng, H.L.; Liu, Z.F.; Cui, Y. Few-layer nanoplates of Bi$_2$Se$_3$ and Bi$_2$Te$_3$ with highly tunable chemical potential. *Nano Lett.* **2010**, *10*, 2245–2250. [CrossRef] [PubMed]

166. Xiao, X.; Yu, H.M.; Jin, H.Y.; Wu, M.H.; Fang, Y.S.; Sun, J.Y.; Hu, Z.M.; Li, T.Q.; Wu, J.B.; Huang, L.; et al. Salt-templated synthesis of 2D metallic MoN and other nitrides. *ACS Nano* **2017**, *11*, 2180–2186. [CrossRef]

167. Yu, Y.Y.; Wang, G.; Qin, S.Q.; Wu, N.N.; Wang, Z.Y.; He, K.; Zhang, X.A. Molecular beam epitaxy growth of atomically ultrathin MoTe$_2$ lateral heterophase homojunctions on graphene substrates. *Carbon* **2017**, *115*, 526–531. [CrossRef]

168. Walsh, L.A.; Yue, R.Y.; Wang, Q.X.; Barton, A.T.; Addoua, R.; Smyth, C.M.; Zhu, H.; Kim, J.; Colombo, L.; Kim, M.J.; et al. WTe$_2$ thin films grown by beam-interrupted molecular beam epitaxy. *2D Mater.* **2017**, *4*, 025044. [CrossRef]

169. Harrison, S.E.; Li, S.; Huo, Y.; Zhou, B.; Chen, Y.L.; Harris, J.S. Two-step growth of high quality Bi$_2$Te$_3$ thin films on Al$_2$O$_3$ (0001) by molecular beam epitaxy. *Appl. Phys. Lett.* **2013**, *102*, 171906. [CrossRef]

170. Song, C.L.; Wang, Y.L.; Jiang, Y.P.; Zhang, Y.; Chang, C.Z.; Wang, L.L.; He, K.; Chen, X.; Jia, J.F.; Wang, Y.Y.; et al. Topological insulator Bi$_2$Se$_3$ thin films grown on double-layer graphene by molecular beam epitaxy. *Appl. Phys. Lett.* **2010**, *97*, 143118. [CrossRef]

171. Roy, A.; Movva, H.C.P.; Satpati, B.; Kim, K.; Dey, R.; Rai, A.; Pramanik, T.; Guchhait, S.; Tutuc, E.; Banerjee, S.K. Structural and electrical properties of MoTe$_2$ and MoSe$_2$ grown by molecular beam epitaxy. *ACS Appl. Mater. Interfaces* **2016**, *8*, 7396–7402. [CrossRef] [PubMed]

172. Nakano, M.; Wang, Y.; Kashiwabara, Y.; Matsuoka, H.; Iwasa, Y. Layer-by-layer epitaxial growth of scalable WSe$_2$ on sapphire by molecular beam epitaxy. *Nano Lett.* **2017**, *17*, 5595–5599. [CrossRef] [PubMed]

173. Khan, U.; Luo, Y.T.; Tang, L.; Teng, C.J.; Liu, J.M.; Liu, B.L.; Cheng, H.M. Controlled vapor solid deposition of millimeter-size single crystal 2D Bi$_2$O$_2$Se for high-performance phototransistors. *Adv. Funct. Mater.* **2019**, *29*, 1807979. [CrossRef]

174. Xiao, X.; Song, H.B.; Lin, S.Z.; Zhou, Y.; Zhan, X.J.; Hu, Z.M.; Zhang, Q.; Sun, J.Y.; Yang, B.; Li, T.Q.; et al. Scalable salt-templated synthesis of two-dimensional transition metal oxides. *Nat. Commun.* **2016**, *7*, 112960. [CrossRef]

175. Gattass, R.R.; Mazur, E. Femtosecond laser micromachining in transparent materials. *Nat. Photonics* **2008**, *2*, 219–225. [CrossRef]

176. Li, Z.; Heidt, A.M.; Simakov, N.; Jung, Y.; Daniel, J.M.O.; Alam, S.U.; Richardson, D.J. Diode-pumped wideband thulium-doped fiber amplifiers for optical communications in the 1800–2050 nm window. *Opt. Express* **2013**, *21*, 26450–26455. [CrossRef]

177. Scholle, K.; Lamrini, S.; Koopmann, P.; Fuhrberg, P. 2 µm laser sources and their possible applications. In *Frontiers in Guided Wave Optics and Optoelectronics*; IntechOpen: London, UK, 2010. [CrossRef]

178. Marcinkevičius, A.; Juodkazis, S.; Watanabe, M.; Miwa, M.; Matsuo, S.; Misawa, H.; Nishii, J. Femtosecond laser-assisted three-dimensional microfabrication in silica. *Opt. Lett.* **2001**, *26*, 277–279. [CrossRef]

179. Fu, B.; Zhang, C.; Lyu, W.; Sun, J.; Shang, C.; Cheng, Y.; Xu, L. Recent progress on laser absorption spectroscopy for determination of gaseous chemical species. *Appl. Spectrosc. Rev.* **2020**. [CrossRef]

180. Ghelfi, P.; Laghezza, F.; Scotti, F.; Serafino, G.; Capria, A.; Pinna, S.; Onori, D.; Porzi, C.; Scaffardi, M.; Malacarne, A.; et al. A fully photonics-based coherent radar system. *Nature* **2014**, *507*, 341–345. [CrossRef] [PubMed]
181. Sotor, J.; Sobon, G.; Kowalczyk, M.; Macherzynski, W.; Paletko, P.; Abramski, K.M. Ultrafast thulium-doped fiber laser mode locked with black phosphorus. *Opt. Lett.* **2015**, *40*, 3885–3888. [CrossRef] [PubMed]
182. Mary, R.; Brown, G.; Beecher, S.J.; Torrisi, F.; Milana, S.; Popa, D.; Hasan, T.; Sun, Z.; Lidorikis, E.; Ohara, S. 1.5 GHz picosecond pulse generation from a monolithic waveguide laser with a graphene-film saturable output coupler. *Opt. Express* **2013**, *21*, 7943–7950. [CrossRef]
183. Li, P.; Zhang, G.; Zhang, H.; Zhao, C.; Chi, J.; Zhao, Z.; Yang, C.; Hu, H.; Yao, Y. Q-switched mode-locked Nd:YVO$_4$ laser by topological insulator Bi$_2$Te$_3$ saturable absorber. *IEEE Photonics Technol. Lett.* **2014**, *26*, 1912–1915. [CrossRef]
184. Guo, B. 2D noncarbon materials-based nonlinear optical devices for ultrafast photonics [Invited]. *Chin. Opt. Lett.* **2018**, *16*, 020004. [CrossRef]
185. Bonaccorso, F.; Sun, Z.; Hasan, T.; Ferrari, A.C. Graphene photonics and optoelectronics. *Nat. Photonics* **2010**, *4*, 611–622. [CrossRef]
186. Zhang, H.; Bao, Q.; Tang, D.; Zhao, L.; Loh, K. Large energy soliton erbium-doped fiber laser with a graphene-polymer composite mode locker. *Appl. Phys. Lett.* **2009**, *95*, 141103. [CrossRef]
187. Wang, C.; Liu, J.; Zhang, H. Ultrafast pulse lasers based on two-dimensinal nanomaterials. *Acta Phys. Sin.* **2019**, *68*, 188101. [CrossRef]
188. Sun, Z.; Popa, D.; Hasan, T.; Torrisi, F.; Wang, F.; Kelleher, E.J.R.; Travers, J.C.; Nicolosi, V.; Ferrari, A.C. A stable, wideband tunable, near transform-limited, graphene-mode-locked, ultrafast laser. *Nano Res.* **2010**, *3*, 653–660. [CrossRef]
189. Shang, C.; Zhang, Y.; Qin, H.; He, B.; Zhang, C.; Sun, J.; Li, J.; Ma, J.; Ji, X.; Xu, L.; et al. Review on wavelength-tunable pulsed fiber lasers based on 2D materials. *Opt. Laser Technol.* **2020**, *131*, 106375. [CrossRef]
190. Guo, B.; Xiao, Q.L.; Wang, S.H.; Zhang, H. 2D layered materials: Synthesis, nonlinear optical properties, and device applications. *Laser Photonics Rev.* **2019**, *13*, 1800327. [CrossRef]
191. Popa, D.; Sun, Z.; Hasan, T.; Torrisi, F.; Wang, F.; Ferrari, A.C. Graphene Q-switched, tunable fiber laser. *Appl. Phys. Lett.* **2011**, *98*, 073106. [CrossRef]
192. Duarte, F.J. *Tunable Laser Applications*; CRC Press: Boca Raton, FL, USA, 2008; Volume 150.
193. Olesberg, J.T.; Arnold, M.A.; Mermelstein, C.; Schmitz, J.; Wagner, J. Tunable laser diode system for noninvasive blood glucose measurements. *Appl. Spectrosc.* **2005**, *59*, 1480–1484. [CrossRef] [PubMed]
194. Besson, J.P.; Schilt, S.; Thévenaz, L. Multi-gas sensing based on photoacoustic spectroscopy using tunable laser diodes. *Spectrochim. Acta Part A* **2004**, *60*, 3449–3456. [CrossRef]
195. Gao, C.; Wang, R.; Zhu, L.; Gao, M.; Wang, Q.; Zhang, Z.; Wei, Z.; Lin, J.; Guo, L. Resonantly pumped 1.645 μm high repetition rate Er:YAG laser Q-switched by a graphene as a saturable absorber. *Opt. Lett.* **2012**, *37*, 632–634. [CrossRef]
196. Sobon, G.; Sotor, J.; Abramski, K.M. Passive harmonic mode-locking in Er-doped fiber laser based on graphene saturable absorber with repetition rates scalable to 2.22 GHz. *Appl. Phys. Lett.* **2012**, *100*, 161109. [CrossRef]
197. Di Dio Cafiso, D.S.; Ugolotti, E.; Schmidt, A.; Petrov, V.; Griebner, U.; Agnesi, A.; Cho, W.B.; Jung, B.H.; Rotermund, F.; Bae, S.; et al. Sub-100-fs Cr:YAG laser mode-locked by monolayer graphene saturable absorber. *Opt. Lett.* **2013**, *38*, 1745–1747. [CrossRef]
198. Sotor, J.; Pasternak, I.; Krajewska, A.; Strupinski, W.; Sobon, G. Sub-90 fs a stretched-pulse mode-locked fiber laser based on a graphene saturable absorber. *Opt. Express* **2015**, *23*, 27503–27508. [CrossRef]
199. Fu, B.; Li, J.; Cao, Z.; Popa, D. Bound states of solitons in a harmonic graphene-mode-locked fiber laser. *Photon. Res.* **2019**, *7*, 116–120. [CrossRef]
200. Yu, H.; Chen, X.; Zhang, H.; Xu, X.; Hu, X.; Wang, Z.; Wang, J.; Zhuang, S.; Jiang, M. Large energy pulse generation modulated by graphene epitaxially grown on silicon carbide. *ACS Nano* **2010**, *4*, 7582–7586. [CrossRef] [PubMed]
201. Zhao, L.M.; Tang, D.Y.; Zhang, H.; Wu, X.; Bao, Q.; Loh, K.P. Dissipative soliton operation of an ytterbium-doped fiber laser mode locked with atomic multilayer graphene. *Opt. Lett.* **2010**, *35*, 3622–3624. [CrossRef] [PubMed]
202. Liu, J.; Wu, S.; Yang, Q.H.; Wang, P. Stable nanosecond pulse generation from a graphene-based passively Q-switched Yb-doped fiber laser. *Opt. Lett.* **2011**, *36*, 4008–4010. [CrossRef] [PubMed]
203. Cho, W.B.; Kim, J.W.; Lee, H.W.; Bae, S.; Hong, B.H.; Choi, S.Y.; Baek, I.H.; Kim, K.; Yeom, D.I.; Rotermund, F. High-quality, large-area monolayer graphene for efficient bulk laser mode-locking near 1.25 μm. *Opt. Lett.* **2011**, *36*, 4089–4091. [CrossRef] [PubMed]
204. Zhao, N.; Liu, M.; Liu, H.; Zheng, X.W.; Ning, Q.Y.; Luo, A.P.; Luo, Z.C.; Xu, W.C. Dual-wavelength rectangular pulse Yb-doped fiber laser using a microfiber-based graphene saturable absorber. *Opt. Express* **2014**, *22*, 10906–10913. [CrossRef] [PubMed]
205. Wang, Q.; Teng, H.; Zou, Y.; Zhang, Z.; Li, D.; Wang, R.; Gao, C.; Lin, J.; Guo, L.; Wei, Z. Graphene on SiC as a Q-switcher for a 2 μm laser. *Opt. Lett.* **2012**, *37*, 395–397. [CrossRef] [PubMed]
206. Ma, J.; Xie, G.Q.; Lv, P.; Gao, W.L.; Yuan, P.; Qian, L.J.; Yu, H.H.; Zhang, H.J.; Wang, J.Y.; Tang, D.Y. Graphene mode-locked femtosecond laser at 2 μm wavelength. *Opt. Lett.* **2012**, *37*, 2085–2087. [CrossRef]
207. Zhang, M.; Kelleher, E.; Torrisi, F.; Sun, Z.; Hasan, T.; Popa, D.; Wang, F.; Ferrari, A.; Popov, S.; Taylor, J. Tm-doped fiber laser mode-locked by graphene-polymer composite. *Opt. Express* **2012**, *20*, 25077–25084. [CrossRef]
208. Liu, J.; Xu, J.; Wang, P. Graphene-based passively Q-switched 2μm thulium-doped fiber laser. *Opt. Commun.* **2012**, *285*, 5319–5322. [CrossRef]

209. Fu, B.; Gui, L.; Li, X.; Xiao, X.; Zhu, H.; Yang, C. Generation of 35-nJ nanosecond pulse from a passively mode-locked Tm, Ho-codoped fiber laser With graphene saturable absorber. *IEEE Photonics Technol. Lett.* **2013**, *25*, 1447–1449. [CrossRef]

210. Jiang, M.; Ma, H.F.; Ren, Z.Y.; Chen, X.M.; Long, J.Y.; Qi, M.; Shen, D.Y.; Wang, Y.S.; Bai, J.T. A graphene Q-switched nanosecond Tm-doped fiber laser at 2 µm. *Laser Phys. Lett.* **2013**, *10*, 79–83. [CrossRef]

211. Zhao, T.; Wang, Y.; Chen, H.; Shen, D. Graphene passively Q-switched Ho:YAG ceramic laser. *Appl. Phys. B* **2014**, *116*, 947–950. [CrossRef]

212. Cizmeciyan, M.N.; Kim, J.W.; Bae, S.; Hong, B.H.; Rotermund, F.; Sennaroglu, A. Graphene mode-locked femtosecond Cr:ZnSe laser at 2500 nm. *Opt. Lett.* **2013**, *38*, 341–343. [CrossRef]

213. Tokita, S.; Murakami, M.; Shimizu, S.; Hashida, M.; Sakabe, S. Graphene Q-switching of a 3 µm Er:ZBLAN fiber laser. In Proceedings of the Advanced Solid State Lasers, Optical Society of America, Paris, France, 27 October–1 November 2013; p. AF2A.9. [CrossRef]

214. Zhu, G.; Zhu, X.; Wang, F.; Xu, S.; Li, Y.; Guo, X.; Balakrishnan, K.; Norwood, R.A.; Peyghambarian, N. Graphene mode-locked fiber laser at 2.8 µm. *IEEE Photonics Technol. Lett.* **2016**, *28*, 7–10. [CrossRef]

215. Pushkin, A.V.; Migal, E.A.; Tokita, S.; Korostelin, Y.V.; Potemkin, F.V. Femtosecond graphene mode-locked Fe:ZnSe laser at 4.4 microm. *Opt. Lett.* **2020**, *45*, 738–741. [CrossRef]

216. Xu, J.; Liu, J.; Wu, S.; Yang, Q.H.; Wang, P. Graphene oxide mode-locked femtosecond erbium-doped fiber lasers. *Opt. Express* **2012**, *20*, 15474–15480. [CrossRef] [PubMed]

217. Zhao, C.; Zhang, H.; Qi, X.; Chen, Y.; Wang, Z.; Wen, S.; Tang, D. Ultra-short pulse generation by a topological insulator based saturable absorber. *Appl. Phys. Lett.* **2012**, *101*, 211106. [CrossRef]

218. Zhang, H.; Liu, C.X.; Qi, X.L.; Dai, X.; Fang, Z.; Zhang, S.C. Topological insulators in Bi_2Se_3, Bi_2Te_3 and Sb_2Te_3 with a single Dirac cone on the surface. *Nat. Phys.* **2009**, *5*, 438–442. [CrossRef]

219. Lee, J.; Koo, J.; Jhon, Y.M.; Lee, J.H. A femtosecond pulse erbium fiber laser incorporating a saturable absorber based on bulk-structured Bi_2Te_3 topological insulator. *Opt. Express* **2014**, *22*, 6165–6173. [CrossRef]

220. Sotor, J.; Sobon, G.; Abramski, K.M. Sub-130 fs mode-locked Er-doped fiber laser based on topological insulator. *Opt. Express* **2014**, *22*, 13244–13249. [CrossRef]

221. Yan, P.; Lin, R.; Ruan, S.; Liu, A.; Chen, H. A 2.95 GHz, femtosecond passive harmonic mode-locked fiber laser based on evanescent field interaction with topological insulator film. *Opt. Express* **2015**, *23*, 154–164. [CrossRef]

222. Boguslawski, J.; Sobon, G.; Zybala, R.; Sotor, J. Dissipative soliton generation in Er-doped fiber laser mode-locked by Sb_2Te_3 topological insulator. *Opt. Lett.* **2015**, *40*, 2786–2789. [CrossRef]

223. Wei, Q.; Niu, K.; Han, X.; Zhang, H.; Zhang, C.; Yang, C.; Man, B. Large energy pulses generation in a mode-locked Er-doped fiber laser based on CVD-grown Bi_2Te_3 saturable absorber. *Opt. Mater. Express* **2019**, *9*, 3535–3545. [CrossRef]

224. Guo, Q.; Pan, J.; Liu, Y.; Si, H.; Lu, Z.; Han, X.; Gao, J.; Zuo, Z.; Zhang, H.; Jiang, S. Output energy enhancement in a mode-locked Er-doped fiber laser using CVD-Bi_2Se_3 as a saturable absorber. *Opt. Express* **2019**, *27*, 24670–24681. [CrossRef] [PubMed]

225. Guo, Q.; Fan, X.; Gao, J.; Han, X.; Zhang, H.; Han, Y.; Jiang, S. Bi_2Se_3/mica optical modulator for high-energy mode-locked Er-doped fiber laser. *Infrared Phys. Technol.* **2020**, *111*, 103453. [CrossRef]

226. Luo, Z.; Huang, Y.; Weng, J.; Cheng, H.; Lin, Z.; Xu, B.; Cai, Z.; Xu, H. 1.06 µm Q-switched ytterbium-doped fiber laser using few-layer topological insulator Bi_2Se_3 as a saturable absorber. *Opt. Express* **2013**, *21*, 29516–29522. [CrossRef] [PubMed]

227. Chi, C.; Lee, J.; Koo, J.; Han Lee, J. All-normal-dispersion dissipative-soliton fiber laser at 1.06 µm using a bulk-structured Bi_2Te_3 topological insulator-deposited side-polished fiber. *Laser Phys.* **2014**, *24*, 105106. [CrossRef]

228. Xu, B.; Wang, Y.; Peng, J.; Luo, Z.; Xu, H.; Cai, Z.; Weng, J. Topological insulator Bi_2Se_3 based Q-switched Nd:LiYF$_4$ nanosecond laser at 1313 nm. *Opt. Express* **2015**, *23*, 7674–7680. [CrossRef]

229. Xu, J.L.; Sun, Y.J.; He, J.L.; Wang, Y.; Zhu, Z.J.; You, Z.Y.; Li, J.F.; Chou, M.M.; Lee, C.K.; Tu, C.Y. Ultrasensitive nonlinear absorption response of large-size topological insulator and application in low-threshold bulk pulsed lasers. *Sci. Rep.* **2015**, *5*, 14856. [CrossRef]

230. Wang, Y.R.; He, J.L.; Lee, C.K.; Sung, W.H.; Su, X.C.; Zhao, Y.; Zhang, B.T.; Wu, C.L.; He, G.B.; Lin, Y.Y.; et al. Ultralow saturation intensity topological insulator saturable absorber for gigahertz mode-locked solid-state lasers. *IEEE Photonics J.* **2018**, *10*, 1–10. [CrossRef]

231. Luo, Z.; Liu, C.; Huang, Y.; Wu, D.; Wu, J.; Xu, H.; Cai, Z.; Lin, Z.; Sun, L.; Weng, J. Topological-insulator passively Q-switched double-clad fiber laser at 2 µm wavelength. *IEEE J. Sel. Top. Quantum Electron.* **2014**, *20*, 6739071. [CrossRef]

232. Jung, M.; Lee, J.; Koo, J.; Park, J.; Song, Y.W.; Lee, K.; Lee, S.; Lee, J.H. A femtosecond pulse fiber laser at 1935 nm using a bulk-structured Bi_2Te_3 topological insulator. *Opt. Express* **2014**, *22*, 7865–7874. [CrossRef] [PubMed]

233. Yin, K.; Zhang, B.; Li, L.; Jiang, T.; Zhou, X.; Hou, J. Soliton mode-locked fiber laser based on topological insulator Bi_2Te_3 nanosheets at 2 µm. *Photonics Res.* **2015**, *3*, 72–76. [CrossRef]

234. Lee, J.; Ju, H.L. Femtosecond Tm–Ho co-doped fiber laser using a bulk-structured Bi_2Se_3 topological insulator. *Chin. Phys. B* **2018**, *27*, 152–159. [CrossRef]

235. Loiko, P.; Bogusławski, J.; Serres, J.M.; Kifle, E.; Kowalczyk, M.; Mateos, X.; Sotor, J.; Zybała, R.; Mars, K.; Mikuła, A.; et al. Sb_2Te_3 thin film for the passive Q-switching of a Tm:GdVO$_4$ laser. *Opt. Mater. Express* **2018**, *8*, 1723. [CrossRef]

236. Yin, K.; Jiang, T.; Zheng, X.; Yu, H.; Cheng, X.; Hou, J. Mid-infrared ultra-short mode-locked fiber laser utilizing topological insulator Bi_2Te_3 nano-sheets as the saturable absorber. *arXiv* **2015**, arXiv:1505.06322.

237. Li, J.; Luo, H.; Wang, L.; Zhao, C.; Zhang, H.; Li, H.; Liu, Y. 3-μm Mid-infrared pulse generation using topological insulator as the saturable absorber. *Opt. Lett.* **2015**, *40*, 3659–3662. [CrossRef]

238. Tang, P.; Wu, M.; Wang, Q.; Miao, L.; Huang, B.; Liu, J.; Zhao, C.; Wen, S. 2.8-μm pulsed Er^{3+}: ZBLAN fiber laser modulated by topological insulator. *IEEE Photonics Technol. Lett.* **2016**, *28*, 1573–1576. [CrossRef]

239. Li, W.; Wang, K.; Du, T.; Zou, J.; Li, Y.; Luo, Z. Miniaturized mid-Infrared all-fiber laser passively Q-switched by topological insulator Bi_2Se_3. In Proceedings of the 2018 Asia Communications and Photonics Conference (ACP), Hangzhou, China, 26–29 October 2018; pp. 1–3. [CrossRef]

240. Chen, S.; Zhao, C.; Li, Y.; Huang, H.; Lu, S.; Zhang, H.; Wen, S. Broadband optical and microwave nonlinear response in topological insulator. *Opt. Mater. Express* **2014**, *4*, 587–596. [CrossRef]

241. Lu, S.; Zhao, C.; Zou, Y.; Chen, S.; Chen, Y.; Li, Y.; Zhang, H.; Wen, S.; Tang, D. Third order nonlinear optical property of Bi_2Se_3. *Opt. Express* **2013**, *21*, 2072–2082. [CrossRef]

242. Yu, H.; Zhang, H.; Wang, Y.; Zhao, C.; Wang, B.; Wen, S.; Zhang, H.; Wang, J. Topological insulator as an optical modulator for pulsed solid-state lasers. *Laser Photonics Rev.* **2013**, *7*, L77–L83. [CrossRef]

243. Wu, D.; Cai, Z.; Zhong, Y.; Peng, J.; Weng, J.; Luo, Z.; Chen, N.; Xu, H. 635-nm visible Pr^{3+}-doped ZBLAN fiber lasers Q-switched by topological insulators SAs. *IEEE Photonics Technol. Lett.* **2015**, *27*, 2379–2382. [CrossRef]

244. Lin, H.Y.; Li, W.S.; Lan, J.L.; Guan, X.F.; Xu, H.Y.; Cai, Z.P. All-fiber passively Q-switched 604 nm praseodymium laser with a Bi_2Se_3 saturable absorber. *Appl. Opt.* **2017**, *56*, 802–805. [CrossRef] [PubMed]

245. Glinka, Y.D.; Babakiray, S.; Johnson, T.A.; Bristow, A.D.; Holcomb, M.B.; Lederman, D. Ultrafast carrier dynamics in thin-films of the topological insulator Bi_2Se_3. *Appl. Phys. Lett.* **2013**, *103*, 151903. [CrossRef]

246. Boguslawski, J.; Sotor, J.; Sobon, G.; Tarka, J.; Jagiello, J.; Macherzynski, W.; Lipinska, L.; Abramski, K.M. Mode-locked Er-doped fiber laser based on liquid phase exfoliated Sb_2Te_3 topological insulator. *Laser Phys.* **2014**, *24*, 105111. [CrossRef]

247. Sotor, J.; Sobon, G.; Boguslawski, J.; Tarka, J.; Abramski, K. Sb_2Te_3 topological insulator based saturable absorber for Er-doped mode-locked fiber lasers. In Proceedings of the SPIE LASE, San Francisco, CA, USA, 9–12 February 2015; Volume 9344. [CrossRef]

248. Wang, K.; Wang, J.; Fan, J.; Lotya, M.; O'Neill, A.; Fox, D.; Feng, Y.; Zhang, X.; Jiang, B.; Zhao, Q.; et al. Ultrafast saturable absorption of two-dimensional MoS_2 nanosheets. *ACS Nano* **2013**, *7*, 9260–9267. [CrossRef]

249. Xu, B.; Cheng, Y.; Wang, Y.; Huang, Y.; Peng, J.; Luo, Z.; Xu, H.; Cai, Z.; Weng, J.; Moncorge, R. Passively Q-switched $Nd:YAlO_3$ nanosecond laser using MoS_2 as saturable absorber. *Opt. Express* **2014**, *22*, 28934–28940. [CrossRef] [PubMed]

250. Zhao, G.; Han, S.; Wang, A.; Wu, Y.; Zhao, M.; Wang, Z.; Hao, X. "Chemical Weathering" exfoliation of atom-thick transition metal dichalcogenides and their ultrafast saturable absorption properties. *Adv. Funct. Mater.* **2015**, *25*, 5292–5299. [CrossRef]

251. Hou, J.; Zhao, G.; Wu, Y.; He, J.; Hao, X. Femtosecond solid-state laser based on tungsten disulfide saturable absorber. *Opt. Express* **2015**, *23*, 27292–27298. [CrossRef]

252. Lin, J.; Hu, Y.; Chen, C.; Gu, C.; Xu, L. Wavelength-tunable Yb-doped passively Q-switching fiber laser based on WS_2 saturable absorber. *Opt. Express* **2015**, *23*, 29059–29064. [CrossRef] [PubMed]

253. Cheng, C.; Liu, H.; Tan, Y.; Vazquez de Aldana, J.R.; Chen, F. Passively Q-switched waveguide lasers based on two-dimensional transition metal diselenide. *Opt. Express* **2016**, *24*, 10385–10390. [CrossRef] [PubMed]

254. Wang, X.; Wang, Y.; Duan, L.; Li, L.; Sun, H. Passively Q-switched Nd:YAG laser via a WS_2 saturable absorber. *Opt. Commun.* **2016**, *367*, 234–238. [CrossRef]

255. Liu, H.; Luo, A.P.; Wang, F.Z.; Tang, R.; Liu, M.; Luo, Z.C.; Xu, W.C.; Zhao, C.J.; Zhang, H. Femtosecond pulse erbium-doped fiber laser by a few-layer MoS_2 saturable absorber. *Opt. Lett.* **2014**, *39*, 4591–4594. [CrossRef] [PubMed]

256. Liu, M.; Zheng, X.W.; Qi, Y.L.; Liu, H.; Luo, A.P.; Luo, Z.C.; Xu, W.C.; Zhao, C.J.; Zhang, H. Microfiber-based few-layer MoS_2 saturable absorber for 2.5 GHz passively harmonic mode-locked fiber laser. *Opt. Express* **2014**, *22*, 22841–22846. [CrossRef]

257. Huang, Y.; Luo, Z.; Li, Y.; Zhong, M.; Xu, B.; Che, K.; Xu, H.; Cai, Z.; Peng, J.; Weng, J. Widely-tunable, passively Q-switched erbium-doped fiber laser with few-layer MoS_2 saturable absorber. *Opt. Express* **2014**, *22*, 25258–25266. [CrossRef] [PubMed]

258. Khazaeizhad, R.; Kassani, S.H.; Jeong, H.; Yeom, D.I.; Oh, K. Mode-locking of Er-doped fiber laser using a multilayer MoS_2 thin film as a saturable absorber in both anomalous and normal dispersion regimes. *Opt. Express* **2014**, *22*, 23732–23742. [CrossRef]

259. Mao, D.; Wang, Y.; Ma, C.; Han, L.; Jiang, B.; Gan, X.; Hua, S.; Zhang, W.; Mei, T.; Zhao, J. WS_2 mode-locked ultrafast fiber laser. *Sci. Rep.* **2015**, *5*, 7965. [CrossRef] [PubMed]

260. Khazaeinezhad, R.; Kassani, S.H.; Hwanseong, J.; Kyung Jun, P.; Byoung Yoon, K.; Dong-Il, Y.; Kyunghwan, O. Ultrafast pulsed all-fiber laser based on tapered fiber enclosed by few-layer WS_2 nanosheets. *IEEE Photonics Technol. Lett.* **2015**, *27*, 1581–1584. [CrossRef]

261. Kassani, S.H.; Khazaeinezhad, R.; Jeong, H.; Nazari, T.; Yeom, D.I.; Oh, K. All-fiber Er-doped Q-Switched laser based on Tungsten Disulfide saturable absorber. *Opt. Mater. Express* **2015**, *5*, 373–379. [CrossRef]

262. Ferrari, A.C.; Bonaccorso, F.; Fal'ko, V.; Novoselov, K.S.; Roche, S.; Boggild, P.; Borini, S.; Koppens, F.H.; Palermo, V.; Pugno, N.; et al. Science and technology roadmap for graphene, related two-dimensional crystals, and hybrid systems. *Nanoscale* **2015**, *7*, 4598–4810. [CrossRef]

263. Luo, Z.; Li, Y.; Zhong, M.; Huang, Y.; Wan, X.; Peng, J.; Weng, J. Nonlinear optical absorption of few-layer molybdenum diselenide ($MoSe_2$) for passively mode-locked soliton fiber laser [Invited]. *Photonics Res.* **2015**, *3*, A79–A86. [CrossRef]

264. Koo, J.; Park, J.; Lee, J.; Jhon, Y.M.; Lee, J.H. Femtosecond harmonic mode-locking of a fiber laser at 3.27 GHz using a bulk-like, $MoSe_2$-based saturable absorber. *Opt. Express* **2016**, *24*, 10575–10589. [CrossRef]

265. Liu, W.; Pang, L.; Han, H.; Liu, M.; Lei, M.; Fang, S.; Teng, H.; Wei, Z. Tungsten disulfide saturable absorbers for 67 fs mode-locked erbium-doped fiber lasers. *Opt. Express* **2017**, *25*, 2950–2959. [CrossRef] [PubMed]

266. Liu, W.; Liu, M.; OuYang, Y.; Hou, H.; Lei, M.; Wei, Z. CVD-grown MoSe$_2$ with high modulation depth for ultrafast mode-locked erbium-doped fiber laser. *Nanotechnology* **2018**, *29*, 394002. [CrossRef] [PubMed]

267. Wang, S.; Yu, H.; Zhang, H.; Wang, A.; Zhao, M.; Chen, Y.; Mei, L.; Wang, J. Broadband few-layer MoS$_2$ saturable absorbers. *Adv. Mater.* **2014**, *26*, 3538–3544. [CrossRef]

268. Luo, Z.; Huang, Y.; Zhong, M.; Li, Y.; Wu, J.; Xu, B.; Xu, H.; Cai, Z.; Peng, J.; Weng, J. 1-, 1.5-, and 2-μm fiber lasers Q-switched by a broadband few-layer MoS$_2$ saturable absorber. *J. Light. Technol.* **2014**, *32*, 4679–4686. [CrossRef]

269. Kong, L.; Xie, G.; Yuan, P.; Qian, L.; Wang, S.; Yu, H.; Zhang, H. Passive Q-switching and Q-switched mode-locking operations of 2 μm Tm: CLNGG laser with MoS$_2$ saturable absorber mirror. *Photonics Res.* **2015**, *3*, A47–A50. [CrossRef]

270. Tian, Z.; Wu, K.; Kong, L.; Yang, N.; Wang, Y.; Chen, R.; Hu, W.; Xu, J.; Tang, Y. Mode-locked thulium fiber laser with MoS$_2$. *Laser Phys. Lett.* **2015**, *12*, 065104. [CrossRef]

271. Jung, M.; Lee, J.; Park, J.; Koo, J.; Jhon, Y.M.; Lee, J.H. Mode-locked, 1.94-μm, all-fiberized laser using WS$_2$ based evanescent field interaction. *Opt. Express* **2015**, *23*, 19996–20006. [CrossRef]

272. Lee, J.; Koo, J.; Lee, J.; Jhon, Y.M.; Lee, J.H. All-fiberized, femtosecond laser at 1912 nm using a bulk-like MoSe$_2$ saturable absorber. *Opt. Mater. Express* **2017**, *7*, 2968–2979. [CrossRef]

273. Wang, J.; Xu, Z.; Liu, W.; Yan, P.; Lu, W.; Li, J.; Chen, H.; Jiang, Z.; Wang, J.; Zhang, W.; et al. Ultrafast thulium-doped fiber laser mode locked by monolayer WSe$_2$. *IEEE J. Sel. Top. Quant.* **2018**, *24*, 1–6. [CrossRef]

274. Fan, M.; Li, T.; Zhao, S.; Li, G.; Ma, H.; Gao, X.; Krankel, C.; Huber, G. Watt-level passively Q-switched Er:Lu$_2$O$_3$ laser at 2.84 μm using MoS$_2$. *Opt. Lett.* **2016**, *41*, 540–543. [CrossRef]

275. Wei, C.; Luo, H.; Zhang, H.; Li, C.; Xie, J.; Li, J.; Liu, Y. Passively Q-switched mid-infrared fluoride fiber laser around 3 μm using a tungsten disulfide (WS$_2$) saturable absorber. *Laser Phys. Lett.* **2016**, *13*, 105108. [CrossRef]

276. Liu, X.; Zhang, S.; Yan, Z.; Guo, L.; Fan, X.; Lou, F.; Wang, M.; Gao, P.; Guo, G.; Li, T.; et al. WSe$_2$ as a saturable absorber for a passively Q-switched Ho,Pr:LLF laser at 295 μm. *Opt. Mater. Express* **2018**, *8*, 1213. [CrossRef]

277. Zhang, S.; Liu, X.; Guo, L.; Fan, M.; Lou, F.; Gao, P.; Guo, G.; Yang, J.; Liu, J.; Li, T.; et al. Passively Q-switched Ho,Pr:LLF bulk slab laser at 2.95 μm based on MoS$_2$ saturable absorber. *IEEE Photonics Technol. Lett.* **2017**, *29*, 2258–2261. [CrossRef]

278. Guo, C.; Wei, J.; Yan, P.; Luo, R.; Ruan, S.; Wang, J.; Guo, B.; Hua, P.; Lue, Q. Mode-locked fiber laser at 2.8 μm using a chemical-vapor-deposited WSe$_2$ saturable absorber mirror. *Appl. Phys. Express* **2020**, *13*, 012013. [CrossRef]

279. Chen, B.; Zhang, X.; Wu, K.; Wang, H.; Wang, J.; Chen, J. Q-switched fiber laser based on transition metal dichalcogenides MoS$_2$, MoSe$_2$, WS$_2$, and WSe$_2$. *Opt. Express* **2015**, *23*, 26723–26737. [CrossRef] [PubMed]

280. Du, J.; Wang, Q.; Jiang, G.; Xu, C.; Zhao, C.; Xiang, Y.; Chen, Y.; Wen, S.; Zhang, H. Ytterbium-doped fiber laser passively mode locked by few-layer Molybdenum Disulfide (MoS$_2$) saturable absorber functioned with evanescent field interaction. *Sci. Rep.* **2014**, *4*, 6346. [CrossRef]

281. Liu, S.; Lv, R.; Wang, Y.; Wang, J.; Wang, Y.; Wang, H. Passively mode-locked fiber laser with WS$_2$/SiO$_2$ saturable absorber fabricated by Sol-Gel technique. *ACS Appl. Mater. Interfaces* **2020**, *12*, 29625–29630. [CrossRef] [PubMed]

282. Cheng, C.; Li, Z.; Dong, N.; Wang, J.; Chen, F. Tin diselenide as a new saturable absorber for generation of laser pulses at 1 μm. *Opt. Express* **2017**, *25*, 6132–6140. [CrossRef]

283. Li, J.; Zhao, Y.; Chen, Q.; Niu, K.; Sun, R.; Zhang, H. Passively mode-locked ytterbium-doped fiber laser based on SnS$_2$ as saturable absorber. *IEEE Photonics J.* **2017**, *9*, 1–7. [CrossRef]

284. Niu, K.; Chen, Q.; Sun, R.; Man, B.; Zhang, H. Passively Q-switched erbium-doped fiber laser based on SnS$_2$ saturable absorber. *Opt. Mater. Express* **2017**, *7*, 3934–3943. [CrossRef]

285. Niu, K.; Sun, R.; Chen, Q.; Man, B.; Zhang, H. Passively mode-locked Er-doped fiber laser based on SnS$_2$ nanosheets as a saturable absorber. *Photonics Res.* **2018**, *6*, 72–76. [CrossRef]

286. Yao, Y.; Zhang, F.; Chen, B.; Zhao, Y.; Cui, N.; Sun, D.; Liu, S.; Zhang, Y.; Zhang, H.; Zhang, H. Nonlinear optical property and mid-infrared Q-switched laser application at 2.8 μm of PtSe$_2$ material. *Opt. Laser Technol.* **2021**, *139*, 106983. [CrossRef]

287. Chen, Y.; Chen, S.; Liu, J.; Gao, Y.; Zhang, W. Sub-300 femtosecond soliton tunable fiber laser with all-anomalous dispersion passively mode locked by black phosphorus. *Opt. Express* **2016**, *24*, 13316–13324. [CrossRef]

288. Song, Y.; Chen, S.; Zhang, Q.; Li, L.; Zhao, L.; Zhang, H.; Tang, D. Vector soliton fiber laser passively mode locked by few layer black phosphorus-based optical saturable absorber. *Opt. Express* **2016**, *24*, 25933–25942. [CrossRef]

289. Yun, L. Black phosphorus saturable absorber for dual-wavelength polarization-locked vector soliton generation. *Opt. Express* **2017**, *25*, 32380–32385. [CrossRef]

290. Jin, X.; Hu, G.; Zhang, M.; Hu, Y.; Albrow-Owen, T.; Howe, R.C.T.; Wu, T.C.; Wu, Q.; Zheng, Z.; Hasan, T. 102 fs pulse generation from a long-term stable, inkjet-printed black phosphorus-mode-locked fiber laser. *Opt. Express* **2018**, *26*, 12506–12513. [CrossRef]

291. Zhang, B.; Lou, F.; Zhao, R.; He, J.; Li, J.; Su, X.; Ning, J.; Yang, K. Exfoliated layers of black phosphorus as saturable absorber for ultrafast solid-state laser. *Opt. Lett.* **2015**, *40*, 3691–3694. [CrossRef]

292. Ma, J.; Lu, S.; Guo, Z.; Xu, X.; Zhang, H.; Tang, D.; Fan, D. Few-layer black phosphorus based saturable absorber mirror for pulsed solid-state lasers. *Opt. Express* **2015**, *23*, 22643–22648. [CrossRef]

293. Al-Masoodi, A.H.H.; Ahmed, M.H.M.; Latiff, A.A.; Arof, H.; Harun, S.W. Q-switched ytterbium-doped fiber laser using black phosphorus as saturable absorber. *Chin. Phys. Lett.* **2016**, *33*, 054206. [CrossRef]

294. Su, X.; Wang, Y.; Zhang, B.; Zhao, R.; Yang, K.; He, J.; Hu, Q.; Jia, Z.; Tao, X. Femtosecond solid-state laser based on a few-layered black phosphorus saturable absorber. *Opt. Lett.* **2016**, *41*, 1945–1948. [CrossRef]

295. Rashid, F.A.A.; Azzuhri, S.R.; Salim, M.A.M.; Shaharuddin, R.A.; Ismail, M.A.; Ismail, M.F.; Razak, M.Z.A.; Ahmad, H. Using a black phosphorus saturable absorber to generate dual wavelengths in a Q-switched ytterbium-doped fiber laser. *Laser Phys. Lett.* **2016**, *13*, 085102. [CrossRef]

296. Ahmad, H.; Salim, M.A.M.; Thambiratnam, K.; Norizan, S.F.; Harun, S.W. A black phosphorus-based tunable Q-switched ytterbium fiber laser. *Laser Phys. Lett.* **2016**, *13*, 095103. [CrossRef]

297. Huang, K.X.; Lu, B.L.; Li, D.; Qi, X.Y.; Chen, H.W.; Wang, N.; Wen, Z.R.; Bai, J.T. Black phosphorus flakes covered microfiber for Q-switched ytterbium-doped fiber laser. *Appl. Opt.* **2017**, *56*, 6427–6431. [CrossRef]

298. Wang, D.; Song, H.; Long, X.; Li, L. Switchable and tunable multi-wavelength emissions in pulsed ytterbium fiber lasers with black phosphorus saturable absorbers and polarization-maintaining fiber Bragg gratings. *Opt. Commun.* **2019**, *452*, 373–379. [CrossRef]

299. Yu, H.; Zheng, X.; Yin, K.; Cheng, X.; Jiang, T. Nanosecond passively Q-switched thulium/holmium-doped fiber laser based on black phosphorus nanoplatelets. *Opt. Mater. Express* **2016**, *6*, 603–609. [CrossRef]

300. Chu, Z.Z.; Liu, J.; Guo, Z.N.; Zhang, H. 2 μm passively Q-switched laser based on black phosphorus. *Opt. Mater. Express* **2016**, *6*, 2374–2379. [CrossRef]

301. Zhang, H.; He, J.; Wang, Z.; Hou, J.; Zhang, B.; Zhao, R.; Han, K.; Yang, K.; Nie, H.; Sun, X. Dual-wavelength, passively Q-switched Tm:YAP laser with black phosphorus saturable absorber. *Opt. Mater. Express* **2016**, *6*, 2328–2335. [CrossRef]

302. Pawliszewska, M.; Ge, Y.; Li, Z.; Zhang, H.; Sotor, J. Fundamental and harmonic mode-locking at 2.1 μm with black phosphorus saturable absorber. *Opt. Express* **2017**, *25*, 16916–16921. [CrossRef]

303. Qin, Z.; Xie, G.; Zhao, C.; Wen, S.; Yuan, P.; Qian, L. Mid-infrared mode-locked pulse generation with multilayer black phosphorus as saturable absorber. *Opt. Lett.* **2016**, *41*, 56–59. [CrossRef]

304. Kong, L.; Qin, Z.; Xie, G.; Guo, Z.; Zhang, H.; Yuan, P.; Qian, L. Black phosphorus as broadband saturable absorber for pulsed lasers from 1 μm to 2.7 μm wavelength. *Laser Phys. Lett.* **2016**, *13*, 045801. [CrossRef]

305. Liu, J.; Liu, J.; Guo, Z.; Zhang, H.; Ma, W.; Wang, J.; Su, L. Dual-wavelength Q-switched $Er:SrF_2$ laser with a black phosphorus absorber in the mid-infrared region. *Opt. Express* **2016**, *24*, 30289–30295. [CrossRef]

306. Woodward, R.I.; Majewski, M.R.; Macadam, N.; Hu, G.; Albrow-Owen, T.; Hasan, T.; Jackson, S.D. Q-switched Dy:ZBLAN fiber lasers beyond 3 μm: comparison of pulse generation using acousto-optic modulation and inkjet-printed black phosphorus. *Opt. Express* **2019**, *27*, 15032–15045. [CrossRef]

307. Guo, Z.; Zhang, H.; Lu, S.; Wang, Z.; Tang, S.; Shao, J.; Sun, Z.; Xie, H.; Wang, H.; Yu, X.F.; et al. From black phosphorus to phosphorene: basic solvent exfoliation, evolution of raman scattering, and applications to ultrafast photonics. *Adv. Funct. Mater.* **2015**, *25*, 6996–7002. [CrossRef]

308. Morita, A. Semiconducting black phosphorus. *Appl. Phys. A* **1986**, *39*, 227–242. [CrossRef]

309. Tran, V.; Soklaski, R.; Liang, Y.; Yang, L. Layer-controlled band gap and anisotropic excitons in few-layer black phosphorus. *Phys. Rev. B* **2014**, *89*, 235319. [CrossRef]

310. Island, J.O.; Steele, G.A.; van der Zant, H.S.; Castellanos-Gomez, A. Environmental instability of few-layer black phosphorus. *2D Mater.* **2015**, *2*, 011002. [CrossRef]

311. Wang, X.; Jones, A.M.; Seyler, K.L.; Tran, V.; Jia, Y.; Zhao, H.; Wang, H.; Yang, L.; Xu, X.; Xia, F. Highly anisotropic and robust excitons in monolayer black phosphorus. *Nat. Nanotechnol.* **2015**, *10*, 517–521. [CrossRef]

312. Castellanos-Gomez, A.; Vicarelli, L.; Prada, E.; Island, J.O.; Narasimha-Acharya, K.; Blanter, S.I.; Groenendijk, D.J.; Buscema, M.; Steele, G.A.; Alvarez, J. Isolation and characterization of few-layer black phosphorus. *2D Mater.* **2014**, *1*, 025001. [CrossRef]

313. Mikulla, B.; Leng, L.; Sears, S.; Collings, B.C.; Arend, M.; Bergman, K. Broad-band high-repetition-rate source for spectrally sliced WDM. *IEEE Photonics Technol. Lett.* **1999**, *11*, 418–420. [CrossRef]

314. McFerran, J.J. Échelle spectrograph calibration with a frequency comb based on a harmonically mode-locked fiber laser: A proposal. *Appl. Opt.* **2009**, *48*, 2752–2759. [CrossRef]

315. Jhon, Y.I.; Koo, J.; Anasori, B.; Seo, M.; Lee, J.H.; Gogotsi, Y.; Jhon, Y.M. Metallic MXene saturable absorber for femtosecond mode-locked lasers. *Adv. Mater.* **2017**, *29*, 1702496. [CrossRef]

316. Jiang, X.; Liu, S.; Liang, W.; Luo, S.; He, Z.; Ge, Y.; Wang, H.; Cao, R.; Zhang, F.; Wen, Q.; et al. Broadband nonlinear photonics in few-layer MXene $Ti_3C_2T_x$ (T = F, O, or OH). *Laser Photonics Rev.* **2018**, *12*, 1700229. [CrossRef]

317. Kim, J.J.; Kim, H.; Koo, C.M.; Lee, J.H.; Lee, S.B.; Lee, K. Femtosecond mode-locked fiber laser Using an etched optical fiber immersed in liquid Mxene as a saturable absorber. In Proceedings of the 23rd Opto-Electronics and Communications Conference, Institute of Electrical and Electronics Engineers Inc., Jeju, Korea, 2–6 July 2018; p. 8730133. [CrossRef]

318. Li, J.; Zhang, Z.; Du, L.; Miao, L.; Yi, J.; Huang, B.; Zou, Y.; Zhao, C.; Wen, S. Highly stable femtosecond pulse generation from a MXene $Ti_3C_2T_x$ (T = F, O, or OH) mode-locked fiber laser. *Photonics Res.* **2019**, *7*, 260–264. [CrossRef]

319. Feng, J.; Li, X.; Feng, T.; Wang, Y.; Liu, J.; Zhang, H. Harmonic mode-locked Er-doped fiber laser by evanescent field-based MXene $Ti_3C_2T_x$ (T = F, O, or OH) saturable absorber. *Ann. Phys.* **2020**, *532*, 1900437. [CrossRef]

320. Wu, Q.; Jin, X.; Chen, S.; Jiang, X.; Hu, Y.; Jiang, Q.; Wu, L.; Li, J.; Zheng, Z.; Zhang, M.; et al.. MXene-based saturable absorber for femtosecond mode-locked fiber lasers. *Opt. Express* **2019**, *27*, 10159–10170. [CrossRef] [PubMed]

321. Huang, W.; Ma, C.; Li, C.; Zhang, Y.; Hu, L.; Chen, T.; Tang, Y.; Ju, J.; Zhang, H. Highly stable MXene (V$_2$CT$_x$)-based harmonic pulse generation. *Nanophotonics* **2020**, *9*, 2577–2585. [CrossRef]

322. Li, G.; Yang, L.; Zhao, R.; Wang, F.; Nie, H.; Wang, R.; Yang, K.; Zhang, B.; He, J. Generation of a square-shaped pulse in mode-locked fiber lasers with a microfiber-based few-layer Nb$_2$C saturable absorber. *Appl. Opt.* **2020**, *59*, 11240–11245. [CrossRef] [PubMed]

323. Jafry, A.A.A.; Muhammad, A.R.; Kasim, N.; Rosol, A.H.A.; Rusdi, M.F.M.; Ab Alim, N.N.N.; Harun, S.W.; Yupapin, P. Ultrashort pulse generation with MXene Ti$_3$C$_2$T$_x$ embedded in PVA and deposited onto D-shaped fiber. *Opt. Laser Technol.* **2021**, *136*, 106780. [CrossRef]

324. Feng, X.Y.; Ding, B.Y.; Liang, W.Y.; Zhang, F.; Ning, T.Y.; Liu, J.; Zhang, H. MXene Ti$_3$C$_2$T$_x$ absorber for a 1.06 µm passively Q-switched ceramic laser. *Laser Phys. Lett.* **2018**, *15*, 085805. [CrossRef]

325. Sun, X.; Zhang, B.; Yan, B.; Li, G.; Nie, H.; Yang, K.; Zhang, C.; He, J. Few-layer Ti$_3$C$_2$T$_x$ (T = O, OH, or F) saturable absorber for a femtosecond bulk laser. *Opt. Lett.* **2018**, *43*, 3862–3865. [CrossRef]

326. Shi, Y.; Xu, N.; Wen, Q. Ti$_2$CT$_x$ (T = O, OH or F) nanosheets as new broadband saturable absorber for ultrafast photonics. *J. Light. Technol.* **2020**, *38*, 1975–1980. [CrossRef]

327. Ma, C.; Huang, W.; Wang, Y.; Adams, J.; Wang, Z.; Liu, J.; Song, Y.; Ge, Y.; Guo, Z.; Hu, L.; et al. MXene saturable absorber enabled hybrid mode-locking technology: A new routine of advancing femtosecond fiber lasers performance. *Nanophotonics* **2020**, *9*, 2451–2458. [CrossRef]

328. Zu, Y.; Zhang, C.; Guo, X.; Liang, W.; Liu, J.; Su, L.; Zhang, H. A solid-state passively Q-switched Tm,Gd:CaF2laser with a Ti$_3$C$_2$T$_x$MXene absorber near 2 µm. *Laser Phys. Lett.* **2019**, *16*, 015803. [CrossRef]

329. Jiang, Q.; Zhang, M.; Zhang, Q.; Jin, X.; Wu, Q.; Jiang, X.; Zhang, H.; Zheng, Z. Thulium-doped mode-locked fiber laser with MXene saturable absorber. In Proceedings of the CLEO: Science and Innovations, Optical Society of America, San Jose, CA, USA, 5–10 May 2019; p. SF3O.3. [CrossRef]

330. Wang, S.; Li, L.; Song, Y.F.; Tang, D.Y.; Shen, D.Y.; Zhao, L.M. Vector soliton and noise-like pulse generation using a Ti$_3$C$_2$ MXene material in a fiber laser. *Front. Inf. Technol. Electron. Eng.* **2020**, *22*, 318–324. [CrossRef]

331. Ahmad, H.; Ramli, R.; Yusoff, N.; Samion, M.Z.; Ismail, M.F.; Bayang, L.; Aidit, S.N.; Zamzuri, A.K.; Thambiratnam, K. 155 nm-wideband and tunable q-switched fiber laser using an MXene Ti$_3$C$_2$T$_x$ coated microfiber based saturable absorber. *Laser Phys. Lett.* **2020**, *17*, 085103. [CrossRef]

332. Gao, L.; Ma, C.; Wei, S.; Kuklin, A.V.; Zhang, H.; Agren, H. Applications of Few-Layer Nb$_2$C MXene: Narrow-Band Photodetectors and Femtosecond Mode-Locked Fiber Lasers. *ACS Nano* **2021**, *15*, 954–965. [CrossRef]

333. Niu, Z.; Feng, T.; Yang, K.; Li, T.; Zhao, J.; Li, G.; Li, D.; Zhao, S.; Jiang, X.; Zhang, H.; et al. MXene Ti$_3$C$_2$T$_x$ (T = F, O, or OH) saturable absorber for a 2 µm doubly Q-switched laser with AOM. *Opt. Laser Technol.* **2021**, *134*, 106642. [CrossRef]

334. Zhou, L.; Wei, C.; Wang, D.; Chi, H.; Li, Q.; Zhang, H.; Liu, Y. Q-switched mid-infrared Er^{3+}: ZBLAN fiber laser at 2.8 µm with a MXene-based Saturable Absorber. In Proceedings of the 2019 Asia Communications and Photonics Conference, Optical Society of America, No. 1736 Tianfu Avenue North, OSA Technical Digest, Chengdu, China, 2–5 November 2019; p. S4A.2.

335. Gayathri, B.; Xiantao, J.; Han, Z.; Feng, C.; Ziqi, L.; Stuart, D.J.; Alex, F. Mode-locked mid-IR fibre laser based on 2D nanomaterials. In *AOS Australian Conference on Optical Fibre Technology (ACOFT) and Australian Conference on Optics, Lasers, and Spectroscopy (ACOLS) 2019*; International Society for Optics and Photonics: Bellingham, WA, USA, 2019, Volume 11200. [CrossRef]

336. Wei, C.; Zhou, L.; Wang, D.; Chi, H.; Huang, H.; Zhang, H.; Liu, Y. MXene-Ti$_3$C$_2$T$_x$ for watt-level high-efficiency pulse generation in a 2.8 µm mid-infrared fiber laser. *Photonics Res.* **2020**, *8*, 972–977. [CrossRef]

337. Feng, C.; Qiao, W.; Liu, Y.; Huang, J.; Liang, Y.; Zhao, Y.; Song, Y.; Li, T. Modulation of MXene Nb$_2$CT$_x$ saturable absorber for passively Q-switched 2.85 microm Er:Lu$_2$O$_3$ laser. *Opt. Lett.* **2021**, *46*, 1385–1388. [CrossRef] [PubMed]

338. Dong, Y.; Chertopalov, S.; Maleski, K.; Anasori, B.; Hu, L.; Bhattacharya, S.; Rao, A.M.; Gogotsi, Y.; Mochalin, V.N.; Podila, R. Saturable absorption in 2D Ti$_3$C$_2$ MXene thin films for passive photonic diodes. *Adv. Mater.* **2018**, *30*, 1705714. [CrossRef] [PubMed]

339. Geim, A.K.; Grigorieva, I.V. Van der Waals heterostructures. *Nature* **2013**, *499*, 419–425. [CrossRef] [PubMed]

340. Mu, H.; Wang, Z.; Yuan, J.; Xiao, S.; Chen, C.; Chen, Y.; Chen, Y.; Song, J.; Wang, Y.; Xue, Y.; et al. Graphene-Bi$_2$Te$_3$ heterostructure as saturable absorber for short pulse generation. *ACS Photonics* **2015**, *2*, 832–841. [CrossRef]

341. Jiang, Y.; Miao, L.; Jiang, G.; Chen, Y.; Qi, X.; Jiang, X.f.; Zhang, H.; Wen, S. Broadband and enhanced nonlinear optical response of MoS$_2$/graphene nanocomposites for ultrafast photonics applications. *Sci. Rep.* **2015**, *5*, 1–12. [CrossRef]

342. Liu, S.; Li, Z.; Ge, Y.; Wang, H.; Yue, R.; Jiang, X.; Li, J.; Wen, Q.; Zhang, H. Graphene/phosphorene nano-heterojunction: Facile synthesis, nonlinear optics, and ultrafast photonics applications with enhanced performance. *Photonics Res.* **2017**, *5*, 662–668. [CrossRef]

343. Li, Z.; Cheng, C.; Dong, N.; Romero, C.; Lu, Q.; Wang, J.; de Aldana, J.R.V.; Tan, Y.; Chen, F. Q-switching of waveguide lasers based on graphene/WS$_2$ van der Waals heterostructure. *Photonics Res.* **2017**, *5*, 406–410. [CrossRef]

344. Tan, Y.; Liu, X.; He, Z.; Liu, Y.; Zhao, M.; Zhang, H.; Chen, F. Tuning of interlayer coupling in large-area graphene/WSe$_2$ van der Waals heterostructure via ion irradiation: Optical evidences and photonic applications. *ACS Photonics* **2017**, *4*, 1531–1538. [CrossRef]

345. You, Z.Y.; Sun, Y.J.; Sun, D.L.; Zhu, Z.J.; Wang, Y.; Li, J.F.; Tu, C.Y.; Xu, J.L. High performance of a passively Q-switched mid-infrared laser with Bi$_2$Te$_3$/graphene composite SA. *Opt. Lett.* **2017**, *42*, 871–874. [CrossRef]

346. Zhao, G.; Lv, X.; Xie, Z.; Xu, J. 2.8 μm Passively Q-switched solid state pulse laser based on MoS_2/Graphene heterojunction. In Proceedings of the 2017 Conference on Lasers and Electro-Optics Pacific Rim (CLEO-PR), Singapore, 31 July–4 August 2017; p. s1175. [CrossRef]

347. Liu, W.; Zhu, Y.N.; Liu, M.; Wen, B.; Fang, S.; Teng, H.; Lei, M.; Liu, L.M.; Wei, Z. Optical properties and applications for MoS_2-Sb_2Te_3-MoS_2 heterostructure materials. *Photonics Res.* **2018**, *6*, 220–227. [CrossRef]

348. Xue, Y.; Xie, Z.; Ye, Z.; Hu, X.; Xu, J.; Zhang, H. Enhanced saturable absorption of MoS_2 black phosphorus composite in 2 μm passively Q-switched Tm:YAP laser. *Chin. Opt. Lett.* **2018**, *16*, 020018. [CrossRef]

349. Liu, W.; Liu, M.; Liu, B.; Quhe, R.; Lei, M.; Fang, S.; Teng, H.; Wei, Z. Nonlinear optical properties of MoS_2-WS_2 heterostructure in fiber lasers. *Opt. Express* **2019**, *27*, 6689–6699. [CrossRef] [PubMed]

350. Xia, X.; Ma, C.; Chen, H.; Khan, K.; Tateen, A.K.; Xiao, Q. Nonlinear optical properties and ultrafast photonics of 2D BP/Ti_3C_2 heterostructures. *Opt. Mater.* **2021**, *112*, 110809. [CrossRef]

351. Du, W.; Li, H.; Lan, C.; Li, C.; Li, J.; Wang, Z.; Liu, Y. Graphene/WS_2 heterostructure saturable absorbers for ultrashort pulse generation in L-band passively mode-locked fiber lasers. *Opt. Express* **2020**, *28*, 11514–11523. [CrossRef]

352. Wang, Z.; Zhang, B.; Liu, J.; Song, Y.; Zhang, H. Recent developments in mid-infrared fiber lasers: Status and challenges. *Opt. Laser Technol.* **2020**, *132*, 106497. [CrossRef]

353. Zhang, W.; Wang, Q.; Chen, Y.; Wang, Z.; Wee, A.T. Van der Waals stacked 2D layered materials for optoelectronics. *2D Mater.* **2016**, *3*, 022001. [CrossRef]

354. Jiang, T.; Yin, K.; Wang, C.; You, J.; Ouyang, H.; Miao, R.; Zhang, C.; Wei, K.; Li, H.; Chen, H.; et al. Ultrafast fiber lasers mode-locked by two-dimensional materials: Review and prospect. *Photonics Res.* **2020**, *8*, 78–90. [CrossRef]

355. Ye, L.; Li, H.; Chen, Z.; Xu, J. Near-infrared photodetector based on MoS_2/black phosphorus heterojunction. *ACS Photonics* **2016**, *3*, 692–699. [CrossRef]

356. Qiao, H.; Yuan, J.; Xu, Z.; Chen, C.; Lin, S.; Wang, Y.; Song, J.; Liu, Y.; Khan, Q.; Hoh, H.Y.; et al. Broadband photodetectors based on graphene-Bi_2Te_3 heterostructure. *ACS Nano* **2015**, *9*, 1886–1894. [CrossRef]

357. Chen, C.; Xie, X.; Anasori, B.; Sarycheva, A.; Makaryan, T.; Zhao, M.; Urbankowski, P.; Miao, L.; Jiang, J.; Gogotsi, Y. MoS_2-on-MXene heterostructures as highly reversible anode materials for lithium-ion batteries. *Angew. Chem. Int. Ed.* **2018**, *57*, 1846–1850. [CrossRef]

358. Du, Y.T.; Kan, X.; Yang, F.; Gan, L.Y.; Schwingenschlögl, U. MXene/graphene heterostructures as high-performance electrodes for Li-ion batteries. *ACS Appl. Mater. Interfaces* **2018**, *10*, 32867–32873. [CrossRef]

359. Georgiou, T.; Jalil, R.; Belle, B.D.; Britnell, L.; Gorbachev, R.V.; Morozov, S.V.; Kim, Y.J.; Gholinia, A.; Haigh, S.J.; Makarovsky, O.; et al. Vertical field-effect transistor based on graphene-WS_2 heterostructures for flexible and transparent electronics. *Nat. Nanotechnol.* **2013**, *8*, 100–103. [CrossRef]

360. Yan, P.; Liu, A.; Chen, Y.; Chen, H.; Ruan, S.; Guo, C.; Chen, S.; Li, I.L.; Yang, H.; Hu, J.; et al. Microfiber-based WS_2-film saturable absorber for ultra-fast photonics. *Opt. Mater. Express* **2015**, *5*, 479–489. [CrossRef]

361. Wei, C.; Zhu, X.; Wang, F.; Xu, Y.; Balakrishnan, K.; Song, F.; Norwood, R.A.; Peyghambarian, N. Graphene Q-switched 2.78 μm Er^{3+}-doped fluoride fiber laser. *Opt. Lett.* **2013**, *38*, 3233–3236. [CrossRef] [PubMed]

362. Wang, S.; Tang, Y.; Yang, J.; Zhong, H.; Fan, D. MoS_2 Q-switched 2.8 μm Er:ZBLAN fiber laser. *Laser Phys.* **2019**, *29*, 025101. [CrossRef]

363. Li, Y.; He, Y.; Cai, Y.; Chen, S.; Liu, J.; Chen, Y.; Yuanjiang, X. Black phosphorus: Broadband nonlinear optical absorption and application. *Laser Phys. Lett.* **2018**, *15*, 025301. [CrossRef]

364. Cihan, C.; Kocabas, C.; Demirbas, U.; Sennaroglu, A. Graphene mode-locked femtosecond Alexandrite laser. *Opt. Lett.* **2018**, *43*, 3969–3972. [CrossRef]

365. Komsa, H.P.; Krasheninnikov, A.V. Electronic structures and optical properties of realistic transition metal dichalcogenide heterostructures from first principles. *Phys. Rev. B* **2013**, *88*, 085318. [CrossRef]

366. Zhao, W.; Ribeiro, R.M.; Toh, M.; Carvalho, A.; Kloc, C.; Castro Neto, A.; Eda, G. Origin of indirect optical transitions in few-layer MoS_2, WS_2, and WSe_2. *Nano Lett.* **2013**, *13*, 5627–5634. [CrossRef]

367. Qin, Z.; Hai, T.; Xie, G.; Ma, J.; Yuan, P.; Qian, L.; Li, L.; Zhao, L.; Shen, D. Black phosphorus Q-switched and mode-locked mid-infrared Er:ZBLAN fiber laser at 3.5 μm wavelength. *Opt. Express* **2018**, *26*, 8224–8231. [CrossRef]

368. Purdie, D.G.; Popa, D.; Wittwer, V.J.; Jiang, Z.; Bonacchini, G.; Torrisi, F.; Milana, S.; Lidorikis, E.; Ferrari, A.C. Few-cycle pulses from a graphene mode-locked all-fiber laser. *Appl. Phys. Lett.* **2015**, *106*, 253101. [CrossRef]

369. Yu, C.; Chujun, Z.; Shuqing, C.; Juan, D.; Pinghua, T.; Guobao, J.; Han, Z.; Shuangchun, W.; Dingyuan, T. Large energy, wavelength widely tunable, topological insulator Q-switched erbium-doped fiber laser. *IEEE J. Sel. Top. Quantum Electron.* **2014**, *20*, 315–322. [CrossRef]

370. Lee, J.; Kim, Y.; Lee, K.; Lee, J.H. Femtosecond mode-locking of a fiber laser using a $CoSb_3$-skutterudite-based saturable absorber. *Photonics Res.* **2018**, *6*, C36–C43. [CrossRef]

371. Liu, W.J.; Liu, M.L.; OuYang, Y.Y.; Hou, H.R.; Ma, G.L.; Lei, M.; Wei, Z.Y. Tungsten diselenide for mode-locked erbium-doped fiber lasers with short pulse duration. *Nanotechnology* **2018**, *29*, 174002. [CrossRef]

372. Wei, C.; Chi, H.; Jiang, S.; Zheng, L.; Zhang, H.; Liu, Y. Long-term stable platinum diselenide for nanosecond pulse generation in a 3-μm mid-infrared fiber laser. *Opt. Express* **2020**, *28*, 33758–33766. [CrossRef]

373. Yan, X.; Jiang, M.; Li, E.; Kang, X.; Ren, Z.; Li, D.; Wang, T.; Lu, B. Tunable high-order harmonic and dual-wavelength mode-locking in Er-doped fiber laser based on $Ti_3C_2T_x$-MXene. *Appl. Phys. Express* **2021**, *14*, 012009. [CrossRef]

374. Zhang, C.; Zhang, F.; Fan, X.; Yang, J.; Liu, J.; Zhang, H. Passively Q-switched operation of in-band pumped Ho:YLF based on Ti$_3$C$_2$T$_x$ MXene. *Infrared Phys. Technol.* **2019**, *103*, 103076. [CrossRef]

375. Li, G.; Liu, J.; Wang, F.; Nie, H.; Wang, R.; Yang, K.; Zhang, B.; He, J. Third-order nonlinear optical response of few-layer MXene Nb$_2$C and applications for square-wave laser pulse generation. *Adv. Mater. Interfaces* **2021**, *8*, 2001805. [CrossRef]

376. Tuo, M.; Xu, C.; Mu, H.; Bao, X.; Wang, Y.; Xiao, S.; Ma, W.; Li, L.; Tang, D.; Zhang, H.; et al. Ultrathin 2D transition metal carbides for ultrafast pulsed fiber lasers. *ACS Photonics* **2018**, *5*, 1808–1816. [CrossRef]

377. Sun, X.; Zhang, B.; Li, Y.; Luo, X.; Li, G.; Chen, Y.; Zhang, C.; He, J. Tunable ultrafast nonlinear optical properties of graphene/MoS$_2$ van der Waals heterostructures and their application in solid-state bulk lasers. *ACS Nano* **2018**, *12*, 11376–11385. [CrossRef]

378. Meng, S.; Kong, T.; Ma, W.; Wang, H.; Zhang, H. 2D Crystal–Based Fibers: Status and Challenges. *Small* **2019**, *15*, 1902691. [CrossRef] [PubMed]

379. Zhang, H. Ultrathin two-dimensional nanomaterials. *ACS Nano* **2015**, *9*, 9451–9469. [CrossRef] [PubMed]

380. Liu, Y.; Xiao, C.; Li, Z.; Xie, Y. Vacancy engineering for tuning electron and phonon structures of two-dimensional materials. *Adv. Energy Mater.* **2016**, *6*, 1600436. [CrossRef]

381. Jung, N.; Kim, B.; Crowther, A.C.; Kim, N.; Nuckolls, C.; Brus, L. Optical reflectivity and raman scattering in few-layer-thick graphene highly doped by K and Rb. *ACS Nano* **2011**, *5*, 5708–5716. [CrossRef]

382. Hartmann, S.J.; Iurchenkova, A.A.; Kallio, T.; Fedorovskaya, E.O. Electrochemical properties of nitrogen and oxygen doped reduced graphene oxide. *Energies* **2020**, *13*, 312. [CrossRef]

383. Shao, L.S.; Li, J.J.; Guang, Y.; Zhang, Y.L.; Zhang, H.; Che, X.Y.; Wang, Y.H. PVA/polyethyleneimine-functionalized graphene composites with optimized properties. *Mater. Des.* **2016**, *99*, 235–242. [CrossRef]

384. Sun, Z.; Hasan, T.; Torrisi, F.; Popa, D.; Privitera, G.; Wang, F.; Bonaccorso, F.; Basko, D.M.; Ferrari, A.C. Graphene mode-locked ultrafast laser. *ACS Nano* **2010**, *4*, 803–810. [CrossRef]

385. Xia, H.; Li, H.; Lan, C.; Li, C.; Zhang, X.; Zhang, S.; Liu, Y. Ultrafast erbium-doped fiber laser mode-locked by a CVD-grown molybdenum disulfide (MoS$_2$) saturable absorber. *Opt. Express* **2014**, *22*, 17341–17348. [CrossRef]

386. Novoselov, K.S.; Mishchenko, A.; Carvalho, A.; Neto, A.H.C. 2D materials and van der Waals heterostructures. *Science* **2016**, *353*, aac9439. [CrossRef]

387. Zhou, K.G.; Withers, F.; Cao, Y.; Hu, S.; Yu, G.L.; Casiraghi, C. Raman modes of MoS$_2$ Used as fingerprint of van der waals interactions in 2-D crystal-based heterostructures. *ACS Nano* **2014**, *8*, 9914–9924. [CrossRef]

388. Sakakura, M.; Lei, Y.H.; Wang, L.; Yu, Y.H.; Kazansky, P.G. Ultralow-loss geometric phase and polarization shaping by ultrafast laser writing in silica glass. *Light. Sci. Appl.* **2020**, *9*, 15. [CrossRef]

389. Baig, Z.; Mamat, O.; Mustapha, M.; Mumtaz, A.; Munir, K.S.; Sarfraz, M. Investigation of tip sonication effects on structural quality of graphene nanoplatelets (GNPs) for superior solvent dispersion. *Ultrason. Sonochem.* **2018**, *45*, 133–149. [CrossRef]

390. Lee, X.J.; Hiew, B.Y.Z.; Lai, K.C.; Lee, L.Y.; Gan, S.; Thangalazhy-Gopakumar, S.; Rigby, S. Review on graphene and its derivatives: Synthesis methods and potential industrial implementation. *J. Taiwan Inst. Chem. Eng.* **2019**, *98*, 163–180. [CrossRef]

391. Xu, J.; Hu, J.; Li, Q.; Wang, R.; Li, W.; Guo, Y.; Zhu, Y.; Liu, F.; Ullah, Z.; Dong, G.; et al. Fast batch production of high-quality graphene films in a sealed thermal molecular movement system. *Small* **2017**, *13*, 1700651. [CrossRef] [PubMed]

392. Goyal, V.; Teweldebrhan, D.; Balandin, A.A. Mechanically-exfoliated stacks of thin films of Bi$_2$Te$_3$ topological insulators with enhanced thermoelectric performance. *Appl. Phys. Lett.* **2010**, *97*, 133117. [CrossRef]

393. Krumrain, J.; Mussler, G.; Borisova, S.; Stoica, T.; Plucinski, L.; Schneider, C.; Grützmacher, D. MBE growth optimization of topological insulator Bi$_2$Te$_3$ films. *J. Cryst. Growth* **2011**, *324*, 115–118. [CrossRef]

394. Aabdin, Z.; Peranio, N.; Winkler, M.; Bessas, D.; König, J.; Hermann, R.; Böttner, H.; Eibl, O. Sb$_2$Te$_3$ and Bi$_2$Te$_3$ thin films grown by room-temperature MBE. *J. Electron. Mater.* **2012**, *41*, 1493–1497. [CrossRef]

395. Fei, F.; Wei, Z.; Wang, Q.; Lu, P.; Wang, S.; Qin, Y.; Pan, D.; Zhao, B.; Wang, X.; Sun, J.; et al. Solvothermal synthesis of lateral heterojunction Sb$_2$Te$_3$/Bi$_2$Te$_3$ nanoplates. *Nano Lett.* **2015**, *15*, 5905–5911. [CrossRef]

396. Tian, W.; Yu, W.; Shi, J.; Wang, Y. The property, preparation and application of topological insulators: a review. *Materials* **2017**, *10*, 814. [CrossRef]

397. Brom, J.E.; Weiss, L.; Choudhury, T.H.; Redwing, J.M. Hybrid physical–chemical vapor deposition of Bi$_2$Se$_3$ films. *J. Cryst. Growth* **2016**, *452*, 230–234. [CrossRef]

398. Manzeli, S.; Ovchinnikov, D.; Pasquier, D.; Yazyev, O.V.; Kis, A. 2D transition metal dichalcogenides. *Nat. Rev. Mater.* **2017**, *2*, 1–15. [CrossRef]

399. Radisavljevic, B.; Radenovic, A.; Brivio, J.; Giacometti, V.; Kis, A. Single-layer MoS$_2$ transistors. *Nat. Nanotechnol.* **2011**, *6*, 147–150. [CrossRef]

400. Jia, J.; Jang, S.K.; Lai, S.; Xu, J.; Choi, Y.J.; Park, J.H.; Lee, S. Plasma-treated thickness-controlled two-dimensional black phosphorus and its electronic transport properties. *ACS Nano* **2015**, *9*, 8729–8736. [CrossRef] [PubMed]

401. Wang, Z.; Kochat, V.; Pandey, P.; Kashyap, S.; Chattopadhyay, S.; Samanta, A.; Sarkar, S.; Manimunda, P.; Zhang, X.; Asif, S.; et al. Metal immiscibility route to synthesis of ultrathin carbides, borides, and nitrides. *Adv. Mater.* **2017**, *29*, 1700364. [CrossRef] [PubMed]

402. Zhang, F.; Zhang, Z.; Wang, H.; Chan, C.H.; Chan, N.Y.; Chen, X.X.; Dai, J.Y. Plasma-enhanced pulsed-laser deposition of single-crystalline Mo$_2$C ultrathin superconducting films. *Phys. Rev. Mater.* **2017**, *1*, 034002. [CrossRef]